Some Principles of Somatosensory Cortical Organization in Rats and Humans

by

Christopher I. Moore

B.A., Neuroscience and Philosophy
Oberlin College, 1990

Submitted to the Department of Brain and Cognitive Sciences in partial fulfillment of the requirements for the degree of

DOCTOR OF PHILOSOPHY

at the

MASSACHUSETTS INSTITUTE OF TECHNOLOGY

April 1998
[June 1998]

Signature of Author_____
Department of Brain and Cognitive Sciences
April 30, 1998

Certified by_____
Suzanne Corkin, Ph. D.
Professor of Behavioral Neuroscience

Accepted by_____
Mriganka Sur, Ph. D.
Teuber Professor and Chairman, Department of Brain and Cognitive Sciences

Some Principles of Somatosensory Cortical Organization in Rats and Humans

by

Christopher I. Moore

Submitted to the Department of Brain and Cognitive Sciences in April 1998 in Partial Fulfillment of the Requirements for the Degree of Doctor of Philosophy in Brain and Cognitive Sciences

ABSTRACT

This thesis research elucidated principles of somatosensory cortical organization at the level of the receptive field, cortical map, and cortical area in the rat and human. Throughout these studies, a central focus was on the connection between each level of organization and the capacity for cortical reorganization. The rat and human somatosensory systems each bring unique opportunities to the study of somatosensory function. Rat SI provides a well-researched system in which detailed, invasive studies can be conducted. Human SI, while less readily available to detailed analysis, is ultimately the relevant preparation for studying the relation between cortical map organization and human perception.

In Chapter 1, I examined the convergence of subthreshold (non-action potential evoking) sensory input in individual neurons using whole-cell in vivo recording techniques. Individual neurons in rat SI integrated subthreshold information from an extensive peripheral field, spanning on average 2 vibrissae in each direction from the vibrissa that evoked the largest input (the primary vibrissa). Inputs across the subthreshold receptive field were not homogeneous, as the latency to onset, rise time and prevalence of inhibition varied as a function of the strength of excitatory input and the time poststimulus when they are assessed. These spatial and temporal variables constrain the suprathreshold output of the receptive field, and define the substrate for context-dependent integration of input.

In Chapter 2, I described studies of the rat SI vibrissa representation conducted using intrinsic-signal optical imaging. Studies at this level of abstraction have two principal merits. First, they provide an understanding of how systems of neurons interact. While a great deal can be inferred from single cell recording, the function of larger populations of neurons needs to be assessed directly and simultaneously to construct an understanding of how a cortical area processes sensory input. Secondly, the study of cortical map organization provides a link between studies of single units in animals and the organization of sensory perception in humans. Because research on human cortical organization has been limited to larger scale phenomena, such as map organization and the segregation of cortical areas (Chapter 3), an understanding of the links between single cell activity and map activity in animals provides a bridge for beginning to understand how the detailed function of single neurons supports processes of human perception.

In Experiment 1 of Chapter 2, I addressed frequency dependent reorganization of the vibrissa representation in rat SI. Individual vibrissa were stimulated at 1, 5 and 10 Hz: The higher frequency stimuli (5 and 10 Hz) activated a

more discrete region of cortex than the lowest frequency (1 Hz) stimulation. This finding demonstrates the dynamic reorganization of rat SI cortex over second timescales, and suggests that whisking behavior may serve to enhance the contrast between individual vibrissa. In Experiment 2, I examined the effects of prolonged non-invasive changes in the pattern of sensory input. All the vibrissa except 2 on one side of the rat's face were cut, and after 64-66 hours the cortical representation was assessed (Armstrong-James et al., 1994; Diamond et al., 1992). Following this behavioral manipulation, the amplitude of uncut vibrissa input increased in the neighboring cut and uncut vibrissa representations. This finding suggests that, in addition to the temporal pairing of inputs, deafferentation-type reorganization is also invoked by this manipulation.

In Chapter 3, I investigated the organization and reorganization of human somatosensory cortex using fMRI. In Experiments 1 and 2, the mediolateral position of the palm representation within the postcentral gyrus (PoCG) was assessed. Using 1.5 and 3 Tesla (T) magnets, the palm representation was localized to the region of the PoCG predicted by the Penfield homunculus (Penfield and Rasmussen, 1950; see also Corkin, 1964), and a secondary activation area, potentially corresponding to the representation of the radial palm in the monkey (Merzenich et al., 1978; Nelson et al., 1980), was identified. In Experiment 3, I examined the anterior-posterior segregation of multiple areas within the human PoCG. During tactile stimulation, a precentral gyrus region, corresponding to area 6, and a PoCG region, corresponding to areas 3b,1 and 2, were activated. The borders of these two regions defined an inactive gap in the central sulcus region, corresponding to area 3a. Conversely, during proprioceptive/motor stimulation, all three representations were activated. This pattern of activation suggests a strong analogy between the organization of primate and human somatosensory processing streams within the PoCG.

Experiment 4 of Chapter 3 presents evidence for the reorganization of human somatosensory cortex following massive deafferentation using perceptual report and fMRI. In agreement with the hypothesis that cortical reorganization is the substrate for phantom perceptions (Ramachandran, 1993; Teuber et al., 1949), two spinal-cord injured (SCI) subjects reported a somatotopic pattern of referred sensations. Further, a subject with phantom perceptions demonstrated greater signal change in the palm representation than an SCI subject without phantom sensations, and normal control subjects (NCS). This finding is in good agreement with increased amplitude in the uncut vibrissa representation following vibrissa trimming/pairing, and suggests that the mechanisms of human cortical reorganization are potentially similar to those observed in rat SI.

Taken alone, these studies represent advances in our understanding of the principles of somatosensory cortical organization in rats and humans. In total, these studies provide evidence on three levels of organization, from rat subthreshold receptive fields to human cortical maps, for the importance of dynamic processes in cortical function.

TABLE OF CONTENTS

ACKNOWLEDGMENTS

Giving just a few words of acknowledgment cheapens the appreciation I'd like to show, it damns the recipients with faint praise. Still, it's a good opportunity to give deserving thanks. Now the trick is to figure out a novel way to begin 20 sentences with "I would like to thank...".

Foremost, I would like to thank my two advisors, Mriganka Sur and Suzanne Corkin. Their intellectual guidance and flexibility gave breath to the diverse projects I have pursued. Perhaps as importantly, their friendship has been an essential constant in my time here. They have opened not only their labs but also their homes, and I can't think of how to thank them enough.

Thanks also to the three main collaborators who contributed to the projects in this thesis, Sacha Nelson (Chapter 1), Bhavin Sheth (Chapter 2) and Chantal Stern (Chapter 3). I've learned a tremendous amount from each of you and I've enjoyed our friendships: If you ever need help writing a thesis, let me know. I am also grateful to Sonal Jhaveri and Matt Wilson, for the insight and encouragement, and to Jon Kaas for helpful comments on the thesis and for serving on my thesis committee.

Thanks to Matthew Diamond, for conversations on vibrissa *trimming* plasticity, and for allowing the use of the suprathreshold data in the Appendix. Thanks to the Bizzi lab for the collaboration on the field potential recordings in Chapter 2.

Thanks to Anders Dale, who developed the analysis techniques employed in Chapter 3, to Mary Folley and Terry Campbell who ran the scanner for most of the experiments, to Sandra Kostyk and Alyssa LeBel who referred the spinal-cord injured patients, to Ann Doyle for helping schedule these patients, and to the patients, who made the greatest contribution to this portion of the research.

I am grateful to Joe Locasio for providing insight into a number of probabilistic events I've been concerned about.

I am fortunate to have collaborated with several talented undergraduates, including Alo Basu, who was primarily responsible for the histological data presented in Chapter 2 and the biocytin anatomy described in Chapter 1, and Nina Gray, who contributed to the analysis of data in Chapter 3. I am also thankful to Anil Gehi, who began as a UROP and continued to obtain his MA degree in Mechanical Engineering working with me on the 1.5 T fMRI Experiments presented in Chapter 3. I am also grateful to Steven Yeh, who contributed to psychophysics research in SCI that is not included in this thesis.

Many thanks to Ted Adelson and the Adelson lab for the generous open disk policy.

I would also like to thank Dennison Smith, Michael Browning and Greg Rose for the on-the-job learning prior to graduate school and for their sound counsel then and now.

Now this acknowledgments page enters a nebulous zone of thanking friends who were helpful to this thesis in some less specific but still significant way.

Prominent in this group are a number of current and past members of the Sur and Corkin laboratories, including David "Night Train" Somers, Diana Smetters, Janine Mendola, Peg Jennings, Carsten Hohnke, L. J. Toth, Allessandra Angelucci, Jeff Bucci, Bob Seguira, Mark Snow, Emily "Chili" Rossi, Mary Ann Capehart, Martha Meyer, and Suzanne Kuffler. I guess in this context it's probably good to thank Anna Roe for not dropping me on my head when I was in swaddling clothes. I would also like to warmly thank Sungsil Kim, Louisa Worthington, Jan Ellertsen, Glen Holm, Tim Davis, J. C. Stevens, Denise Heinze, and Kevin Flansburg.

Most learning in graduate school occurs with fellow students, and a lot of the shared knowledge that is exchanged escapes the traditional boundaries of neuroscience. In this vein, I'd like to thank Brad Postle for continued assistance with difficult terminology (e.g., trenchant, dedifferentiation); Stephen Gilbert for his encyclopedic knowledge of all things Texan and administrative; Matt Tresch for the donation of various pieces of equipment, including the sponge used in Chapter 1, the Bizzi lab amplifier and the segments of his anatomy left on the frisbee field; Cristina Sorrentino, for Mind *and* Brain; and, Rose Roberts, for editing everything, twice. All that learning noted, I'd mostly like to thank this list for their wonderful companionship and friendship.

Finally, I'd like to thank my family for their love, support and for any of a number of discussions around the kitchen table, Paul for his unflagging friendship and for continuing to be one of my most important teachers, and Willamarie for her seemingly boundless empathy and support, and patience during the writing of this Acknowledgements page.

PREFACE

This thesis is organized in the following way. Each Chapter begins with a general introduction. Within a Chapter, each Experiment is presented with its own methods, results and discussion, in addition to a small general discussion at the end that considers broader issues. In the Conclusion, I comment upon topics relating to the thesis as a whole, and propose future directions for this work. To help contextualize the measurements made in Chapters 1 and 2, the Appendix describes the relation between hemodynamic signal and subthreshold signal spread.

Abbreviations

PV	Primary vibrissa
i. p.	Intraperitoneal
RS	Regular-spiking neuron
FS	Fast-spiking neuron
IB	Intrinsically bursting neuron
VPm	Ventral posterior medial nucleus of the thalamus
POm	Posterior medial nucleus of the thalamus
PoCG	Postcentral gyrus
PreCG	Precentral gyrus
Hbr	Deoxygenated hemoglobin
HbO_2	Oxygenated hemoglobin
T	Tesla

CHAPTER 1

Spatio-temporal Subthreshold Receptive Fields in Rat SI

"All things are porous to a certain sense, they pass
...it seems they even go through glass..."

Baudelaire

The rodent primary somatosensory cortex (SI) contains a detailed representation of the vibrissae on the rat face. For each vibrissa, there is a corresponding cluster of layer IV neurons in SI (a "barrel") (Woolsey and van der Loos, 1970; Welker and Woolsey, 1974). This unique anatomical homeomorphy in layer IV has inspired a number of physiological studies of action potential receptive fields in the vibrissa representation within rat SI (Armstrong-James and Fox, 1987; Armstrong-James et al., 1992; Chapin, 1986; Chapin and Lin, 1984; Simons, 1985; Simons and Carvell, 1989; Welker, 1971, 1976). These studies have consistently reported that the column extending above and below the layer IV barrel is most responsive to the input from the associated vibrissa (Simons, 1978; Armstrong-James et al., 1992).

Despite this consistent localization of the center of the vibrissa representation with its anatomically corresponding barrel, this system is not a labeled line. Suprathreshold receptive fields within a rat SI vibrissa barrel often extend beyond their homologous vibrissa (Armstrong-James and Fox, 1987; Armstrong-James et al., 1992; Chapin, 1986; Faggin et al., 1997). In addition, evoked responses to stimulation of a vibrissa can be modulated rapidly by the context in which they occur (Sheth et al., 1998; Simons, 1985), and receptive fields within rat SI are plastic over longer time scales following changes in the pattern of peripheral input (Armstrong-James et al., 1994; Delacour et al., 1987; Diamond et al., 1992, 1994). These results imply that suprathreshold receptive fields are based upon larger, subthreshold receptive fields from which they are constructed and rapidly modified.

There are several factors that, together with the cell's intrinsic firing threshold, determine the extent of a suprathreshold receptive field. Primary among these are the spatial extent of the subthreshold receptive field, the temporal dynamics of that input, and the balance of excitation and inhibition within the receptive field. To measure these aspects of subthreshold receptive fields directly, we made whole cell recordings in the adult rat SI vibrissa representation in vivo while stimulating individual vibrissae. Our results show that single neurons can integrate information from a large region of the vibrissa pad, extending several vibrissa from the 'primary vibrissa' that evokes the largest response. Inputs across the subthreshold receptive field are not homogeneous, as the latency to onset, rise time and prevalence of inhibition vary as a function of the spatial location within the receptive field, strength of excitatory input and the time poststimulus they are assessed. These spatial and temporal variables constrain the suprathreshold output of the receptive field, and define the substrate for context-dependent integration of input. Some of these results have been reported previously in abstract form (Moore and Nelson, 1994; Moore, 1998).

Methods

Surgical Methods

Adult Sprague-Dawley rats (190-330g) were anesthetized with urethane (20% in saline solution, 1.25g/kg initial dose, i.p.). Dexamethasone 8 mg/kg i.p. was given to reduce pial and cortical swelling (Istvan and Zarzecki, 1994) and atropine 8 μg/kg, i.p., was given to reduce respiratory secretions. During the experiment, a .125g/kg supplement of urethane was administered if needed to maintain a level of anesthesia at which animals were unresponsive to hindpaw pinch and had a breathing rate of 80-120 breaths/min (Armstrong-James and Callahan, 1991). Core

body temperature of 36° C was maintained with a servo-controlled heating blanket and rectal thermometer (Harvard apparatus).

Following induction of anesthesia, the animal was placed in a stereotaxic device on an air table, and the right scalp and temporal muscle were resected. Using a dremel tool bit, the skull over the vibrissa representation was thinned until translucent, allowing an accurate reconstruction of the cortical vasculature. Using the vascular pattern as a guide, a small (1-3 mm) craniotomy and durotomy were made over the right SI vibrissa representation at approximately 2 mm posterior and 5.5 mm lateral to bregma (Armstrong-James et al., 1989; Simons and Carvell, 1989). To improve recording stability, cerebrospinal fluid was removed through the foramen magnum. The craniotomy and durotomy were enlarged later in the experiment to allow for further electrode penetrations.

Whole-Cell Recording Techniques

All recordings reported here were obtained using "blind" in vivo whole-cell recording techniques (Ferster and Jagadeesh, 1992; Nelson et al., 1994). Recordings were made in bridge mode (Axoclamp 2A amplifier) and the bridge balance was adjusted to compensate for series resistance. Whole-cell recording pipettes were lowered through the cortex with a hand operated Leitz micromanipulator (electrode resistance = 5-7 mΩ; tip width, 2 μm; recording solution, 120 mM potassium gluconate, 20 mM hepes, 1 mM EGTA, 10 mM KCl, 5 mM $MgSO_4$, 3 mM ATP and 1 mM GTP). While the electrode descended through the cortex, a current step (-440 nA, 500msec, .5 Hz) was passed through the electrode tip. Penetrations continued until an increased resistance was observed, at which time back pressure on the electrode tip was removed and a high resistance seal (1-10 gΩ) was allowed to form spontaneously or with application of gentle suction. Additional suction was then used to achieve whole cell recording (Fig. 1). Neurons with a resting membrane potential of less than -50 mV and a spike height of greater than 20 mV were accepted for analysis (Ri = 87.2 MΩ +/- 68.5 SD). Recordings lasted up to 3 hours.

Electrode depth was monitored as the electrode progressed through the cortex. Based on cytochrome oxidase staining in coronal section (60μm: N = 5 animals; A. Basu and C. Moore, unpublished observations) and correspondence with the Paxinos and Watson (1986) rat atlas, we made an adjustment for the angle of the penetrating electrode (electrode depth was multiplied by .86). This calculation was confirmed by biocytin staining in 2 neurons from which intracellular recordings were obtained and in 5 small extracellular deposits of biocytin made using whole-cell electrodes (data not shown). We were unable to estimate accurately the depth in 16/45 neurons due to difficulty in precisely determining the point of contact with the surface of the cortex. The segmentation of cortical depths into supragranular (0-500 μm), granular (500-850 μm), and infragranular divisions (>850 μm) was made from cytochrome oxidase stained sections (N = 5 animals).

Figure 1 Seal formation and intrinsic firing properties A. Prior to entry into the neuron, a several GΩ seal (>9 GΩ) between the electrode and the cell membrane was revealed by current injection. Following break through of the membrane (arrow), the resting membrane potential is -55 mV. *7.* B. and C. Examples of an intrinsically bursting (B) and a regular-spiking neuron (C). *Scale bar* 100 msec, horizontal and 500 pA and 10 mV, vertical. In A and B, small spontaneous events can be observed. These were common in our recordings.

Receptive-field Mapping

Sensory stimuli were provided by a Chubbyk stimulator (Chubbyk, 1969: N = 8 neurons) and a piezoelectric bimorph wafer attached to a thin-wall glass capillary (M. Armstrong-James, personal communication; Simons, 1983; N = 16). Both stimulators employed a 100-300 msec stimulus of 1 mm (initial rate of rise: Chubbyk = 120 mm/sec; Piezoelectric = 100 mm/sec). To prevent ringing in the piezoelectric stimulus, the voltage step driving the piezoelectric stimulator was filtered through an RC filter (τ = 10 msec), and a section of sponge that expanded in the direction of deflection was attached to the back of the piezoelectric wafer. Prior to recording, vibrissae on the left side of the rat's face were clipped to a length of approximately 1 cm and the deflection point of the vibrissa was established at 5-7 mm from the base of the vibrissa. After entering the cell and establishing its intrinsic firing properties, the center of the receptive field was determined using a hand held probe and pre-positioned stimulators. In 9 rats, sensory-evoked field potentials were recorded prior to whole-cell recording to pre-position stimulator(s) accurately in the center of the receptive field. For quantitative receptive field mapping, each vibrissa was stimulated a minimum of 10 times at 2 sec intervals (Armstrong-James et al., 1993). Up to 18 vibrissae were quantitatively mapped during a single neuronal recording.

The latency to the initial post-synaptic potential (PSP) was measured from the onset of vibrissa deflection to the first positive deviation from resting membrane potential. The amplitude of evoked subthreshold responses was measured as the peak mean initial depolarization subtracted from the mean of the resting membrane potential, with baseline defined as the period 1-5 msec prior to vibrissa deflection. The 'primary vibrissa' was defined as the vibrissa that evoked the largest depolarization from rest. If action potentials were evoked by vibrissa deflection, subthreshold amplitude was assessed as the peak underlying depolarization not including the fast action potential transient. Suprathreshold responses were defined as action potentials evoked within 100 msec of onset of deflection (Armstrong-James et al., 1991) on a minimum of 20% of trials after subtracting the probability of spontaneous action potential firing during the period 100 msec prior to deflection (spontaneous action potential firing was relatively rare in our sample, and was not present in the baseline period of neurons possessing action potential receptive fields). Rise time to half maximal was measured as the time from onset of the evoked response to the point one-half the amplitude of the peak depolarization. For analyses requiring identification of a primary vibrissa (PV), only neurons in which 4 or more vibrissae were quantitatively mapped were analyzed. This cut-off was used to further insure that the center of the receptive field had been identified. Probability statistics are reported for 2-tailed t-test comparisons except where otherwise noted.

Results

We obtained stable whole-cell recordings from 45 neurons in 20 animals (mean resting membrane potential = -62.1 mV +/- 9.2 SD: Mean spike height = 52.5 mV +/- 16.6). Neurons in this population exhibited regular-spiking (RS: N = 35), intrinsically-bursting (IB: N = 9) and fast-spiking (FS: N = 1) firing characteristics (Fig. 1: Agmon and Connors, 1992; Istvan and Zarzecki, 1994; McCormick et al., 1985; Pockberger, 1991). Approximately one-third of the neurons classified as RS (N = 13) also fired a burst-like cluster of action potentials riding on a broad depolarization (Amitai and Connors, 1995; Friedman and Gutnick, 1987; Istvan and Zarzecki, 1994;

Montoro et al., 1988). This bursting mode was usually observed during periods of membrane oscillations which are common during urethane anesthesia (.2-5 Hz, Wilson, 1993). Two neurons demonstrated prolonged, complex action potentials suggestive of dendritic recordings (data not shown: Amitai and Connors, 1995; Kim et al., 1995). These neurons were not included in receptive field analyses.

Receptive Field Analyses

We quantitatively assessed the vibrissa receptive field in 24 neurons and 126 vibrissae. In 4 neurons, including 8 vibrissae, we did not observe subthreshold or suprathreshold responses within the vibrissa field. For the 20 neurons in which we observed an evoked response, 96 of 118 vibrissae (81.4%) demonstrated subthreshold receptive field inputs (Fig. 2, grey bars within histogram). Suprathreshold responses were observed in 7 of 20 neurons (35%) quantitatively mapped, and in 12 of 118 vibrissae (10.2%; Fig. 2, black bars within histogram). There was no significant difference in the mean resting membrane potential of neurons with suprathreshold and purely subthreshold receptive fields (suprathreshold, -60.2 mV +/- 2.0 SEM; subthreshold, -61.6 mV +/- 3.1; $p > 0.10$), and both populations readily fired action potentials in response to injection of depolarizing current.

Extensive subthreshold receptive fields were observed in neurons throughout the depth of rat SI. An example of a subthreshold receptive field recorded at a depth of 645 μm, corresponding to layer 4, is shown in Figure 3. In this neuron, responses were evoked from 10 of 10 vibrissae stimulated, and deflection of vibrissae more than 2-away from the PV (e.g., the D4) evoked consistent PSPs. To assess the relative strength of input throughout the receptive field, we normalized the amplitude of surround vibrissa responses to the response of the PV (for a similar approach applied to suprathreshold receptive fields, see Armstrong-James et al., 1991). The majority of neurons had receptive fields with a single-peak, and response amplitudes that diminished with increasing distance from the peak (N = 14/15 receptive fields in which 4 or more vibrissae were assessed, including N = 6 suprathreshold and N = 8 exclusively subthreshold receptive fields). The single exception to the single-peaked receptive field pattern was an infragranular bursting neuron (depth = 860 mm) that showed two distinct peaks (the D4 and the B3) with a trough of non-responsive vibrissae between them. Similar multi-foci receptive fields have been reported for extracellular recordings from infragranular neurons (Armstrong-James and Fox, 1987; Armstrong-James et al., 1992; Chapin, 1986; Chapin and Lin, 1984; Innocenti and Manzoni, 1972). Because we were unable to define a PV for this neuron, it was excluded from summary statistics described below.

Figure 2 Histogram of receptive field sizes per number of vibrissae deflected Each neuron demonstrating an evoked subthreshold receptive field is depicted as a separate interval within the histogram (N = 20). The total number of vibrissae stimulated during quantitative receptive field mapping is shown in the length of each column, the vibrissae that evoked exclusively subthreshold responses are shown in gray, and the those that evoked suprathreshold responses in black. For each neuron, the vibrissa that evoked the largest response amplitude is shown in the column on the right.

Figure 2

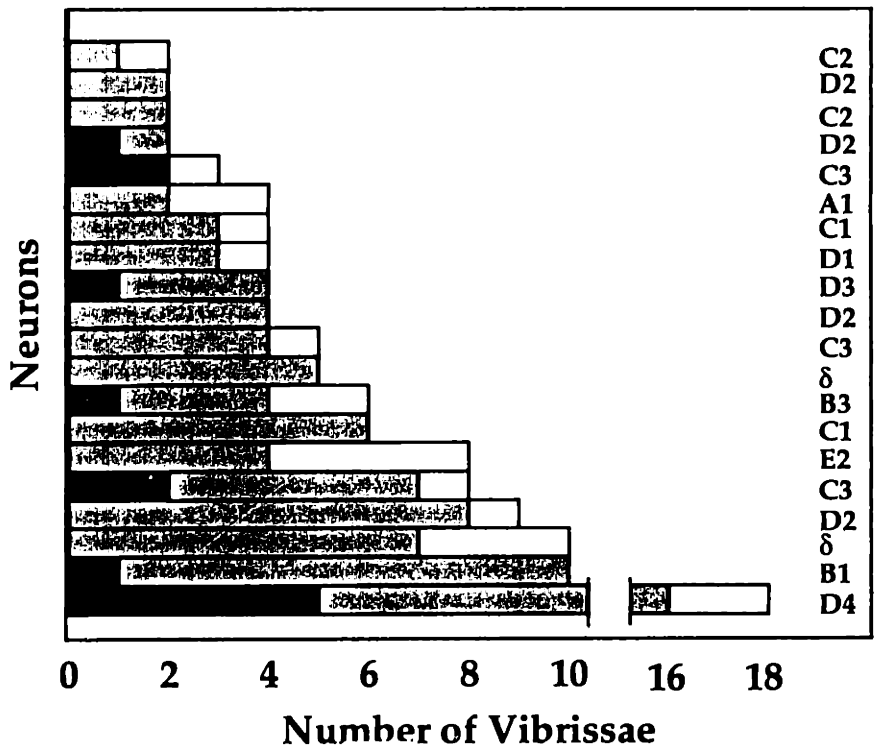
Neurons
C2
D2
C2
D2
C3
A1
C1
D1
D3
D2
C3
δ
B3
C1
E2
C3
D2
δ
B1
D4
0
2
4
6
8
10
16
18
Number of Vibrissae

Figure 3 The subthreshold receptive field of a granular depth neuron A. Evoked responses to the deflection of three individual vibrissae in a granular layer depth neuron (648 μm). B. The receptive field of the same neuron. Each vertical column represents the amplitude of the initial subthreshold depolarization evoked by deflection of a single vibrissa. Responses are normalized to the subthreshold amplitude of the PV (B1) (see text for detail)s.

Figure 3

A.

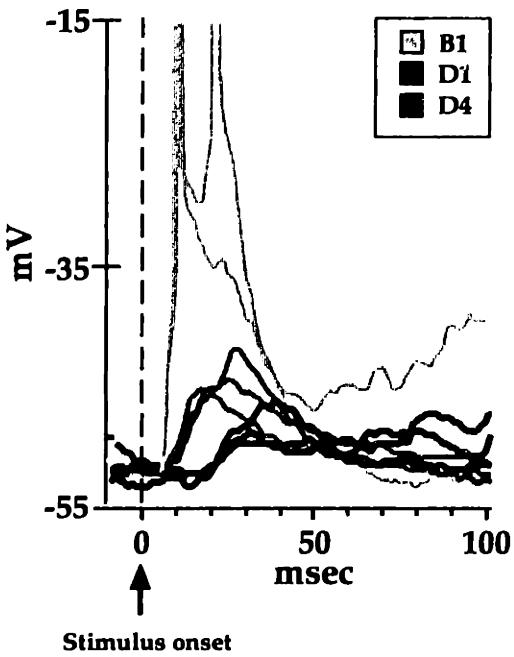
-15
-35
-55
mV
B1
D1
D4
0
50
100
msec
Stimulus onset

B.

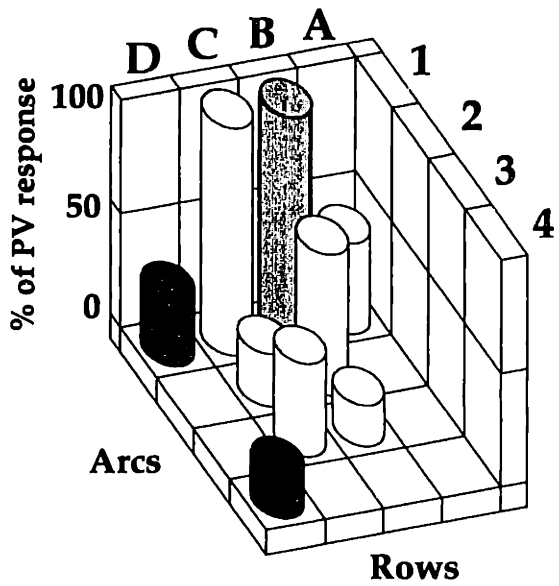
D
C
B
A
1
2
3
4
100
50
0
% of PV response
Arcs
Rows

Figure 4 The amplitude and extent of subthreshold receptive fields A. The amplitude of evoked responses from the PV (white circles, 9.1 mV +/- .84 SEM), vibrissa 1-away (5.1 mV +/- .5) and vibrissa 2-away (3.7 mV +/- .59). B. Receptive fields were normalized as in Figure 3, and then averaged (N = 74 vibrissae, 14 cells). Data are plotted with respect to the within row, arc, or diagonal relation to the PV.

Figure 4

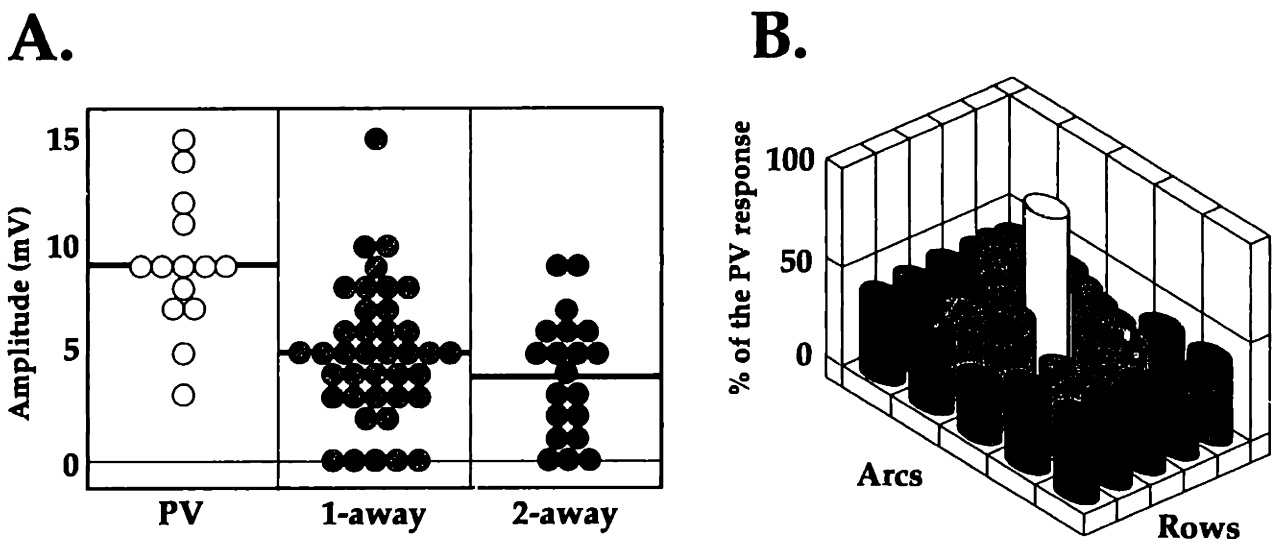
A.
B.
15
10
5
0
Amplitude (mV)
PV
1-away
2-away
100
50
0
% of the PV response
Arcs
Rows

Stimulation of vibrissae one- and two-away (in the same row, arc or diagonal) from the PV consistently evoked sensory responses (Fig. 4A; PV, 9.1 mV +/- .84 SEM, N = 14; 1-away, 5.1 mV +/- .5, N = 39; and 2-away, 3.7 mV +/- .59, N = 20: $p <$ 0.001 for 2-away). The response to stimulation three vibrissa away was not, over the population tested, significantly different from baseline (1.3 mV +/- .70 SEM: $p > .10$), although our limited sample (N = 8) included clear subthreshold responses from vibrissa three-away in neurons from the supragranular, granular and infragranular depths (e.g., the D4 vibrissa input in Fig. 3). To assess the spatial organization of subthreshold receptive field input, we normalized as described above, and averaged across vibrissae (N = 14 neurons and 61 vibrissae). As previously reported for suprathreshold cortical and thalamic receptive fields, there was a trend toward within-row subthreshold signal spread (Armstrong-James et al., 1992; Chapin, 1986; Lee et al., 1994: 1-away within row, 67.8% +/- 6.8 SEM; within arc, 51.9 +/- 9.3; within diagonal, 41 +/- 6.1), although within-row activity was only significantly greater than activity along the diagonal (1-way ANOVA; $p < .05$, Tukeys HSD).

Latency and Rise Time of Subthreshold Inputs

Subthreshold latencies following peripheral stimulation varied with cortical depth as previously reported (Carvell and Simons, 1988; Armstrong-James et al., 1992). The shortest latencies (<= 8 msec) arose from inputs to the granular and the middle of the infragranular depths (Fig. 5), the primary termination zones of VPm thalamocortical inputs (Keller, 1995; Koralek et al., 1988). Latency to onset was more rapid for primary than for non-primary vibrissa inputs (PV, 10.8 msec +/- .80 SEM, N = 14; 1-away, 15.0 +/- 1.2, N = 35: 2-away, 15.7 +/- 2.0, N = 16: $p < 0.05$: Fig. 5). The most rapid latency input was not, however, always or exclusively from the PV: In 10 neurons, the onset latency to the PV occurred within 1 msec of onset of input from a neighboring vibrissa, or after the onset of another input.

The rise time needed to reach one-half amplitude and the initial slope of the sensory response were measured across vibrissae. A significant correlation ($r^2 = .44$: $p < .05$: Fig. 6A) was observed between the latency to subthreshold PSP onset and the rise time, and no correlation ($r^2 = -.02$: $p > .10$: Fig. 6) was observed between response amplitude and rise time. However, the fastest rise times and slopes were evoked by vibrissae that evoked an action potential response (Fig. 6: Rise time of suprathreshold vibrissae inputs, 4.1 msec +/- 1.3 SEM, N = 8; subthreshold vibrissae inputs, 12.4 msec +/- 1.5, N = 61: $p < .01$: Slope of suprathreshold vibrissa inputs, 2.57 mV/msec +/- .58; subthreshold vibrissa inputs, .46 +/- .14 : $p < .01$). An example of the relation between rise time, slope and action potential activity is illustrated in Figure 6 (lower right corner, traces). The grey lines are traces from an action potential evoking vibrissa (C3, the PV) and the black lines are traces from a vibrissa that did not evoke action potentials when stimulated (C4). The responses to C3 and C4 have identical onset latencies (11 msec). Notice, however, that the response to C3 (grey) rises more rapidly (4 ms to 1/2 amplitude; 1.6 mV/msec slope) compared with the response to C4 (20 msec rise time to 1/2 amplitude; .24 mV/msec slope).

Figure 5 Latency to PSP onset A. Each set of circles connected by a single line represents one neuron, and each circle marks the latency to onset following deflection of one vibrissa. White circles show the latency to the PV, black circles show the latency to all other vibrissae. B. The average latency to PSP onset for the PV (10.8 msec +/- .80 SEM), vibrissa 1-away (15.0 +/- 1.2) and vibrissa 2-away (15.7 +/- 2.0). The latency to the PV was significantly faster than the latency to non-primary vibrissae (asterisk, p <.05).

Figure 5

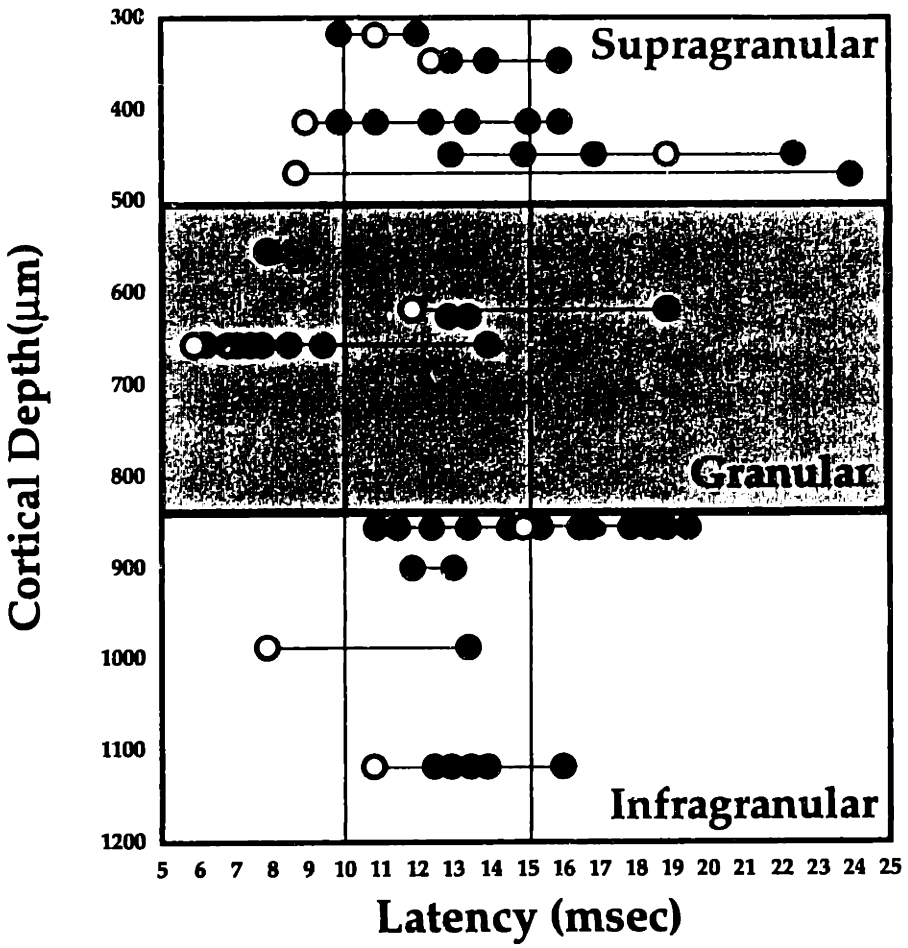
A.
Supragranular
Granular
Infragranular
Cortical Depth(μm)
300
400
500
600
700
800
900
1000
1100
1200
5 6 7 8 9 10 11 12 13 14 15 16 17 18 19 20 21 22 23 24 25
Latency (msec)

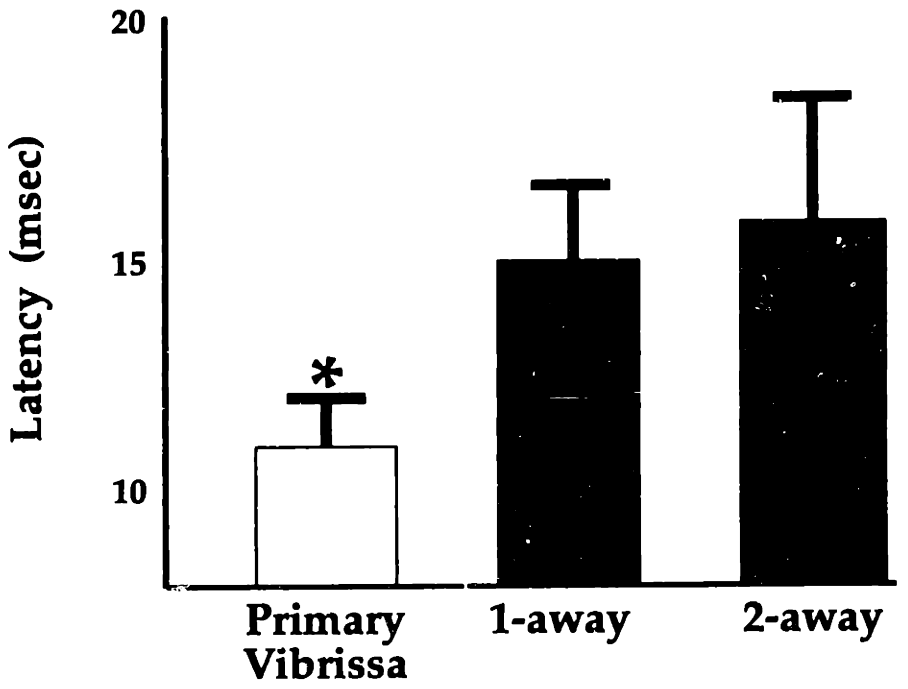
B.
Latency (msec)
20
15
10
*
Primary Vibrissa
1-away
2-away

Figure 6 The relation between rise time and latency in suprathreshold and subthreshold inputs A. Latency to onset and amplitude are plotted as a function of rise time to 1/2 maximal response. White circles represent inputs that evoked suprathreshold responses. There was a significant correlation between latency to onset and rise time (r^2 = .44), but no correlation between amplitude and rise time (r^2 = -.02). B. *Bar graph* Rise time to 1/2 maximal and slope are shown for suprathreshold and subthreshold evoked responses. Subthreshold inputs had significantly longer rise times and lower slopes (rise time to 1/2 maximal; suprathreshold, 4.1 msec +/- 1.3 msec SEM; subthreshold, 12.4 +/- 1.5 msec: Slope, suprathreshold, 2.57 +/- .58 mV/msec; subthreshold, .46 +/- .14 mV/msec: asterisk indicates $p < .01$). *Membrane traces* Evoked responses from two vibrissa (C3 and C4) with identical latency to onset (11 msec). The faster rising C3 response (gray traces, 4 ms rise time to 1/2 amplitude; 1.6 mV/msec slope) is able to evoke a suprathreshold response, while the C4 response (black traces, 20 msec rise time to 1/2 amplitude; .24 mV/msec slope) remains subthreshold.

Figure 6

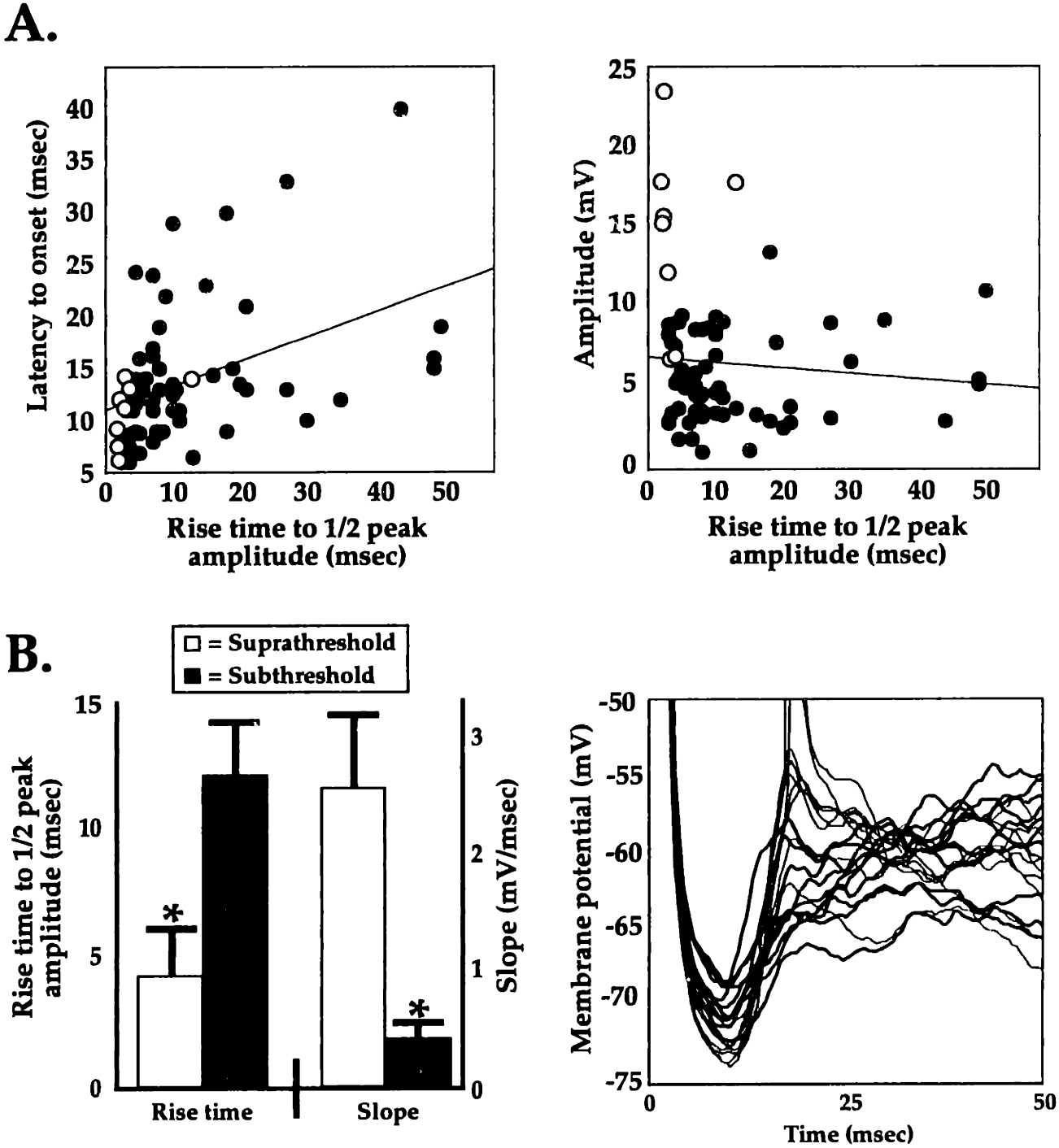
A.
Latency to onset (msec)
40
35
30
25
20
15
10
5
0
10
20
30
40
50
Rise time to 1/2 peak amplitude (msec)
Amplitude (mV)
25
20
15
10
5
0
0
10
20
30
40
50
Rise time to 1/2 peak amplitude (msec)
B.
□ = Suprathreshold
■ = Subthreshold
Rise time to 1/2 peak amplitude (msec)
15
10
5
0
*
*
3
2
1
0
Slope (mV/msec)
Rise time
Slope
Membrane potential (mV)
-50
-55
-60
-65
-70
-75
0
25
50
Time (msec)

Inhibitory and Excitatory Subthreshold Receptive Fields

To assess excitation and inhibition within the subthreshold receptive field, vibrissae were deflected while depolarizing and hyperpolarizing current was injected into the neuron (N = 5 neurons). In all five neurons, IPSPs (defined as evoked responses that reversed at a membrane potential of -45 mV or greater), were evoked in PV (N = 5/5 vibrissae) and non-primary vibrissa (N = 8/13) inputs. Figure 7 (upper two sets of evoked responses) displays responses in a supragranular neuron during stimulation of the D2 and D3 vibrissae. Following deflection of either vibrissa, an initial EPSP followed by an IPSP is revealed in the depolarized traces. In the case of the D3-input, the initial EPSP was sufficient to elicit an action potential (see top trace, Fig. 7A, D3 deflection). These recordings were used to reconstruct the membrane reversal potential at different latencies following vibrissa deflection. For D3, the projected reversal potential 1-3 msec following the onset of the PSP is -10 mV, close to that expected for a glutamatergic EPSP (black circles and black line, Fig. 7, lower right-hand graph). At 10-11 msec (grey circles) and 20-21 msec (white circles) following onset of the PSP, the reversal potential is -60 mV and -62 mV, respectively, indicating the dominance of an inhibitory, GABA-A mediated IPSP. This transition from excitation to inhibition is detailed in Fig. 7C, where the reversal potential is plotted for the D2 and D3 responses as a function of time. While both vibrissae evoked strong inhibition that began within 3 msec of the onset of excitation, the stronger initial response of the D3 vibrissa permitted a window within which action potential firing could occur before IPSPs reach peak amplitude, whereas the D2 input was unable to fire an action potential before the onset of inhibition.

To assess the evolution of excitation and inhibition within the receptive field, we measured the amplitude of evoked responses at or projected to an initial membrane potential of -30 mV, a membrane potential approximately half-way between the expected reversal potentials for excitatory (~0 mV) and inhibitory (~-60 mV) currents. At -30 mV, the driving force on excitatory and inhibitory conductances was assumed to be approximately equal. This method did not differentiate between mixed and isolated excitatory and inhibitory currents, but did provide an estimate of the relative magnitude of inhibitory and excitatory conductances evoked at various times following stimulation throughout the receptive field. Fig. 8 depicts these maps for a supragranular (top; same neuron as in Fig. 7) and an infragranular neuron (bottom). As both examples illustrate, the strongest inhibitory input was centered on the vibrissa that evoked the strongest excitatory input (i.e., those vibrissae capable of firing an action potential in the non-depolarized state). The inhibition had a delayed onset, but quickly overpowered any concurrent excitation, leading to a functional inversion of the center of the receptive field, with inhibition reaching full amplitude at 10-20 ms after the onset of the fastest excitatory response. Stimulation of surrounding vibrissae that previously evoked only subthreshold PSPs could, upon depolarization, evoke action potentials (e.g., the 10 mV upward light grey columns without a dot in the infragranular neuron map). Unlike responses to PV, responses to surrounding vibrissae did not always contain prominent inhibitory components. Prior investigations of barrel cortex circuitry (Agmon and Connors, 1992) and cat somatosensory cortex (Innocenti and Manzoni, 1972; Hellweg et al., 1977) have reported "pure" IPSPs in some neurons. We have not observed an IPSP evoked without an EPSP, but did observe one example of an IPSP arriving prior to an EPSP (vibrissa B4 in the infragranular

neuron; Hellweg et al., 1977). In addition to rapid EPSPs and IPSPs, some responses contained late excitatory components that were more variable in duration and amplitude, and that were more prominent at depolarized membrane potentials (Fig. 7, D2 and D3 depolarized traces). The appearance of IPSPs at only a subset of surround vibrissae and the occurrence of later or longer-duration EPSPs at other vibrissae led to a spatial asymmetry in the temporal progression of excitation and inhibition throughout the receptive field.

Figure 7 Mapping inhibitory and excitatory subthreshold receptive fields A. The D2 (left) or the D3 vibrissa (right) was deflected during depolarizing and hyperpolarizing current injection in a supragranular neuron. In response to deflection of either vibrissa, an EPSP followed by an IPSP was revealed in the more depolarized current traces. At 100 msec after the onset of stimulation, there was, for both vibrissa, a second late depolarizing potential presumably reflecting activation of NMDA receptors or active inward conductances in depolarized, but not hyperpolarized, traces. B. The hyperpolarizing or depolarizing amplitude of evoked responses is plotted as a function of membrane potential. Responses were measured 1-3 msec (black line, black circles), 10-11 msec (dark gray line, gray circles) and 20-21 msec (light gray line, white circles) following response onset. C. The PSP reversal potential for the D2 (grey circles) and D3 vibrissa (white circles) plotted at 1 and 2 msec intervals post-onset of response.

Figure 7

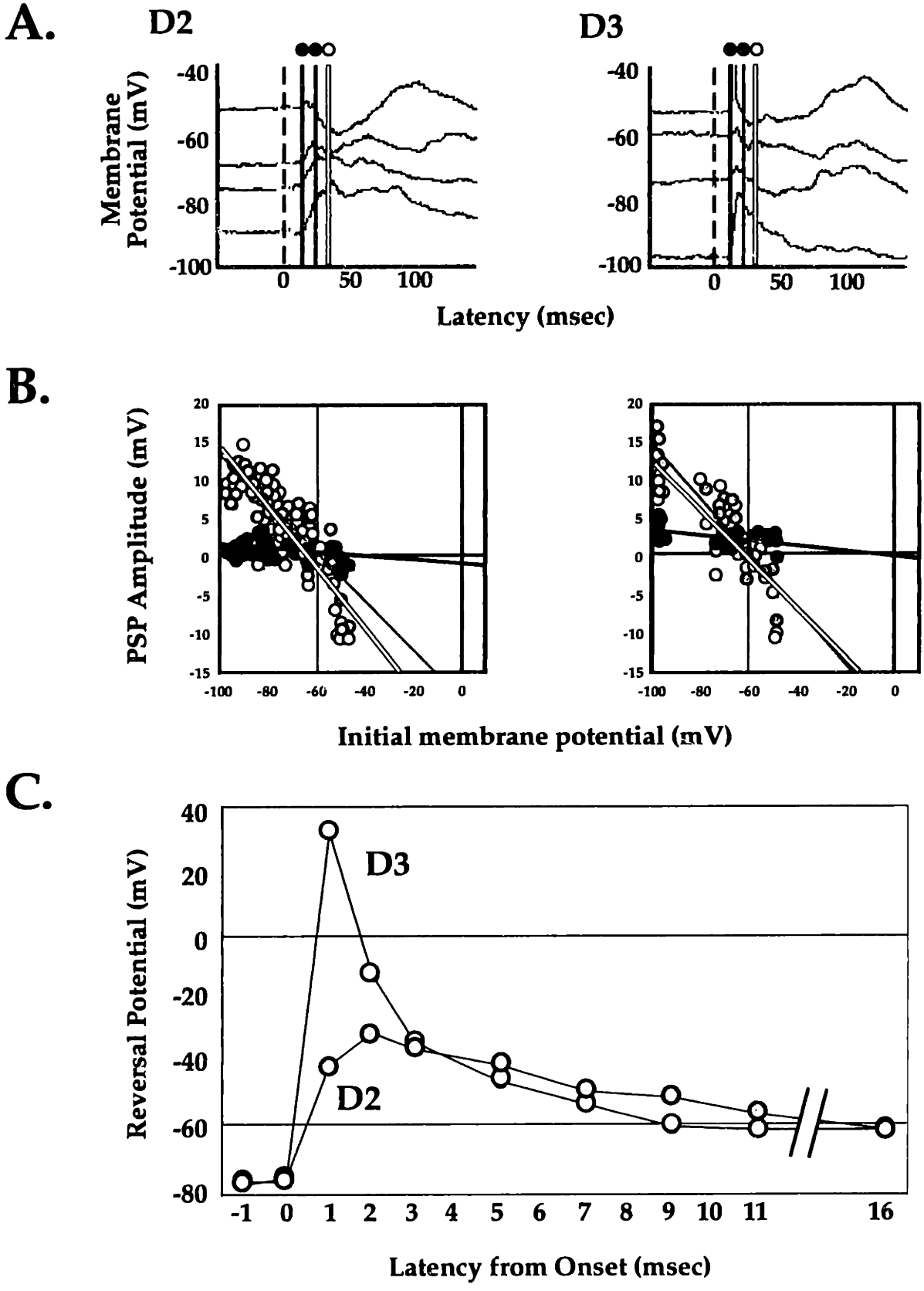
A.
D2
D3
Membrane Potential (mV)
-40
-60
-80
-100
0
50
100
Latency (msec)
B.
PSP Amplitude (mV)
20
15
10
5
0
-5
-10
-15
-100
-80
-60
-40
-20
0
Initial membrane potential (mV)
C.
Reversal Potential (mV)
40
20
0
-20
-40
-60
-80
D3
D2
-1
0
1
2
3
4
5
6
7
8
9
10
11
16
Latency from Onset (msec)

Figure 8 The temporal progression of excitation and inhibition in the receptive fields of a supragranular and an infragranular neuron Excitatory (upward, light grey) and inhibitory (downward, dark grey) events were plotted at 1-3 msec, 10-11 msec and 20-21 msec after the onset of the initial PSP. Responses display the amplitude (mV) of the response projected to a -30 mV resting membrane potential. Any response greater or less than the 20 mV range depicted is plotted as a maximal (10 mV or -10 mV) event. The black dots indicate a vibrissa that evoked suprathreshold responses from the resting membrane potential. The C4, B3, and C2 vibrissae in the infragranular neuron evoked an action potential when depolarized, and are displayed as a 10 mV increase.

Figure 8

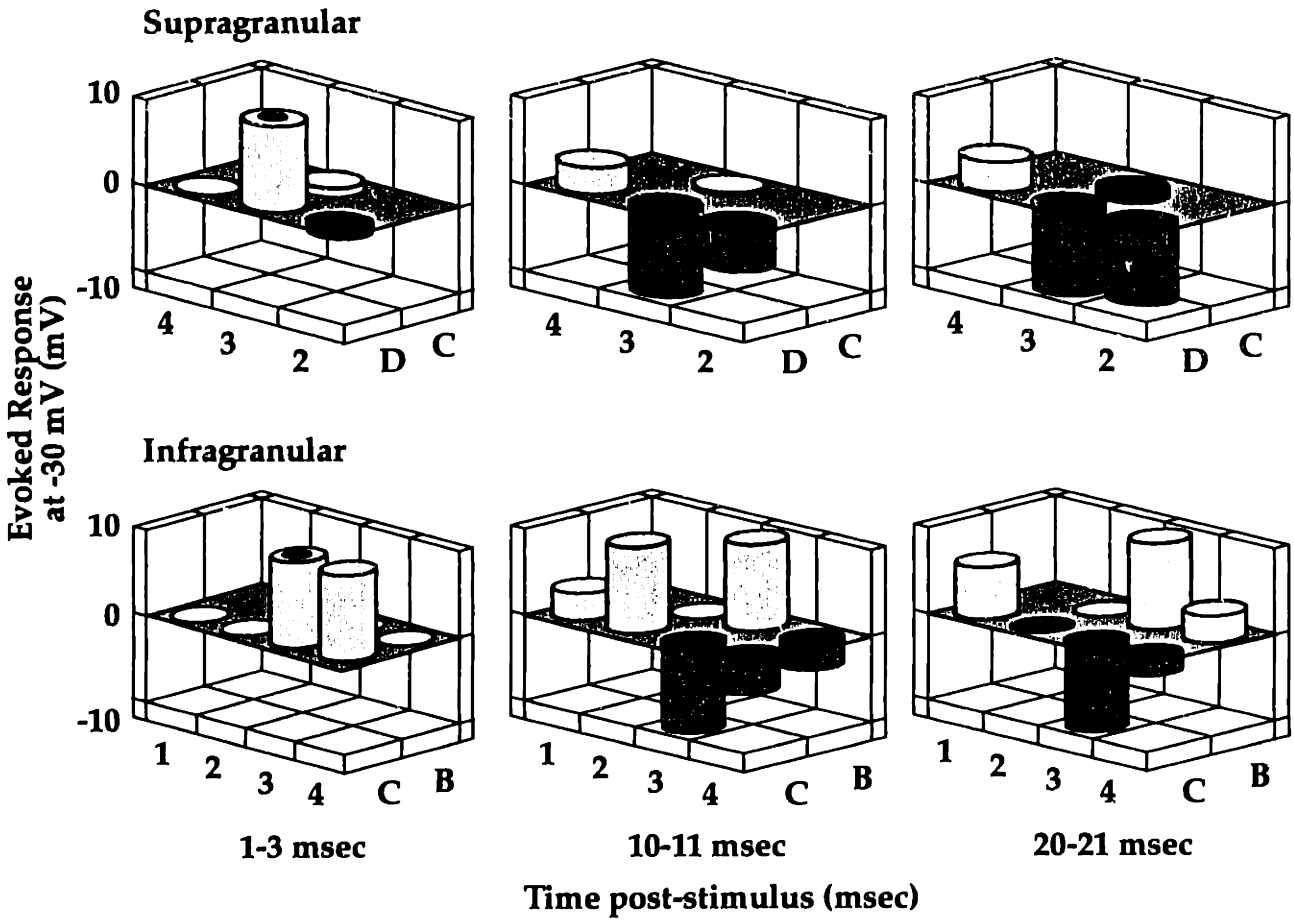
Supragranular
Infragranular
Evoked Response at -30 mV (mV)
10
0
-10
4
3
2
D
C
1
2
3
4
C
B
1-3 msec
10-11 msec
20-21 msec
Time post-stimulus (msec)

Discussion

Organization of Subthreshold Receptive Fields.

Subthreshold inputs to rat SI neurons could be evoked from a large number and a wide spatial extent of vibrissae. Stimulation of vibrissa 1- and 2-away from the PV consistently evoked prominent synaptic responses. Further, subthreshold receptive fields spanning 3 vibrissa from the PV were observed at supragranular, granular and infragranular layers depths. In the context of the vibrissa map, our data predict that the population of neurons within the cortical column corresponding to the C3 vibrissa integrate information from the A5 to the E1 vibrissae, and from at least 25 vibrissae within the vibrissa pad. From the perspective of divergence of information entering the cortex, subthreshold input from a single vibrissa spreads over at least 5 rows and arcs of cortical vibrissa columns.

The extensive subthreshold receptive fields we observed are in agreement with recent intracellular recordings in the rat SI forepaw representation (Li and Waters, 1996: see also Istvan and Zarzecki, 1994 for similar receptive fields recorded in raccoon SI) that demonstrate multi-digit subthreshold receptive fields, and in the rat vibrissa representation (Zhu and Connors, 1994, and personal communication). In both studies, animals were anesthetized with sodium pentobarbital, suggesting that large subthreshold receptive fields are not unique to urethane anesthesia. Further, the stimulus parameters we employed were identical in amplitude to those previously employed in suprathreshold studies of the vibrissa representation (Simons, 1985), suggesting that the divergence of information we observed was not the result of artifactual stimulation of neighboring vibrissae.

The predominance of purely subthreshold receptive fields within our sample may result from several factors. Although all neurons recorded from fired action potentials readily following current injection, our intracellular recordings may have damaged the spike initiation machinery of the neuron, thereby limiting output to only the most robust responses. Our findings may also result from the depth of anesthesia we employed, as our animals were maintained at a level just sub-responsive to reflexive withdrawal, whereas previous suprathreshold studies under urethane anesthesia were performed at levels of slow withdrawal (Armstrong-James et al., 1992; Armstrong-James and Callahan, 1991; Simons et al., 1992; see also Armstrong-James and George, 1988 and Chapin and Lin, 1984). Third, the stimulus we employed, while able to evoke suprathreshold responses in rate of rise and amplitude of deflection (Armstrong-James and Fox, 1987; Simons, 1985), was administered in a single direction, potentially leading to an undersampling of the optimal direction for suprathreshold activity (Simons, 1985). A fourth possibility is that we recorded from neurons usually undetected in extracellular recording studies. The recording bias introduced by our whole-cell recordings is towards neurons in which a satisfactory seal and intracellular recording could be achieved, not neurons that demonstrated spontaneous action potential firing or suprathreshold receptive fields. The subthreshold receptive fields we observed may, therefore, exist without recognition in studies of suprathreshold receptive fields. Using extracellular injection of glutamate and bicuculline to reveal non-spontaneously active neurons, Dykes and Larmour (1988) reported that the majority of neurons recorded in SI of the urethane anesthetized rat did not demonstrate suprathreshold receptive fields. In contrast, in the presence of bicuculline methiodide, over half of the non-responsive neurons revealed suprathreshold

output. Our findings are in good agreement with this report, and with other reports of purely subthreshold receptive fields in somatosensory neurons (Innocenti and Manzoni, 1972; Swadlow, 1992; see also Agmon and Connors, 1992, for a similar suggestion from the thalamocortical slice preparation).

The amplitude and temporal characteristics of subthreshold responses varied as a function of position within the receptive field. By definition, non-primary vibrissae evoked smaller amplitude depolarizations from rest than the central, PV, and the amplitude of evoked inputs decreased with distance from the PV. Non-primary inputs also evoked, on average, subthreshold responses with increasing latency to onset with increased distance from the PV. The rise time of evoked subthreshold responses was not closely correlated with the primary versus non-primary vibrissa distinction. However, rapid rise times (<= 4 msec) were found to be well-correlated with the presence of suprathreshold evoked activity, which occurred in the PV and in the vibrissa adjacent to it within the receptive field.

Sensory-evoked inhibition also varied as a function of the spatial position of sensory input and the time poststimulus. In our limited sample (N = 5), and in previous investigations of rat SI vibrissa-evoked responses (intracellular: Carvell and Simons, 1988; extracellular: Simons, 1985; see also Istvan and Zarzecki, 1994 for similar findings in raccoon SI, and Innocenti and Manzoni, 1972 and Hellweg et al 1977 in cat SI), inhibition developed over the first 10 msec after the arrival of excitation within the cortex. Rapid cortical inhibition arises from the disynaptic (or polysynaptic) activation of intracortical interneurons following the arrival of excitatory input to the cortex, and our latencies to the onset of inhibition are in agreement with this pattern of connectivity (Agmon and Connors, 1992; Istvan and Zarzecki, 1994; Simons, 1995). As in previous reports (Carvell and Simons, 1988), we observed that the strongest inhibition was centered on the input that also evoked the strongest excitation, and that less robust inhibition was also evoked by a subset of non-primary vibrissae. In our sample, non-primary vibrissa evoked inhibition that was asymmetrically organized in neurons from all three cortical depths, with a bias towards spread within a row (e.g., Fig. 8).

Implications for the Spatio-temporal Organization of Suprathreshold Receptive Fields

The spatial organization of the amplitude, onset latency, rise time and slope, and the balance of excitatory/inhibitory inputs over time, suggest the following model for the spatio-temporal evolution of suprathreshold evoked responses. Deflection of the PV (or one of the adjacent vibrissa providing strong input) causes a large amplitude, short latency response, while deflection of a more peripheral vibrissa evokes a smaller amplitude response, that arrives either at the same latency as the primary input or later, and that has a slower rise time to peak amplitude. Because FSs are likely to have lower thresholds for activation following afferent sensory and electrical stimulation (Simons and Carvell, 1989; Agmon and Connors, 1992), both stronger and weaker excitatory inputs are likely to trigger disynaptic inhibition. The fastest-rising, large amplitude inputs are able to fire an action potential prior to the peak of inhibition, while the slower rise time and longer latency of the smaller inputs make them more susceptible to cortical inhibition. There is, then, a dynamic reorganization of the receptive field over time. An initial strong, focal excitatory input is followed by weaker more diffuse excitation and by inhibition, which is strongest at the PV and spreads asymmetrically throughout the

receptive field. The fact that more peripheral inputs are more susceptible to inhibition may explain the finding that administration of bicuculline methiodide, a GABA-A blocker, causes expansion of the receptive field and differential amplification of suprathreshold inputs that are initially less robust (Kyrazi et al., 1996; see also Dykes et al., 1984).

Extracellular mapping studies have repeatedly found that weaker, more peripheral responses occur later, but have disagreed as to whether this reflects underlying inputs that have a longer latency to onset, or inputs that have similar latencies, but rise more slowly (Armstrong-James and Fox, 1987; Armstrong-James et al., 1992; Simons et al., 1992). Our results suggest that both factors are likely to play a role. Non-primary vibrissa inputs do have longer average latencies (by approximately 5 msec; see for example D4 vs. B1 in Fig. 3), but even inputs that have the same latency can have dramatically different initial rates of rise (e.g., B1 vs. D1 in Fig. 3, and C3 vs. C4 in Fig. 6). Differences in this initial slope are likely to be due to differences in both amplitude and kinetics (i.e., rise time) of the underlying EPSP. Differences in EPSP kinetics could occur through multiple mechanisms, including activation of monosynaptic inputs, or differences in electrotonic location. In our recordings, more peripheral inputs that did not rise rapidly enough to escape concurrent inhibition remained subthreshold unless the neuron was artificially depolarized. Presumably, under other recording conditions (e.g.,) these inputs may be expressed as long latency suprathreshold responses.

Implications for Multi-Vibrissa Interactions

Rat vibrissae are seldom deflected in isolation in the natural environment: An object is usually contacted by several whisks of multiple vibrissae (Carvell and Simons, 1990; Nicolelis et al., 1995; Simons, 1995). Our data demonstrate that rat SI cortical neurons possess the large subthreshold receptive fields necessary to integrate input rapidly from a spatially extensive peripheral area. Further, the dynamic shift in the organization of the subthreshold receptive field, with the later arrival and peak of more peripheral inputs and of inhibition, positions these neurons to amplify stronger excitatory inputs differentially. Simons and colleagues (Simons, 1985; Brumberg et al., 1996), have shown this type of context-dependent modulation by demonstrating that preceding stimulation of the same or a neighboring vibrissa typically inhibits the output of suprathreshold receptive fields, with peak inhibition occurring 10 to 20 msec after vibrissa input. In concordance with these findings, and with theoretical modeling of thalamocortical circuitry (Kyrazi and Simons, 1993; Pinto et al., 1996), the observations presented here suggest that during simultaneous or nearly simultaneous contact of multiple vibrissae, the spatio-temporal organization of the subthreshold receptive fields serves to dampen weaker responses selectively.

The asymmetry we observed in the organization of excitation and inhibition within the receptive field is in agreement with previous extracellular (Armstrong-James et al., 1992; Chapin, 1986; Lee et al., 1994; Simons, 1985) and intracellular reports on rat SI (Carvell and Simons, 1988). The asymmetry in the spread of subthreshold input within a row may provide the substrate for the construction of asymmetric suprathreshold receptive fields, because the firing threshold is likely to sharpen subtle differences between surround inputs significantly.

The asymmetric spread of inhibition we observed (e.g., Fig. 8) may provide the substrate for asymmetric inhibitory multivibrissa interactions (Simons, 1985).

Receptive fields in which the latency and duration of excitatory and/or inhibitory influences vary systematically with spatial location have been shown in the visual system to be an important mechanism for generating selectivity for the direction and speed of a moving stimulus (Reid et al., 1991; Jagadeesh et al., 1993). Similarly, the spatio-temporal asymmetry observed here may play a role in generating suprathreshold receptive fields tuned for the direction of motion across several vibrissae (Simons, 1995) and, hence, may represent a general feature of sensory cortical organization.

Implications for Receptive Field Plasticity

The subthreshold receptive fields we observed are consistent with many of the mechanisms that have been hypothesized to underlie the short- and longer-term reorganization of cortical receptive fields (Moore and Sur, 1997). First, the broad subthreshold spread of input to SI cortical neurons may define the region over which expansion via Hebbian mechanisms can occur. Temporal correlation of weak subthreshold inputs with stronger inputs can lead to the emergence a new suprathreshold response (Allard et al., 1991; Clark et al., 1988; Delacour et al., 1987; Diamond et al., 1992; Wang et al., 1995). The broader the subthreshold input to a neuron, the larger the region over which such correlations can be effective. Second, the selective temporal alignment of the peak of inhibition with that of smaller, more slowly rising excitatory inputs, suggests that relatively subtle changes in the strength of inhibition should lead to the emergence of long-latency suprathreshold responses to stimulation of non-primary inputs. Stimulation of vibrissa that previously evoked little or no suprathreshold response elicit longer latency suprathreshold responses following prolonged alterations in the pattern of input from the vibrissae (Armstrong-James et al., 1994; Diamond et al., 1992, 1994). Alternatively, increased temporal synchrony of presynaptic inputs to a cortical neuron (leading to a sharper rate of rise) would allow emergence of new suprathreshold responses without requiring changes in the relative strength of inhibition (Pinto et al., 1996; see also Zarzecki et al., 1993, who report changes in the rise time of evoked responses in a deafferented region of the cortical map).

Our results, taken together with those of prior studies, suggest that even minor alterations in the intrinsic excitability of cortical neurons, or in the balance of excitation and inhibition, are likely to alter the size of the suprathreshold receptive field substantially. Presumably, changes in receptive field size with anesthetic (Armstrong-James and George, 1988; Chapin and Lin, 1984) or following sensory manipulation (Armstrong-James et al., 1994; Diamond et al., 1992, 1994; Delacour et al., 1987; Faggin et al., 1997; Welker et al., 1989) may occur as the result of one of the mechanisms described above. The precise mechanisms by which receptive fields reorganize on short- and long-time scales are difficult to disambiguate with suprathreshold recording techniques, suggesting that a full mechanistic understanding of cortical reorganization will include information gathered using intracellular in vivo recording techniques.

CHAPTER 2

Dynamic and Long-term Reorganization of Vibrissa Representations in Rat SI

"...Light breaks on secret lots,
On tips of thought where thoughts smell in the rain;
When logics die,
The secret of the soil grows through the eye,
And blood jumps in the sun;..."

Dylan Thomas, *Light Breaks Where No Sun Shine*

As described in Chapter 1, rat SI cortical neurons have large subthreshold receptive fields that vary in their amplitude and temporal characteristics as a function of the position of peripheral input. This receptive field organization suggests that the spatial and temporal context of sensory stimulation is an important factor in the cortical processing of sensory input. These findings, along with other recent studies of rat SI cortex (Delacour et al., 1987; Faggin et al., 1997), challenge the conception of a static cortical map, that alters its organization only following extreme changes in the pattern of sensory input (e.g., amputation). To the contrary, these findings suggest that the ability to modify connections rapidly following relatively subtle changes in receptive field input are an important component of the mechanisms of sensory perception.

Context Dependent Modulation of Cortical Organization

Several recent studies have shown that cortical neurons are sensitive to the spatial perceptual context of sensory input (Toth et al., 1996; Zipser et al., 1996). In primate V1, Zipser et al. (1996) have reported modulation of suprathreshold responses dependent on the contrast of the pattern within and outside of the classical receptive field. Similarly, Toth et al. (1996) have demonstrated orientation specific spread of activation from a border region to patches of cortex within a masked topographic region. The subthreshold receptive fields characterized in Chapter 1 provide the substrate for this type of rapid influence. Subthreshold inputs from over 5 arcs and rows on the vibrissa pad impinge on a single cortical column, permitting spatially diffuse modulation of cortical firing. Further, the pattern of input from vibrissa throughout a receptive field is not unimodal, suggesting stimulus specific influences in single neurons (e.g., directional encoding of multiple vibrissa).

The recent temporal history of input to a neuron can also profoundly influence its response (Abbott et al., 1997; Brumberg et al., 1996; Simons, 1985; Turrigiano et al., 1998). Prior stimulation of a vibrissa can alter its evoked response (Brumberg et al., 1996; Simons, 1985). Further, over longer timescales, patterns of stimuli played into a neuron (or population of neurons) evoke greater trial-to-trial variability than between-pattern variability (Zador and Dobrunz, 1997), and the ongoing pattern of a constant train of stimulation can modulate the gain of the evoked response (Abbott et al., 1997) or the firing properties (Turrigiano et al., 1998) of the neuron.

One example of a sensory context that is established by the behaving animal is vibrissa whisking. When exploring an environment, rats move their vibrissae in an ellipsoid motion at a dominant frequency of ~8 Hz (Simons, 1995). An advantage of this behavior is to increase the number of contacts between a single vibrissa and the object and to increase the number of vibrissae contacting the object, thereby improving the resolution of the discrimination.

The prevalence of whisking, and the importance of context in the organization of cortical receptive fields, suggest that a second advantage of whisking may be to dynamically alter cortical organization to improve tactile perception. Simons and colleagues (Simons, 1995; Brumberg et al., 1996) have suggested that one of the functions of the barrel circuitry is to constrain the output of the barrel during multi-vibrissa stimulation by differential inhibition of smaller inputs (see also Chapter 1). Behavioral studies have shown that whisking at 8 Hz frequency improves discrimination of fine gratings (Carvell, unpublished observations as reported in

Simons, 1995), suggesting that a second, potentially important component of whisking may be the frequency of movement.

Longer-term Reorganization in Rat SI

Recent studies have also observed plasticity in the organization of the rat SI vibrissa representation following longer-term changes in the pattern of sensory input (Armstrong-James et al., 1994; Diamond et al., 1992a, 1994; Glazewski and Fox, 1996; Welker et al., 1989, 1992). Using a non-invasive sensory manipulation, Diamond and colleagues (1992a, 1994; Armstrong-James et al., 1994), demonstrated adult rat SI reorganization. In this paradigm, all vibrissae except two were cut on one side of the rat's face, and the animal returned to its home environment. After 64-66 hours, sensory evoked suprathreshold responses were recorded in a barrel corresponding to one of the uncut vibrissa. In response to deflection of the neighboring uncut vibrissa (termed, by them, the "paired" vibrissa), activity was significantly increased, and in response to the neighboring cut vibrissa, activity was non-significantly decreased. This result is provocative, because of the significant change that results from a non-invasive manipulation of sensory input. However, the limited cortical region assessed in these studies (the uncut vibrissa representation) leaves open a variety of hypotheses regarding the underlying mechanisms guiding this reorganization.

There are two broad classes of somatosensory plasticity studies that serve as precedents for the vibrissa trimming/pairing manipulation; temporal-pairing studies and deafferentation studies. In temporal-pairing studies, inputs from two or more spatial locations on the skin surface are temporally correlated, through either a physical attachment of the two inputs (e.g., artificial syndactyl, Allard et al., 1990; Clark et al., 1988) or through the simultaneous administration of external stimuli (Wang et al., 1995). In both cases, increased temporal correlation leads to a blurring of the representational borders between correlated inputs and a sharpening of the borders between decorrelated inputs. For example, in primate SI, Wang et al., (1995) observed that sensory input that is correlated across finger pads, but not along the finger length, induces a shared representation along the costimulated pads. In contrast, the decorrelated sets of pads along the finger length cease to overlap and form sharp representation borders. A "Hebbian" temporal correlation mechanism is believed to underlie these patterns of reorganization (Allard et al., 1990; Clark et al., 1988; Wang et al., 1995). Briefly stated, coactivation of pre- and postsynaptic activity, brought about by the synchrony of two peripheral inputs, leads to strengthening of the synaptic connections from those inputs. Conversely, decorrelation of two inputs should weaken or have no influence on the strength of the connection from the inputs to the cortical neuron.

The second class of potentially relevant studies are deafferentation studies. Studies from the monkey and rat somatosensory system suggests that loss of peripheral input, through anesthesia (Nicolelis et al., 1993; Faggin et al., 1997; Pettit and Schwark, 1993) or through injury/surgery (Merzenich et al., 1983; Jain et al., 1997; but see Jain et al., 1995) induces the takeover of deafferented representations by neighboring inputs. Several mechanisms, including subcortical reorganization, cortical disinhibition and sliding-threshold models of cortical potentiation (e.g., the Bienenstock, Cooper and Munro (BCM) model, Bear et al., 1987) can account for this type of reorganization.

With regard to the vibrissa trimming/pairing paradigm, temporal pairing and deafferentation studies make different predictions as to the spread of activity into the cut vibrisssa representation. Temporal pairing studies predict that vibrissa "pairing" is the relevant sensory manipulation, and that a shared representation between the two uncut vibrissa should emerge, concomitant with a decreased overlap between the decorrelated cut and uncut vibrissa. Conversely, deafferentation studies predict the opposite. These studies suggest that vibrissa "trimming" is the relevant manipulation, and that the uncut vibrissa should invade the perceptually deafferented cut vibrissa territory, leading to an increased overlap between the cut and uncut representation. To examine these predictions, the organization of the cortical map needs to be assessed across both cut and uncut barrels, not simply in the barrel corresponding to the uncut vibrissa.

Intrinsic Signal Optical Imaging

Recently, several techniques have been developed to record the activity across a large population of cortical neurons (Malonek and Grinvald, 1996; Kwong et al., 1992; Nicolelis et al., 1993; Wilson et al., 1993). Many of these techniques, including fMRI and intrinsic-signal optical imaging, measure hemodynamic changes that are associated with neural activation (Kety, 1997; Figure 1A). The intrinsic optical imaging hemodynamic signal, which is the best localized of the hemodynamic markers, is believed to result from the aerobic activity of cortical neurons. Specifically, when cortical neurons are active they consume oxygen at an increased rate, causing a relatively rapid (~300-500 msec latency) and local (50-100μm) increase in the concentration of deoxygenated hemoglobin (Hbr) (Figure 1A). While this increase in [Hbr] is followed by an increase in oxygenated hemoglobin (HbO_2) caused by oxygenated blood flow into an active cortical region (the hemodynamic underpinnings of fMRI, see Chapter 3 for a discussion), there is a 500-2000 msec window following the onset of sensory stimulation when the increase in [Hbr] is prominent (Malonek and Grinvald, 1996; Malonek et al., 1997; but see Fox and Raichle, 1986; Figure 1A). At a wavelength of 632.8 nm, the absorption of Hbr is several orders of magnitude greater than the absorption of HbO_2 (Figure 1B): Measuring changes in the absorption of light at this wavelength permits, therefore, the measurement of increases in the [Hbr] and, indirectly, the measurement of underlying neural activity. This signal has been used to image localized activity in orientation columns in visual cortex (e.g., Toth et al., 1996, 1997), and vibrissa columns in somatosensory cortex (Masino et al., 1993; Sheth et al., 1998).

We used optical imaging to examine changes in the cortical map during dynamic and long-term changes in the pattern of sensory input. In Experiment 1, we varied the rate of vibrissa stimulation from 1 to 10 Hz, and compared the divergence of activity through the cortex to assess the rapid alteration of cortical representations. In Experiment 2, we employed the trimming/pairing paradigm of Diamond and colleagues, and assessed long-term reorganization over several vibrissa columns simultaneously.

Figure 1 Hemodynamic response following neural stimulation and the absorption spectra for Hbr and HbO_2 Adapted from Malonek and Grinvald (1996). A. The concentration of deoxyhemoglobin [Hbr] demonstrates an initial increase in response to neural activation during sensory stimulation. This increase, which constitutes the mapping signal for intrinsic-signal optical imaging, results from the aerobic consumption of O_2. Following this peak, there is a large undershoot in the concentration of oxygenated hemoglobin in the region of neural activation. This undershoot is believed to result from the inflow of oxygenated blood, and is the blood-oxygen level dependent (BOLD) mapping signal of fMRI. The units of the y-axis are arbitrary. B. Both Hbr and HbO_2 show peak absorption at ~550 nm +/- 40 light. This green light was used in optical imaging experiments to obtain a vascular map on the surface of the cortex. At 632.8 nm +/- 10 light, Hbr demonstrates greater absorption of light than HbO_2, allowing observation of the initial Hbr concentration increase described in A at .5-2 sec poststimulus onset.

Figure 1

A.

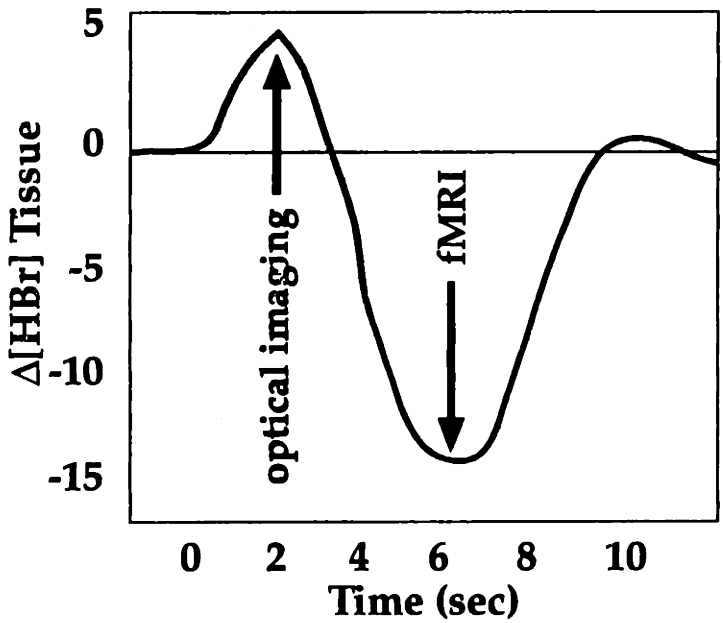
5
0
-5
-10
-15
Δ[HBr] Tissue
optical imaging
fMRI
0
2
4
6
8
10
Time (sec)

B.

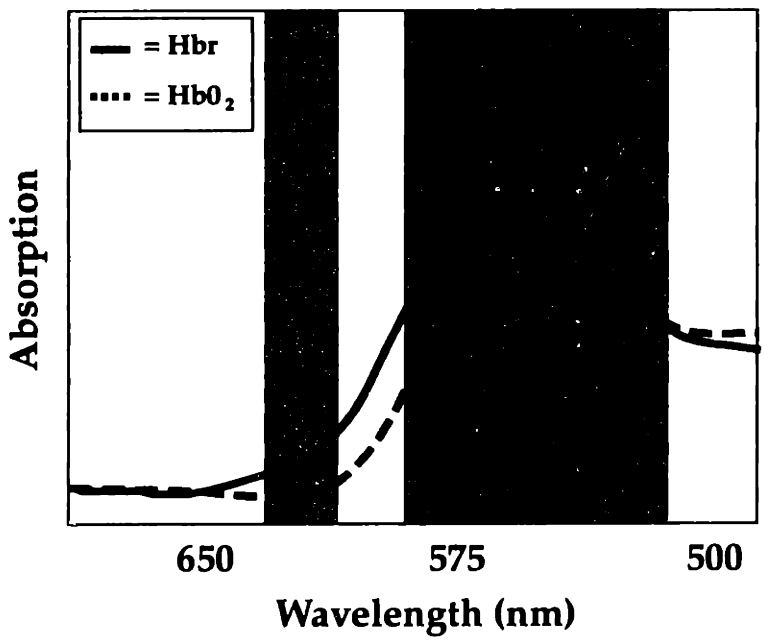
= Hbr
= Hb0 2
Absorption
650
575
500
Wavelength (nm)

Experiment 1: Dynamic Modulation of Representation Borders with Increasing Frequency of Vibrissa Stimulation

To investigate the effect of increasing frequency on the vibrissa representation in rat SI, we stimulated individual vibrissae at 1, 5 and 10 Hz while imaging the cortex with intrinsic signal optical imaging.

Methods

Methods are described here for the two Experiments reported in this chapter and for the Appendix. Specific differences in methods between Experiments are detailed in the appropriate section.

Surgical Methods

Animals were anesthetized and surgery performed as described in Chapter 1. The skull was thinned to form a translucent ~ 5 mm^2 window over the vibrissa representation (Masino et al., 1993). A dental cement or agar (3%) well was then built over the cortical window and filled with 50 cs oil. The stereotaxic frame was tilted to a ~25° angle to permit better camera alignment with the curvature of the cortex over rat SI.

Optical Imaging Recording Techniques

To image surface vasculature and functional changes in reflectance, a slow-scan video camera (Bischke CCD-5014N, RS-170, 30 Hz, 60 dB SN) was focused through a macroscope (back-to-back cameral lenses) onto the cortical surface. The camera imaged an area 4.25 mm x 3.5 mm. The macroscope provided a high numerical aperture and a shallow depth of field, permitting constrained focusing within the cortical depth. The cortex was illuminated with a bifurcated fiber optic light source filtered at one of two wavelengths (see below). Data was collected using the Imager 2001 imaging system (Optical Imaging). A reference image was taken during a period of no stimulation and analog subtracted from the acquired functional image before digitization.

Prior to functional imaging, an image of the surface vasculature of the cortex was taken using light filtered at 550 nm +/- 40. At this wavelength, signals from Hbr and $Hb0_2$ are robust, providing resolution of veins and arteries (Figure 1B, green band). The camera was then focused in a plane 450 µm deep in the cortex, to approximately the level of deep supragranular cortex (Diamond et al., 1994; A. Basu and C. Moore, unpublished observation). Light filtered at 632.8 nm +/- 10 was then applied. This wavelength allows selective detection of changes in the concentration of Hbr (Figure 1B, orange band). Data acquisition began with the onset of vibrissa deflection, and were acquired in 500 msec epochs for a total of 4.5 sec (9 epochs). A 4.5 sec no-stimulation condition was randomly interleaved with each stimulation condition, with a minimum of a 10 sec latency between conditions. Each optical image represents the average of 30 stimulation conditions, acquired over a ~20 min period.

Sensory Stimulation

The parameters of sensory stimulation were identical to those described in Chapter 1 with the following exceptions. The RC filter was not employed on the

piezoelectric stimulator, the ramp and hold stimulus was maintained for 50 msec, and stimuli were applied at a rate of 5 Hz for 2 sec (Masino et al., 1993).

In Experiment 1, using the standard 5 Hz stimulation paradigm, vibrissae showing activation in the exposed region of cortex were tested at deflection rates of 1, 5 and 10 Hz. Averages of 30 trials were obtained at these frequencies under two different stimulus paradigms. In the first, blocks consisting of 10 trials at each frequency were pseudorandomly interleaved for a given vibrissa, in order to avoid any consistent effect of cortical adaptation. Three blocks were run for each frequency. The signal was analyzed as described above. In the second paradigm, a constant number of stimuli (5) was presented at each frequency. Because the duration of stimulation was different for the three frequencies (4 sec, 800 msec, 400 msec), it was not possible to compare the signal over the same time frames. Hence, we summed and averaged the signal over all time frames for the duration of the stimulation and for .5-1 sec following its offset (frames 1-9 for 1 Hz; frames 1-4 for 5 Hz and frames 1-3 for 10 Hz).

Data Analysis

To obtain functional signal, frames 2, 3 and 4 of the no stimulation condition were divided into the analogous frames of the stimulation condition. This method, produced well-defined peaks of optical signal (Masino et al., 1993; Moore et al., 1995; e.g., Figure 3). Resulting maps were analyzed using a program that isolated the peak 280 μm^2 region of highest signal intensity. Two types of signal averaging were then conducted. Six concentric annular rings were centered on the location of peak activation, and the signal averaged for pixels in each ring (center circle of ~133 μm, surrounding rings of outer radii 267 μm, 360 μm, 720 μm, 1080 μm and 1440 μm) (Figure 2). This approach allowed us to view the fall off in optical signal as a function of distance within the cortical map. In Experiments 1 and 3, an "optical receptive field" was constructed by summing the signal at the location of the peak response (over the putative barrel) and at the location of peak responses evoked by other vibrissae mapped during the experiment. This allowed us to measure the input to a single cortical location during stimulation of vibrissa 1-away and 2-away from the vibrissa that evoked the peak response (Figure 2).

For statistical analyses in Experiment 1, two concentric, non-overlapping averaging masks were placed over the activity center (the center was a circle of 133 μm radius; the outer ring circumscribing the center circle had a 133 μm inner radius and a 506 μm outer radius) and the activity averaged over all the pixels falling in each ring was calculated (both rings had the same number of pixels). The average activity in the outer ring thus obtained was then subtracted from the average activity in the center circle. These differences (or slopes of the relative changes in reflectance) obtained for all the stimulated vibrissae were then compared vibrissa-by-vibrissa for all three frequencies. The differences in slope between the three frequencies (1 Hz - 5 Hz, 5 Hz - 10 Hz, 1 Hz - 10 Hz) were then used to evaluate frequency-dependent fall-off in activity from the putative barrel center (one-tailed, paired student's t-test). In an expanded companion analysis, the six concentric annular rings described above were used, and their respective activity averages were calculated and compared. In a similar fashion, fall-off in activity between the center circle and the innermost annular ring (outer radius 267 μm) was obtained, and the two groups of data (1 Hz vs. 5 Hz, 1 Hz vs. 10 Hz) were compared. For both Experiments, data were analyzed with a 1-way ANOVA, a Tukey HSD post-hoc test or with a t-test.

Histology

Rats (N = 3) were euthanized with an overdose of anesthetic and perfused intracardially with saline and 4% paraformaldehyde. Tangential sections (60 μm) were cut through PMBS in a plane approximately parallel to the plane of optical imaging. Sections were stained for cytochrome oxidase to visualize barrels. In one case, camera lucida reconstruction of the barrels was aligned with an electrolytic lesion made in the center of an optical representation.

Electrophysiological Techniques

To examine the correlation between the optical signal and electrophysiological activity, we recorded somatosensory-evoked local field-potential responses with a pair of electrodes (Uwe Thomas Recording, Marburg, Germany) in cortex that was imaged immediately prior to electrophysiological recording. Glass insulated platinum-iridium electrodes (3-5 MΩ impedance at 1 kHz) were used in these recordings. The electrical signal was amplified, sampled at 10 kHz, digitized by an A/D board (Data Translation), and recorded and stored on a computer (Data Wave Technologies).

Figure 2 Two methods of optical intrinsic signal averaging Following identification of the peak evoked response to vibrissa deflection, one of two methods was used to measure the fall-off in optical signal. A. *Top.* A series of concentric rings (see text for details) was centered on the peak of the optical spot and activity under each was averaged. *Bottom.* Fall-off in signal as a function of distance from the center of the vibrissa representation. B. Activity under the peak (133 μm radius mask) of the evoked optical signal, and activity in the center of vibrissa representations 1-vibrissa and 2-vibrissa away was measured.

Results

Intrinsic signal optical imaging routinely produced functional maps that followed the somatotopic order predicted by the anatomical organization of the barrel cortex. As demonstrated in the example in Figure 3, the peak of optical activity shifted systematically as a function of the vibrissa stimulated. There was a significant correlation ($r = .88$, $p < .05$) between the distance between the peak activation of optical signals and the distance between barrel centers (A. Basu, C. Moore and M. Sur, unpublished observations; Masino et al., 1993). Further, the location of the peak of the optical signal following vibrissa stimulation was shown to be aligned with the corresponding SI barrel (Figure 4).

To examine the effect of stimulus frequency on representation borders, we first kept the time of stimulation constant (2 sec) and studied the spatial spread of activation at vibrissa stimulation frequencies of 1 Hz, 5 Hz and 10 Hz. We observed a more diffuse spatial spread of activity under the 1 Hz stimulus condition compared to the 5 Hz and 10 Hz stimulation conditions (Figure 5). There was a sharper fall-off in activation away from the activity center for the 5 Hz and 10 Hz stimulus than for the 1 Hz stimulus (133 μm vs. 506 μm radius, $p < 0.025$: Statistically significant differences, $p < 0.002$, in the fall-off in activation from the optical activity center were also found between 1 Hz and 5 Hz, and between 1 Hz and 10 Hz at a radius of 200 μm). These findings indicate that cortical activation was more discrete at 5 Hz stimulation than at 1 Hz stimulation. No statistical difference ($p > 0.05$) was found between activity spread for 5 Hz and 10 Hz stimuli.

Figure 3 Somatotopy revealed with intrinsic signal optical imaging Intrinsic signal activation maps of stimulation of the C1, C2 or C3 vibrissa at 5 Hz for 2 sec. Note the progression of somatotopic order in the peak signal, and the overlap in divergence of signal.

Figure 3

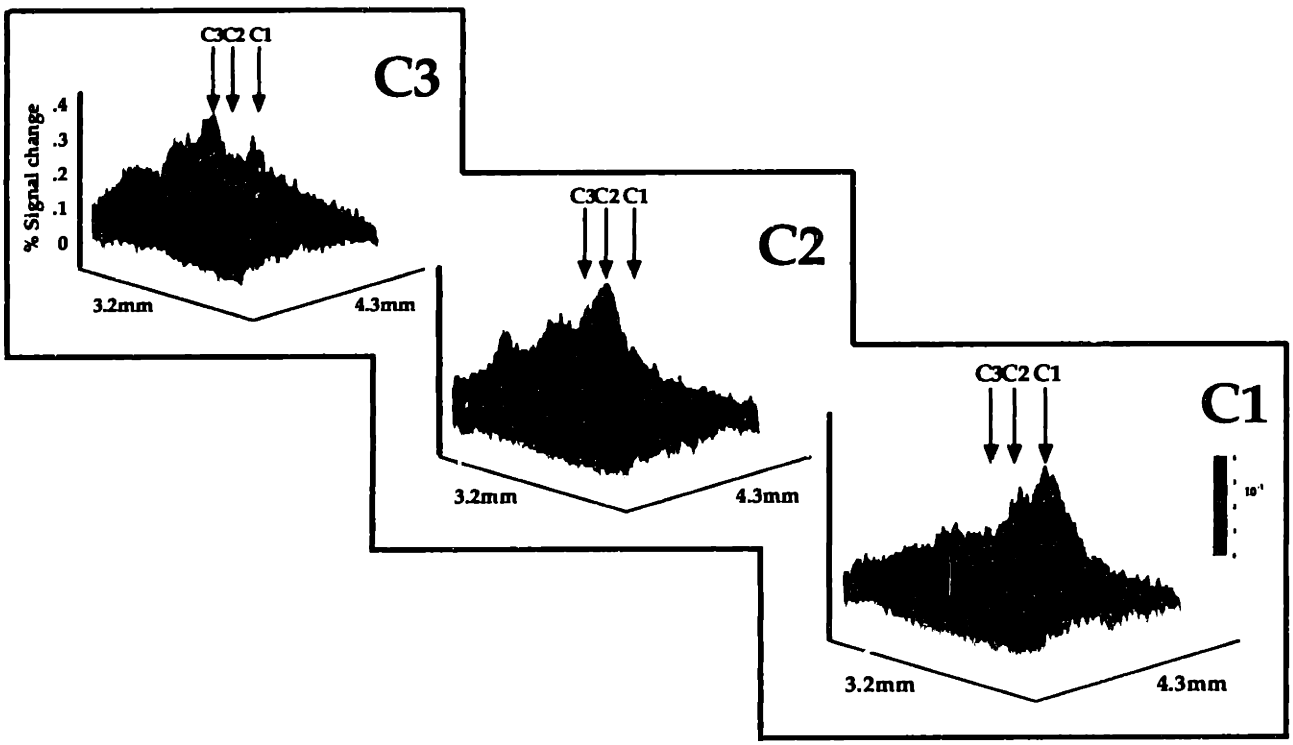
C3C2 C1
C3
% Signal change
.4
.3
.2
.1
0
3.2mm
4.3mm
C3C2 C1
C2
3.2mm
4.3mm
C3C2 C1
C1
3.2mm
4.3mm

Figure 4 Correlation between rat barrel cortex anatomy and optical signal *Lefthand graph* Correlation of the distance between cortical barrels and the peaks of the corresponding optical evoked representations in one rat. *Righthand grey box* A 2D plot of optical signal (lighter coloration corresponds to increased signal) following deflection of the C2 vibrissa. A lesion made in the center of the C2 optical representation was later localized to the corresponding barrel located using cytochrome oxidase histology.

Figure 4

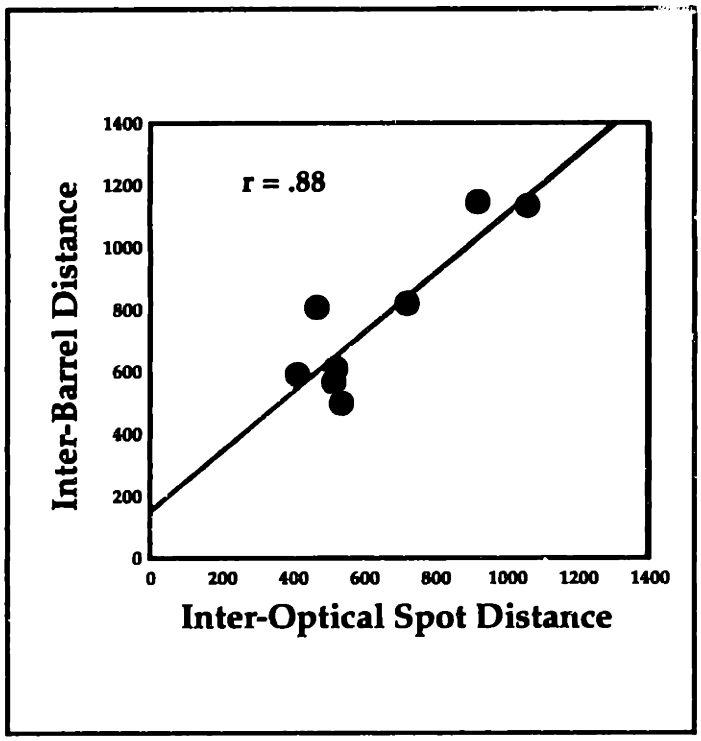
r = .88
Inter-Barrel Distance
Inter-Optical Spot Distance
0
200
400
600
800
1000
1200
1400

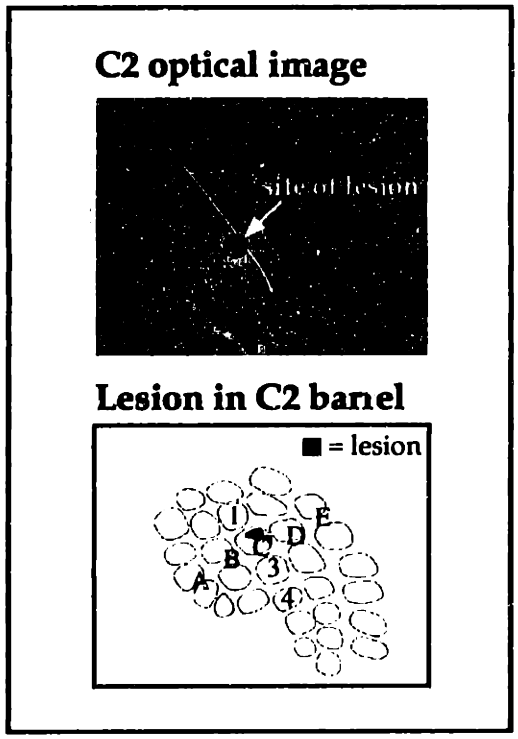
C2 optical image
site of lesion
Lesion in C2 barrel
= lesion
1
E
D
C
B
3
A
4

We obtained similar results when the number of deflections was fixed at five for the three frequencies, while the time of stimulation was varied. For 15 of 16 vibrissae (5 animals), the spread of activity for the 5 Hz stimulus was less than (N = 7) or equal to (N = 8) that for the 1 Hz stimulus. For the population, 1 Hz activation was more discrete than the 5 Hz or the 10 Hz stimulus ($p < 0.05$). In contrast, the signal strength at the optical activity centers for all three frequencies was indistinguishable (activity values in arbitrary units of signal strength: 1 Hz, 1.122 +/- 0.013 SEM; 5 Hz, 1.120 +/- 0.005; 10 Hz, 1.112 +/- 0.007: $p = 0.69$). Thus, although higher frequencies lead to attenuation in the strength of optical signal in the surround, they do not affect the strength of signal in the center of a vibrissa representation.

Because the optical signal represents the activity of populations of neurons, we examined the effect of stimulus frequency on spread of cortical activation by combining optical imaging with electrical recording of local field potentials at two, spatially separated electrodes. Following the imaging session, one electrode was placed in the center of the optical spot generated by stimulation of a vibrissa (C1, marked "center" in Figure 6), and a second electrode was placed at a lateral distance of approximately 700 μm (marked "periphery" in Figure 6). The electrodes were lowered to a depth of 300-600 μm, corresponding to the depth at which the intrinsic signal was measured (450 μm). Figure 6 shows somatosensory-evoked responses to the first and second vibrissa deflections, carried out at 1 Hz and 5 Hz, at each of the two electrodes. Responses were larger in the electrode located at the center of the optical spot, similar to the optically imaged intrinsic signal. After stimulation at 1 Hz, the second deflection evoked a consistent response in both the center and the periphery electrode. In contrast, for 5 Hz stimulation, the response at the periphery electrode following the second deflection of the C1 vibrissa (Figure 6, bottom right) was virtually absent, while a small but clear response was present at the center electrode (Figure 6, bottom left). This differential loss of response in the periphery electrode at 5 Hz replicated the frequency dependent decrease in optical signal in the periphery at higher frequencies.

Figure 5 Rate of fall-off in optical signal at three frequencies during 1, 5 and 10 Hz stimulation Fall-off in optical signal was significantly steeper at 5 and 10 Hz than at 1 Hz (N = 10 vibrissa). Signal in peripheral rings was subtracted from the amplitude of under the central mask.

Figure 5

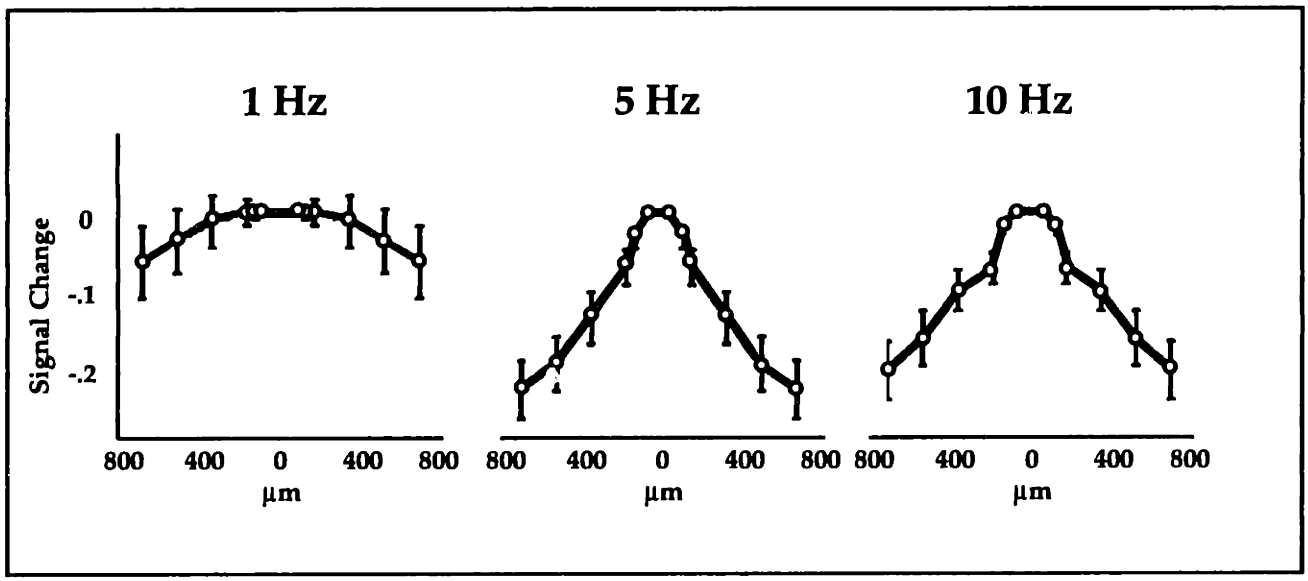

Figure 6 Electrical recordings demonstrate the effect of frequency of vibrissa stimulation on spread of cortical activity. A. Using standard stimulation conditions (5 Hz, 2 sec), an optical map of cortex responding to the C1 vibrissa was obtained. Two electrodes were placed at a depth of 300-600 μm below the cortical surface, one at the activity center of the imaged area (center) and the second ~700 μm away (periphery). The electrode locations are marked by dots. B. Responses recorded in the activity center and the periphery to 1 Hz and 5 Hz C1 vibrissa stimulation. The responses to the initial and second vibrissa deflections are shown in dotted and solid lines respectively. Stimulus onset is marked by an arrow.

Figure 6

A.


1 mm

B.

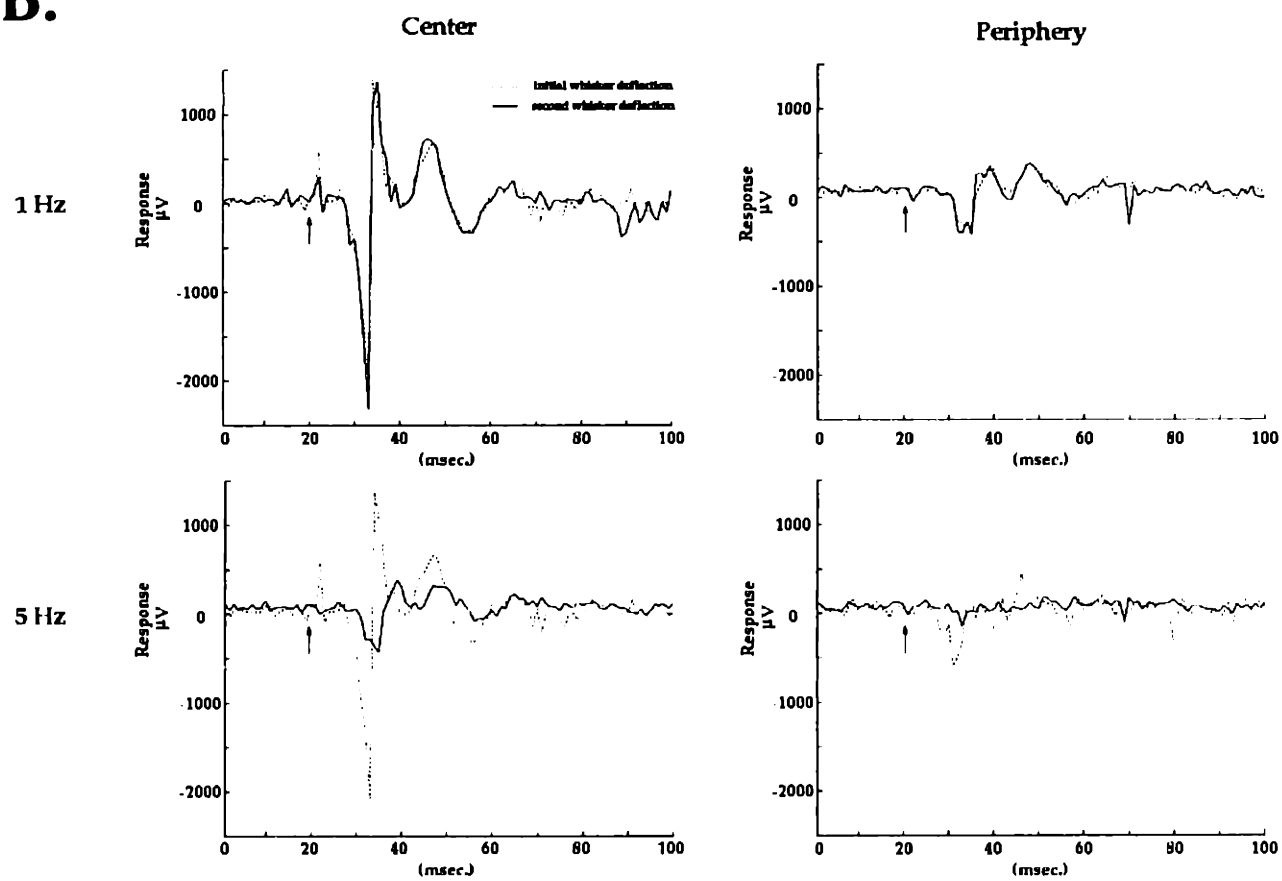
Center
Periphery
1 Hz
5 Hz
Response μV
(msec.)
1000
0
-1000
-2000
0
20
40
60
80
100

Discussion

We found that increased frequency of stimulation of a single vibrissa evoked decreased divergence of activity in the cortex at approximately the level of upper layer IV or lower layer III (450 μm deep to the surface of the cortex). Using optical imaging, we have replicated this finding with a fixed amount of time of stimulation and a fixed number of vibrissa stimulations. This finding was confirmed with extracellular evoked potential recordings.

The choice of anesthetic in the present study is unlikely to account for these results. In contrast to the awake condition, urethane-anesthetized animals have a large late component in their stimulus-evoked neuronal responses in cortex (Simons et al., 1992). However, no significant differential effects of urethane anesthesia have been found on neuronal responses in the barrels versus the inter-barrel areas of rat SI (Simons et al., 1992). To our knowledge, the susceptibility of the ventral posterior medial nucleus of the thalamus (VPm) or the posterior medial nucleus of the thalamus (POm), the two primary thalamic inputs to rat SI, to urethane anesthesia has not been investigated.

Possible Mechanisms Underlying the Decreased Spread of Input

In general, weaker non-primary inputs are nearer to the threshold for action potential firing and are, therefore, the most vulnerable to subtle changes in membrane potential. This can be seen in the non-primary inputs in Chapter 1 (e.g., Figures 3, 4, 6-8). This suggestion is also predicted by Mountcastle and Powell (1959) in primate SI, who observed that responses evoked from the edge of an extracellular receptive field were unable to follow high-frequency trains of sensory stimuli. There are at least three mechanisms that may account for the loss of peripheral signal at higher frequencies: Loss of POm input with increasing frequency, differential adaptation of excitation and inhibition in the barrel, and, specific adaptation of excitatory intracortical connections.

The first mechanism is the selective loss of POm thalamocortical input to the septa with increasing frequency of stimulation. VPm projections synapse in two principle termination zones, the barrels in granular layer IV and the lower part of layer III, and in upper layer VI and lower layer V, (Keller, 1995; Killackey, 1973; Killackey and Leshin, 1975; Jensen and Killackey, 1987; Chmielowska et al., 1989; Lu and Lin, 1993); POm projections synapse in layer IV of septal regions between the barrels (Chmielowska et al., 1989; Lu and Lin, 1993), and in layers I and upper layer V (Lu and Lin, 1993). These two nuclei also differ in their ability to fire action potentials in response to increasing frequency of vibrissa deflection. VPm neurons respond without attenuation to deflection rates of up to 5 Hz, with only moderate (~30%) attenuation at 10 Hz. POm neurons, conversely, show decreased firing at 5 Hz and are almost completely unresponsive to rates of 10 Hz or greater (Diamond et al., 1992b). With respect to our data, one possibility is that at lower frequencies (i.e., 1 Hz) of vibrissa stimulation, deflection of a single vibrissa activates the barrel-specific VPm input as well as the more diffuse POm input. As a result, the appropriate layer IV barrel will become active along with a diffuse cortical region surrounding it. However, at 5 Hz or higher frequencies of vibrissa stimulation, POm neurons will not be significantly activated, and only the barrel-specific VPm projection will carry a thalamocortical signal, creating a discrete region of cortical activity inside the corresponding barrel. We recorded optical signals at a depth corresponding to upper layer IV/lower layer III in the rat barrel cortex. Our results, therefore, may

reflect the anatomical and physiological differences between VPm and POm neurons in layer IV.

A second possible mechanism for our finding is the differential susceptibility of excitatory and inhibitory activity within a barrel to frequency-dependent adaptation. FSs, one class of inhibitory interneurons in the cortex, receive prominent thalamocortical VPm input and are more readily driven by vibrissa deflection, electrical thalamic stimulation and current injection, than RSs, the primary class of excitatory neurons within the layer IV barrel (Simons and Carvell, 1989; Armstrong-James et al., 1994; Agmon and Connors, 1992; McCormick et al., 1985; C. Moore and S. Nelson, unpublished observation). Presumably as a result of this permissive threshold for firing and of their shorter duration after-hyperpolarizations (Agmon and Connors, 1992; McCormick et al., 1985), FSs are less readily adapted than RSs by increasing frequency of sensory stimulation (Simons, 1978). This functional asymmetry could decrease the excitatory output of the barrel at higher frequencies through maintained feedforward flow of inhibitory activity during a concomitant decrease in the output of RSs. The filtering of the local output from a barrel would limit the lateral intracortical spread of signal to the surround cortical territories, and thereby decrease the optical signal at higher frequencies. In support of this model, Castro-Alamancos and Connors (1995) found that paired pulse electrical stimulation of the VPm at interstimulus intervals of 25-200 msec (5-40 Hz) evoked decreased spread of signal beyond layer IV of SI following the second stimulus.

This enhanced filtering would be augmented by the pattern of differential inhibition described in Chapter 1. Non-primary excitatory inputs in the cortex are smaller than more central inputs, and are more effectively suppressed by inhibition (Chapter 1; Kyrazi et al., 1996). Our data from Chapter 1 predict that these inputs should be the most easily suppressed by maintained strength of inhibitory activity in the context of decreased excitatory current flow. A relatively small difference, then, in the sensitivity of inhibition and excitation to frequency would amplify the sharpening of the barrel in two ways: First, by limiting the intracortical output of strong barrel inputs, and, second, by differentially suppressing more peripheral inputs from non-primary vibrissa.

A third mechanism that could explain these results is a decreased lateral spread of intracortical activity due to preferential intracortical adaptation at excitatory horizontal projection synapses. Using a thalamocortical slice preparation through the barrel cortex, Gil et al. (1996) demonstrated that paired pulse stimulation of thalamocortical pathways at a range of stimulus frequencies (.5 to 100 Hz) leads to significantly greater adaptation than stimulation of layer 3 intracortical pathways at the same frequencies (see also Agmon and Connors, 1991; Diesz and Prince, 1991). This dissociation predicts that the frequency-dependent decrease in signal in surrounding cortex should be scaled to decreases in the center of the representation at higher frequencies. We observed the opposite effect, suggesting that selective adaptation of cortical activation through horizontal connections is an unlikely explanation of our results.

Perceptual Implications of the Sharpening of the Vibrissa Representation

Simons and colleagues (Simons, 1985, 1996; Brumberg et al., 1996; Kyrazi and Simons, 1993) have suggested that one purpose of the circuitry of the barrel is to amplify primary vibrissa signal during whisking. Because inhibition differentially

suppresses smaller inputs (Chapter 1; Brumberg et al., 1996), contact of multiple vibrissae (inducing inhibition) would suppress the firing of weaker, non-primary inputs. We have shown that increasing the frequency of stimulation of the vibrissa also serves to sharpen the cortical representation of a single vibrissa. Our findings, in the context of this previous work, suggest that whisking may establish a *sensitivity* versus *specificity* trade-off in the processing of perceptual input. When the whisking rat is palpating objects, frequency of whisking and simultaneous contact with multiple vibrissae lead to a sharpening of the input to the corresponding cortical barrel representation. This sharpening in turn would lead to a decreased sensitivity to less robust non-primary inputs, but a greater relative input from the primary vibrissa, allowing for increased discrimination. Conversely, in the resting, non-whisking state, a broader spatial divergence of activity in the cortex compromises the ability to discriminate the precise origin of that input, but allows for greater sensitivity to input from a number of vibrissae.

A second implication of our studies is the grouping and ungrouping of distinct septal and barrel processing systems within rat SI. Several authors have suggested that the barrels and their intervening septa form two discrete somatosensory processing areas (Diamond et al., 1992b; Olavarria et al., 1984; Chmielowska et al., 1989). The frequency-dependent reorganization we observed here, interpreted under this scheme, suggests the functional uncoupling of two independent somatosensory processing systems, a cortical region with larger receptive fields (septa) from a more discrete representation (barrels). From a different perspective, this framework again supports the view that the functional effect of whisking is to establish a sensitivity/specificity trade-off, by a frequency dependent suppression of the large-receptive field septa.

Experiment 2: Reorganization of the Rat SI Vibrissa Representation Following Prolonged Vibrissa Trimming/Pairing

Experiment 1 demonstrated that adult rat SI is capable of dynamic, temporary reorganization during the stimulation of a single vibrissa. To investigate the reorganization of the cortex following a prolonged change in the pattern of perceptually relevant stimulation, I examined cortical reorganization after vibrissa trimming/pairing.

Methods

Behavioral Manipulation

Experimental animals were taken briefly from their home cage and lightly anesthetized with metaphane. While lightly anesthetized, all of the vibrissae on the left side of the rat's face were cut to a length of ~5 mm, except for two which were left at their normal length (either the C2-C3 or the D1-D2). The vibrissae on the right side were not cut. The animals were then returned to their home cage for 64 hours, after which they were removed and prepared for optical imaging. Control animals were imaged without prior manipulations.

Results

We recorded optical signals evoked by stimulation of 20 vibrissae in 7 control animals, and 17 vibrissae in 3 experimental animals. Following trimming/pairing, we observed a significant expansion of the uncut vibrissa representation. This effect is demonstrated in Figure 8, where the mean fall-off in signal strength is plotted as a function of distance from the center of the uncut (N = 5), control (N = 20) and cut (N = 12) evoked signals. To quantify the pattern of this signal spread, we calculated the activity in neighboring representations during stimulation using a mask with a 133 μm radius. Uncut vibrissae demonstrated significantly greater activation in neighboring representation centers (.31% +/- .01 SEM, N = 18) than control vibrissae (.06 +/- .01, N = 40; $p < .0001$) or cut vibrissae (.03 +/- .01, N = 29; $p < .0001$; Figure 8). This signal spread was greater into the neighboring cut vibrissa representation (.34% +/- .02, N = 14) than into the neighboring uncut representation (.20 +/- .07, N = 4; Figure 8), but this difference was not significant ($p > .05$). The spread of activity from cut vibrissae to neighboring centers was not significantly different from control vibrissa signal spread ($p > 0.05$).

Activity in the center of the uncut vibrissa representation (.34 +/- .05, N = 5) was significantly higher than activity in the center of the cut vibrissa representations (.16 +/- .03, N = 12: $p = 0.059$, student's 1-tailed t-test). Optical signal in the center of the uncut vibrissa representation was not significantly greater than activation in the center of control vibrissa representations (.22 +/- .03, N = 20: $p > 0.05$). The cut vibrissa representation was also not significantly different from control ($p > 0.05$: Figure 8).

Figure 7 Increased signal strength from uncut vibrissa stimulation compared with control and cut vibrissa following vibrissa trimming/pairing A. Using the concentric summation approach, increased spread of signal can be observed in the periphery. Input from uncut vibrissae demonstrated a significantly greater amplitude in the center of the representation as compared to cut vibrissae. B. Signal spread into the cut (green) and uncut (red) neighboring representations following cut (left) and uncut (right) vibrissa representation. Error bars show standard deviation.

Figure 7

A.

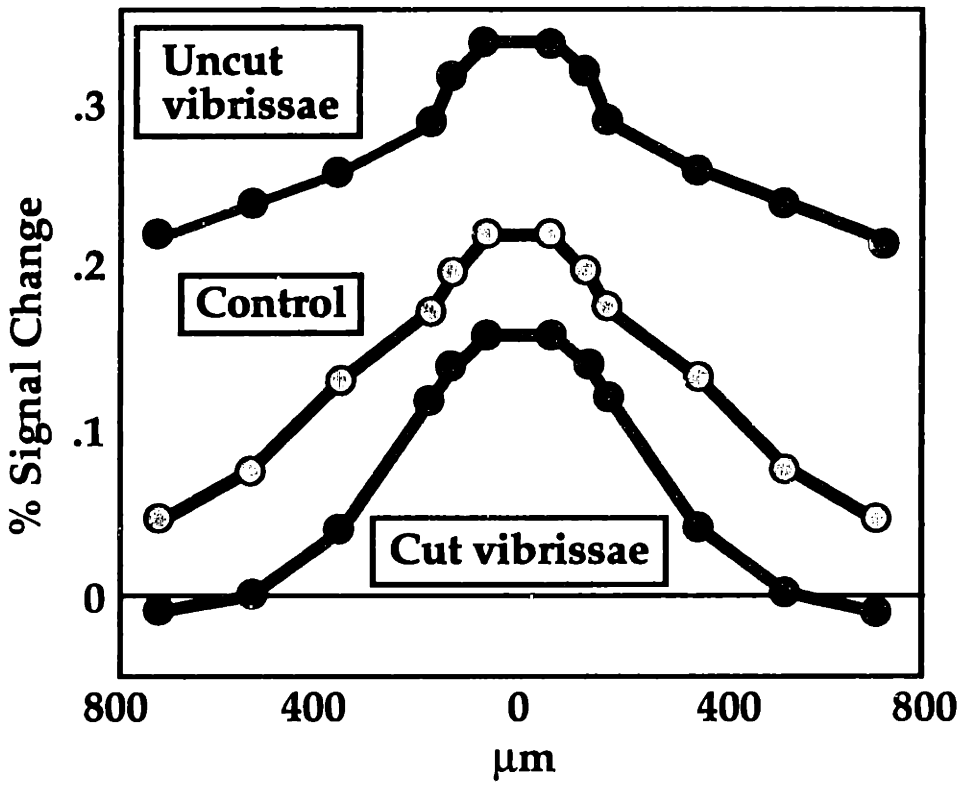
Uncut vibrissae
Control
Cut vibrissae
% Signal Change
.3
.2
.1
0
800
400
0
400
800
µm

B.

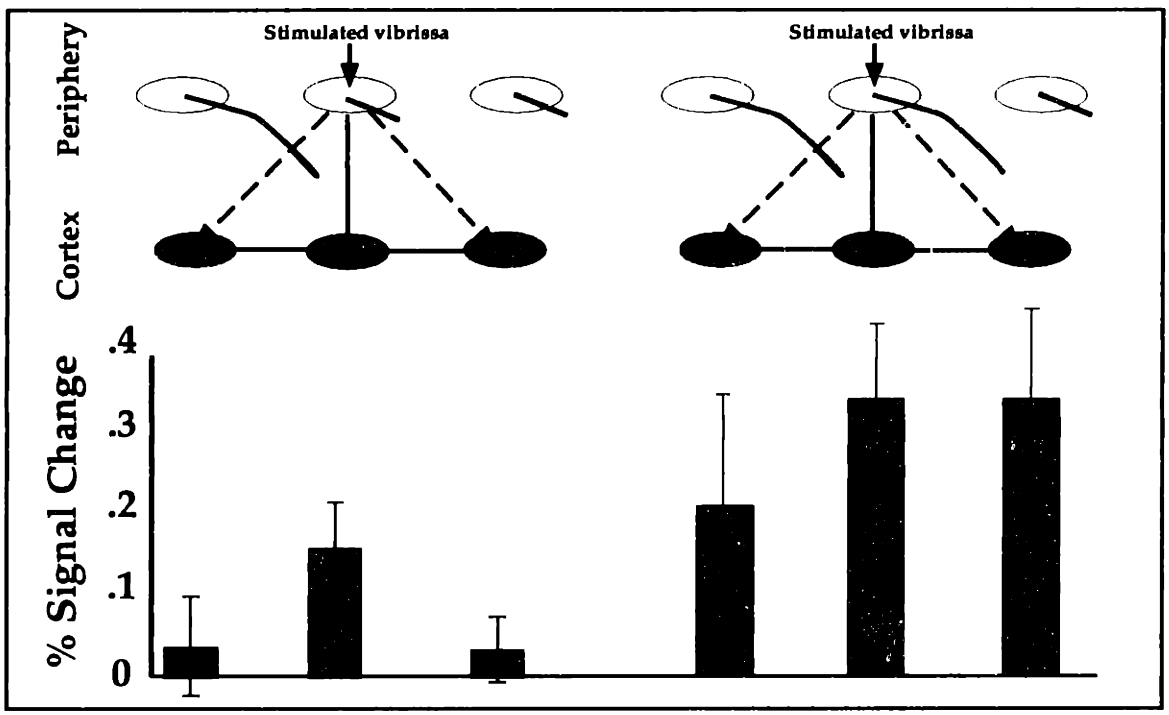
Stimulated vibrissa
Stimulated vibrissa
Periphery
Cortex
% Signal Change
.4
.3
.2
.1
0

Discussion

Our findings replicate and extend the receptive field plasticity studies of Armstrong-James et al. (1994) and Diamond et al. (1992a). Using intrinsic-signal optical imaging, we observed a significantly enhanced spread of signal from uncut vibrissae to their neighboring vibrissa representations. This finding is in agreement with the observation of enhanced action potential firing in the neighboring, uncut barrel. Also in agreement with previous studies, we observed an increase in the activation in the center of the vibrissa representation.

The unique contribution of this study is the observation that input from the uncut vibrissa spreads significantly into the adjacent cut representation. A plasticity model relying on the temporal synchrony of input to drive cortical change would predict that the decreased correlation between the uncut and recently cut vibrissa would weaken (or have no effect on) the strength of activation in the cut vibrissa representation. The increased signal in the cut vibrissa representation in our data suggests that temporal synchrony cannot explain all of the changes observed following vibrissa trimming/pairing. In contrast, the spread of activity from a viable input (the uncut vibrissa), into cortical territory that receives decreased input (the cut vibrissa representation), is similar in nature to takeover following peripheral anesthesia, amputation or nerve-section (Faggin et al., 1997; Florence and Kaas, 1996; Jain et al., 1997; Merzenich et al., 1983, 1984; but see Jain et al., 1995). These studies typically do not report whether changes in the amplitude of input in the *extant* portions of the representation occurred, although Merzenich et al. (1983) have demonstrated reorganization of receptive field size within the radial nerve representation following section of the medial nerve, in agreement with the suggestion that reorganization occurs within the extant representation (see also Chapter 3, Experiment 4, where a similar increased amplitude in the human palm representation is observed following SCI).

Mechanisms of Cortical Reorganization Following Vibrissa Trimming/Pairing

A mechanistic explanation of vibrissa trimming/pairing plasticity must account for at least three phenomena: The spread of activity from an uncut vibrissa into a cut vibrissa representation; increased signal within an uncut vibrissa representation during stimulation of the corresponding vibrissa; and, the spread of activity from an uncut vibrissa into a neighboring uncut vibrissa representation. Three mechanisms can explain some part of our results: Alteration in the strength of intracortical inhibition, increases in the strength of excitatory connections within the cortex, and subcortical reorganization.

Several lines of evidence support disinhibition as a mechanism for receptive field expansion. Subthreshold receptive fields within rat SI demonstrate substantial inhibition (Chapter 1; Brumberg et al., 1996; Carvell and Simons, 1988; Kyrazi et al., 1996; Simons, 1985). A direct prediction of the recordings in Chapter 1 is that a decrease in the strength of inhibition within the cortex would lead to the revelation of slower-rising, non-primary sensory inputs that are differentially suppressed by inhibitory currents (e.g., Figures 6-8 of Chapter 1; Kyrazi et al., 1996). In close agreement with this prediction, Diamond et al. (1992a) and Armstrong-James et al. (1994) have reported that changes in receptive field organization after trimming/pairing occur in longer-latency inputs (> 10 msec). These authors have attributed this increase in longer-latency inputs to stengthening of intracortical projections. Our data in Chapter 1 cannot speak directly to the question of the

origin of synaptic inputs, but both latency and rise time vary with the efficacy of cortical input, suggesting that even inputs with the same arrival time would reveal later action potential responses following cortical reorganization (e.g., Figure 6 of Chapter 1, evoked responses). Further, the prevalence of inhibition in primary vibrissa inputs suggests that decreased inhibition would permit an increase in longer-latency responses in these inputs as well. This increase could explain the increased amplitude of response we observed in the center of the uncut vibrissa representation.

In further support of inhibitory regulation as a mechanism for cortical reorganization, Welker et al (1989) observed a down regulation of GAD staining in the corresponding vibrissa barrel 3 days after vibrissa plucking (see also Garraghty et al., 1991). Such a down regulation in deafferented representations would explain the spread of the uncut vibrissa representation into the cut representation: A similar down regulation of inhibitory gain in the uncut representation would also explain the increased signal in the uncut representation. However, we did not observe increased cortical activation in the cut or uncut vibrissa representation centers after stimulation of the cut vibrissa, which would be predicted by a non-specific down regulation of the inhibitory gain within the cortex. A disinhibitory mechanism would, therefore, have to engage the cut and uncut inputs differentially to support the reorganization we observe.

An increase in the synaptic strength of excitatory uncut inputs in the cortex could also explain our findings. In support of this proposal, several studies have demonstrated in vivo potentiation of the strength of cortical synapses. Lee and Ebner (1992) have shown that bursts of sensory or electrical stimulation to the VPm can induce a cortical-specific enhancement in the response to vibrissa deflection in the corresponding layer IV barrel, and Dinse et al. (1993) have shown that electrical stimulation of a somatotopically defined cortical representation induced shifts in neighboring receptive field centers such that they overlap with the stimulation site (see also Cahusac, 1995). In addition to these studies, several *in vitro* studies have demonstrated the capacity for potentiation of rat SI cortical synapses (Bindman et al., 1988; Markram and Tsodyks, 1996; Lee et al., 1991).

Two types of models of plasticity have been invoked to explain cortical potentiation. The first model is a sliding threshold model of cortical plasticity. Bensukova et al. (1994) have proposed a BCM model of cortical potentiation to explain vibrissa trimming/pairing plasticity. In this model, the capacity for plasticity is scaled to the pattern and amplitude of input. The general decrease in input to the cortex following trimming of the majority of vibrissae would lower the threshold for plastic change, allowing uncut inputs to increase their input strength, especially into the cut barrel, in the context of the loss of cut inputs. This framework provides a single explanation for the increased representation of input in the uncut and cut representations, and for the non-significant decrease in input from the cut vibrissa.

The second is the "Hebbian" temporal synchrony of inputs described above. In support of this model, Glazewski and Fox (1996), working in the adolescent rat (p28), did not observe reorganization in layer IV after 60 days of trimming all the vibrissa but one. In contrast, we observed changes at approximately the level of layer IV at 64 hr after leaving two vibrissa intact. The failure to achieve single-vibrissa plasticity in layer IV suggests that, in favor of a Hebbian mechanism, the temporal synchrony of the two inputs may be crucial to the increased representation

in the uncut representation. In addition, two vibrissa may encode more perceptually viable information than one vibrissa, leading the rat to continue to employ these vibrissa for perception, and thereby promoting reorganization (e.g., Merzenich et al., 1996).

Subcortical reorganization of input from the uncut vibrissa could also lead to an increased spread of signal in the cortex. This suggestion is predicted by several studies that have demonstrated subcortical reorganization in the rat somatosensory system (trigeminal nuclei and thalamus) following anesthesia or deafferentation (Faggin et al., 1997; Nicolelis et al., 1993; Parker et al., 1998; see also Devor and Wall, 1981 and Wall, 1977). Using the more subtle manipulation of vibrissa trimming/pairing, however, Diamond et al. (1994) have observed that layer IV responses do not reorganize within 24 hours. In contrast, supragranular and infragranular receptive fields do demonstrate reorganization at this timescale. These authors have interpreted this finding to mean that subcortical change in this paradigm follows, and may be a result of, prior cortical plasticity.

What is the Utility of the Long-term Cortical Reorganization?

There are several potential uses for longer-term plasticity in primary sensory cortex. One function of longer term cortical change (i.e., change that persists beyond the cessation of the context) may be to support low-level perceptual learning phenomena (see Postle, 1997 for a review). This suggestion is supported by the neuropsychological literature, as lesions of sensory cortex in humans lead to specific deficits in priming for sensory, as opposed to conceptual, stimuli (Keane, 1991). The mechanism(s) underlying this type of learning would require specific correlation-based interactions to encode the features of individual stimuli. A crude version of this type of mechanism is suggested by the studies of Wang et al. (1995), who observed reorganization of spatial correlations between representations in the cortex following increased temporal correlation. Another proposed role for longer-term plasticity is a more general maximization of cortical utility: If one representation is going unused through perceptual deprivation or deafferentation, that neural machinery should be employed by more active inputs. In this context, deafferentation plasticity can be viewed as an adaptive phenomenon, insofar as it utilizes available cortex in the context of a loss of input to optimize perceptual capability (Merzenich et al., 1988; see also Chapter 3).

With vibrissa trimming/pairing, we observed changes that may reflect both of these proposed uses of cortical reorganization. The overlap in representation we observed between the neighboring, correlated uncut vibrissa inputs is suggestive of the specific temporal correlation of inputs, and the increased spread of signal from the uncut to the cut representation is analogous to the more general maximization of cortical utility. In all likelihood, several mechanisms, operating at different levels of the somatosensory system and working on different timescales, work in concert to reorganize cortical vibrissa representation following trimming/pairing plasticity (Moore and Sur, 1997).

General Discussion

The first single unit examinations of the rat SI vibrissa representation (Welker, 1971, 1976), emphasized the pointilistic nature of its representations. In the barbiturate anesthetized rat, neurons in a given layer IV barrel responded to input from only the corresponding vibrissa (Welker, 1976). The importance of this

correspondence was reinforced by the dramatic segregation of cytoarchitecture (Woolsey and van der Loos, 1970) and afferent projection patterns (e.g., Olavarria, 1984) within each barrel. This cortical system appeared to be an extreme example along the continuum of cortex parcellated into columns, if not actually a labeled line.

Barrel Cortex is not a Labeled Line

While this view has persisted[1], more recent studies mitigate against a simple conception of the segregation of input within rat SI. Simons (1985) was one of the first to suggest a more complex organization of the spatial representation within the rat SI vibrissa representation, by reporting that stimulation of surrounding vibrissa could inhibit the evoked response of an adjacent vibrissa. His work was followed by recordings in the urethane anesthetized (Armstrong-James and Fox, 1987) and unanesthesthetized rat (Chapin, 1986) that demonstrated that, under different anesthetic regimines, vibrissa receptive fields in rat barrel cortex could express much larger peripheral receptive fields (Armstrong-James and George, 1988). In turn, a series of studies have demonstrated that the vibrissa representation of adult rat SI is malleable following alteration in the pattern of peripheral input (Delacour et al., 1987; Welker et al., 1989, 1992; Diamond et al., 1992a, 1994; Armstrong-James et al., 1994; Glazewski and Fox, 1996), further suggesting that this cortex has an extensive vocabulary of possible dynamic changes.

Our data contribute significantly to this emerging conception of adult rat SI organization. As described in Chapter 1, subthreshold receptive fields in rat SI are large and complex, suggesting multi-vibrissa integration of inputs as an active part of sensory processing. Further, as described in Chapter 2, temporal context and perceptual history can invoke rapid and longer-term reorganization of the cortex. The use of a noninvasive stimulation paradigm to evoke cortical reorganization in both Experiments suggests that reorganization is not a phenomenon limited to large-scale changes in the pattern of cortical input (e.g., deafferentation), but, rather, may be an active component of normal sensory processing.

Suprathreshold Receptive Fields are Discrete

Although the barrel cortex is not as segregated as previously believed, it does possess discrete suprathreshold receptive fields. The suprathreshold receptive fields within a layer IV barrel are, on average, smaller than or equal in size to the input from the VPm (Simons and Carvell, 1989; see also the discrete suprathreshold receptive fields in Chapter 1). In this vein, Simons and Carvell (1989) have suggested that the primary thalamocortical response transformation within this cortex is to *reduce* the size of the suprathreshold receptive field, and many of the consequences of whisking appear to limit these receptive fields further (Brumberg et al., 1996; Chapter 2). These relatively smaller layer IV receptive fields within the barrel make it disanalogous to area VI, where single receptive fields integrate the output of several thalamic neurons to produce larger suprathreshold receptive fields (Reid et al., 1991). Further, these smaller receptive fields counter the trend towards expansion of receptive field size with increasing distance from the periphery (see Kaas, 1989 for a review). Thus, a more complex understanding of rat

[1] As recently as 1993, no less than a pioneer of squirrel SI cortex continued to view rat SI as a system unlikely to demonstrate dynamic modulation (Moore, unpublished observation).

SI cortical organization, that incorporates the active constraint of larger subthreshold receptive fields to form discrete output receptive fields, is necessary.

The Relevance of Experiments 1 and 2

Experiments 1 and 2 are clearly aphysiological. High-frequency stimulation of a single vibrissa seldom, if ever occurs in the behaving rat, and anesthesia is not a natural environmental variable (although the case could be made for the Sprague-Dawley strain). Similarly, while rats will occasionally lose a single vibrissa, they seldom if ever lose effective sensory input from all but two vibrissae on one side of the face. The importance of these two studies is, then, fourfold. First, they provide another existence proof of cortical reorganization, i.e., that it is possible to observe this kind of rapid and longer-term plasticity following non-invasive manipulation of sensory input. Second, while not physiological, they suggest mechanisms that may underlie physiological reorganization. Third, they demonstrate the effective use of intrinsic-signal optical imaging for the exploration of temporal phenomena and behaviorally induced cortical reorganization. Fourth, these findings suggest experiments that address the physiological relevance of these phenomena and their mechanistic underpinnings (see Conclusion).

CHAPTER 3

Organization of Human Somatosensory Cortex Examined Using fMRI

"...Quietness again lifts and planes out
blood in our heads gliding
in the sky of the brain."

Rumi, *12*

The cortical organization of somatosensory input possesses several common features across species (Kaas, 1983; Krubitzer, 1995; Merzenich and Kaas, 1980). These commonalties include a) the representation of neighboring peripheral inputs in neighboring populations of cortical neurons (the somatotopic "map", e.g., Penfield and Rasmussen, 1950; Woolsey et al., 1942; Chapter 2), b) the presence of multiple cortical areas (Merzenich and Kaas, 1983; Kaas, 1989), and c) the ability to reorganize representation borders following changes in the pattern of peripheral input (Diamond et al., 1992a, 1994; Jain et al., 1997; Merzenich et al., 1983; Chapter 2). The explication of these features in the human and monkey is reviewed here as an introduction to my study of human cortical organization using fMRI.

Maps within the Primate PoCG

Within the human somatosensory cortex, the mediolateral extent of the PoCG is organized into a series of adjacent body representations, the somatotopic map. Penfield and colleagues (e.g., Penfield and Rasmussen, 1950) defined this map using patient reports during electrical stimulation. They observed that stimulation of the PoCG at the midline evoked the sensation of contact on the foot, followed in lateral progression by the lower body, trunk, arm, hand, and, near the juncture of the PoCG and the Sylvian fissure, the face (e.g., Figure 4 of Chapter 3). Within this "homunculus," each body part had a single representation, though stimulation often induced the perception of contact in body regions that had neighboring cortical representations. The organization of this homunculus was further supported by human lesion studies (Head, 1920; Corkin, 1964; Corkin et al., 1970; Taylor et al., 1997) wherein damage to specific representations within the PoCG was related to deficits in tactile perception in corresponding areas in the sensory periphery.

This map is recapitulated in the PoCG of the monkey (e.g., Kaas et al., 1979; Merzenich et al., 1978; Nelson et al., 1980; Woolsey et al., 1942). Owl and macaque monkey cortex possess a similar progression of body representations in the PoCG, stretching from the foot (medial) to the face (lateral) (Merzenich et al., 1978, Nelson et al., 1980; Pons et al., 1991). There are, however, some differences between the description of the somatosensory representation in the monkey and human PoCG. First, within a given representation, individual parts of a dermal surface may display a fractured representation. For example, in the macaque palm representation, the palm is represented as two distinct islands of cortex representing the ulnar and radial palm regions (Nelson et al., 1980). This difference in the map could be one of emphasis: Penfield and Rasmussen (1950) observed such breaks in representation but accounted it to variability in the technique. It might also have arisen from the method of gross electrical stimulation, which is more aphysiological in its mapping method (i.e., stimulating the cortex versus observing the cortical response to natural stimuli). A second, more profound difference between nonhuman and human primate studies is the report of several distinct representations within the PoCG of the monkey that code for separate submodalities of somatosensory input.

Segregation of Sensory Cortical Areas in the Monkey

A consistent feature of sensory systems is the rerepresentation of the sensory periphery in distinct cortical areas. Sensory cortical areas are defined by several criteria, including their cytoarchitecture, pattern of connectivity, and receptive field response properties (Kaas, 1983). Over 30 areas have been delineated within the

visual system of the non-human primate (Kaas, 1989; Van Essen et al., 1992), and several analogous regions, with similar response properties, have been recently defined in the human cortex (Tootell et al., 1997; DeYoe et al., 1996). Similarly, multiple auditory areas, segregated by the pattern of responsiveness in tonotopic space, have been isolated in monkey (reviewed in Merzenich and Kaas, 1980) and human cortex (T. Talavage, personal communication).

Within the PoCG of the monkey, four somatosensory body representations with distinct receptive field properties and anatomical connectivity have been described (Kaas et al., 1979; Iwamura et al., 1985, 1993; Jones and Porter, 1980; Merzenich et al., 1978; Merzenich and Kaas, 1980; Nelson et al., 1980; Paul et al., 1972; Sur et al., 1980; Tommerdahl et al., 1996). These physiologically defined areas correspond to Brodmann areas 3a, 3b, 1, and 2 (Brodmann, 1909). Area 3a, located in the depth of the central sulcus, has been found to be almost exclusively responsive to deep and proprioceptive input (Iwamura et al., 1993; Jones and Porter, 1980; Kaas et al., 1979; Rencanzone et al., 1992a). Areas 3b and 1, located on the anterior face and crest of the PoCG (Kaas et al., 1979), possess receptive fields responsive to light touch (Kaas et al., 1979; Sur et al., 1984). Neurons in these areas also demonstrate premovement activity (Nelson, 1996) and a minority of proprioceptive and deep receptive fields (Iwamura et al., 1993; but see Merzenich et al., 1978). Along the posterior wall of the PoCG, area 2 contains tactile and proprioceptive receptive fields (Hyvarinen and Poranen, 1978; Iwamura et al., 1993). Area 2 receptive fields are often complex, as they can be responsive to the direction of movement (Hyvarinen and Poranen, 1978; Constanza and Gardener, 1980), the coordination of multi-digit movements or inputs (Iwamura and Tanaka, 1996), and the integration of multimodal input (Ageranioti-Belanger and Chapman, 1992; Iwamura et al., 1985).

In addition to these areas within the PoCG, there are at least three somatosensory representations located within the precentral gyrus (PreCG) of the primate. Distinct tactile and proprioceptive maps have been defined in the anterior bank of the central sulcus, areas 4a and 4b, respectively (Strick and Preston, 1982; Geyer et al., 1995). Further, the crest and posterior bank of the PreCG, Brodmann area 6, also possesses a tactile map (Penfield and Rasmussen, 1950; Gentilucci et al., 1994). The importance of these regions to tactile perception is significant: Following lesions of the PoCG, PreCG stimulation can evoke tactile sensations (e.g., Penfield and Rasmussen, 1950), and lesions of the PreCG in monkeys can lead to somatosensory neglect (Rizzolatti et al., 1983).

The effects of discrete lesions within the PoCG in monkeys suggest that distinct subregions of the PoCG support specific submodalities of somatosensory perception. In the macaque, lesions of areas 1 and 3b lead to specific deficits in tactile discrimination, i.e., the perception of roughness, grating orientation, and texture, and lesions of area 2 induce selective deficits in tasks requiring tactile and proprioceptive integration, i.e., the perception of the shape or angle of an object (Carlson, 1980; Semmes and Porter, 1972; Semmes et al., 1974). Neither set of lesions induced a deficit in the perception of position sense (Semmes et al., 1974), presumably because this submodality of somatosensory perception is mediated in large part by area 3a.

Segregation of Cortical Areas within the Human PoCG

Although a great deal is known about the somatosensory areas in the monkey, there has been little extrapolation of this prevalent and seemingly important pattern

of organization to the human somatosensory cortex. The investigation of adjacent somatosensory areas within the anterior-posterior extent of the central sulcus has been limited by the spatial resolution of lesion-based approaches and presurgical stimulation techniques (Nii et al., 1996; Penfield and Rasmussen, 1950). Using electrical stimulation during neurosurgery, Penfield and Rasmussen (1950) described evoked tactile perceptions following stimulation of the PreCG. However, they did not detect a separate map of proprioceptive input, and went on to suggest that only important proprioceptive capacities were represented in the cortex, and that these were represented in series with the PoCG tactile map (but see Head, 1920, for an early conjecture on the presence of a separate cortical proprioceptive area). More recent studies using subdural electrode grids have also reported tactile sensations from the PreCG and motoric output from the PoCG (Nii et al., 1996), leading these authors to conclude that the position of motor and tactile representations is variable across subjects, and that the central sulcus is an unreliable indicator of the position of sensory and motor maps, contrary to the findings in the monkey. Functional imaging studies using positron emission tomography (PET) have also defined activation within the PoCG during different types of somatosensory input, but have lacked the functional resolution (> 1 cm) to segregate cortical areas (e.g., Burton et al., 1997).

Plasticity in the Primate Cortical Map Following Deafferentation

The somatosensory cortex of the monkey is orderly, but it is not static: Several studies have demonstrated reorganization in the primate cortical map following lesions of the peripheral nervous system (PNS) (Florence and Kaas, 1995; Garraghty and Kaas, 1991; Merzenich et al., 1983, 1984). Many of these studies were inspired by the work of Merzenich et al. (1983), that demonstrated takeover of deafferented cortical territory in areas 3b and 1 following transection of the median nerve of the hand. Subsequent reports have shown that reorganization after discrete lesions of the PNS can occur following a variety of manipulations, including amputation (Florence and Kaas, 1995; Merzenich et al., 1984) and multiple-nerve transection (Garraghty and Kaas, 1991), and that the pattern of deafferentation plays a crucial role in the extent of reorganization observed (e.g., Garraghty and Kaas, 1991; Garraghty et al., 1994).

A few studies have also reported reorganization in the human cortex following PNS lesions. In traumatic unilateral amputees, PET signal generated by a shoulder rotation above the stump was increased in extent and amplitude over the contralateral "M1/S1" cortex (Kew et al., 1994). Similarly, Taub and colleagues (Elbert et al., 1994; Flor et al., 1995; Knecht et al., 1996) have also reported reorganization of human somatosensory cortex following traumatic amputation. Using magnetic source imaging, these authors have observed a shift in the center of extant cortical somatosensory representations towards the predicted location of the deafferented cortex.

Extending the work conducted with PNS lesions, recent studies in adult monkeys have investigated the effects of extensive central nervous system (CNS) deafferentation on cortical reorganization in area 3b (Jain et al., 1997; Pons et al., 1991). Jain et al. (1997) demonstrated that transection of the dorsal columns causes a loss of cutaneous input to the hand representation in 3b that was not immediately remapped by neighboring peripheral inputs. After 6 months, the cortex that had responded to the lesioned section of the cord (the arm and hand representation) was

completely remapped by inputs from above the level of section (the chin). This pattern of reorganization was accompanied by changes in neural responsiveness: Neurons in the remapped cortical territory adapted more rapidly than normal inputs and were less easily driven by punctate (von Frey filament) stimulation. This work suggests that reorganization following extreme CNS lesions occurs on a relatively slow timescale, but that remapping is eventually complete. In a study of a different kind of CNS deafferentation, dorsal root ganglion lesions at the level of C2-T4, Pons et al. (1991) observed an extensive remapping of deafferented cortex, such that inputs from the hand totaling over a centimeter of cortex were taken over by the extant inputs from the face (but see Lund et al., 1994, for a more conservative estimate of the extent of the reorganization, i.e., ~5mm). Contrary to the results of Jain et al. (1997), Pons and colleagues found that the amplitude and latency of neuronal responsiveness in the remapped cortical territory was normal.

The Link Between Perception and Cortical Plasticity

Principles of cortical map organization suggest several perceptual consequences of cortical reorganization. As noted by Weinstein (1968), there is a strong correlation between the cortical territory devoted to a given representation and the perceptual acuity of that region. The relation between acuity and the extent of cortical representation arises in part from the increased density in peripheral receptors in regions with large cortical representations (Valbo et al., 1979), but also may be the result of the relation between receptive field size and cortical extent. Sur et al. (1980) demonstrated that receptive field size is an inverse function of the extent of a cortical representation in areas 3b and 1: The larger a cortical representation relative to body area, the smaller the receptive fields in that representation. This relation is maintained following cortical expansion after deafferentation (Merzenich et al., 1983, 1984; but see Rencanzone et al., 1992b). The implication of this finding is that cortical representations that increase their extent should demonstrate higher perceptual acuity as the result of more discrete cortical receptive fields. In agreement with this prediction, Teuber et al., (1949) and Haber (1958) have observed better two-point and pressure sensitivity thresholds above the stump region of unilateral amputees, as compared with the contralateral homologous region. Further, amputees and spinal cord injured (SCI) patients often report bands of increased sensitivity in the region bordering the deafferented zone (Bors, 1951; Tasker, 1990).

A second perceptual implication of cortical plasticity was originally suggested by Teuber et al., (1949), and recently has been brought to light by Ramachandran (1993). Following deafferentation, amputees commonly report a "phantom" sensation emanating from the deafferented zone. This percept can take a variety of forms, including, a burning, cramped, or pins and needles sensation (Bors et al., 1951; Riddoch, 1941). The phantom is often evoked by contact in a reference zone, a skin region that projects sensation of contact to the phantom region (Halligan et al., 1993; Knecht et al., 1996; Ramachandran, 1993). Ramachandran (1993) has suggested that the origin of the phantom sensation is the perceptual misattribution of activity in a deafferented region of cortex to the peripheral region that previously activated that region. In support of this hypothesis, regions that would be predicted to inherit cortical territory following deafferenation (e.g., the face following amputation of the hand) demonstrate reference zones. In further support of the connection between phantom perceptions and cortical reorganization, Flor et al.

(1995) demonstrated that the degree of shift in the cortical map following deafferentation was correlated with the subjective report of the intensity of phantom pain sensations, and Teuber et al. (1949) noted lower 2-point discrimination thresholds were related to the presence of phantom sensations, suggesting that a shared mechanism supports both phenomena.

Functional Magnetic Resonance Imaging

Functional magnetic resonance imaging (fMRI) provides a relatively high-resolution (1.5 mm, Engel, 1996; 500 μm, Shulman, 1997; but see Malonek and Grinvald, 1996, where they estimate a resolution of 6 mm), relatively robust (.5-10% signal change, C. Moore, A. Gray and S. Corkin, unpublished observations), non-invasive means for imaging activity in the human brain. Like intrinsic-signal imaging, fMRI measures hemodynamic changes in the brain that are the result of neurophysiological activity. Following an initial increase in [Hbr] after neuronal activation, there is a subsequent increase in the flow of oxygenated blood to that region that causes a decrease in the [Hbr][2] (see also Chapter 2, Introduction). Because Hbr is paramagnetic, and HbO_2 is significantly less so (diamagnetic), the decreased concentration of Hbr leads to an increased homogeneity in the field, and a subsequent change in the rate of relaxation in the coherence of the precession of hydrogen atoms following a radio-frequency pulse that has temporarily aligned them. This change in the coherence relaxation rate in the presence of increased HbO_2 generates what is known as the blood oxygen-level dependent (BOLD) signal, the mapping signal for fMRI (Kwong et al., 1992; Ogawa et al., 1992; Cohen and Bookheimer, 1994). Correlation studies show reasonable agreement in localization between fMRI (<2 cm) and electrophysiological techniques (MEG; Liu, personal communication, 4/14/98: Electrical stimulation; Jack et al., 1994) and other metabolic imaging techniques, e.g., PET (Dettmers et al., 1996; for a review of integration of imaging techniques, see Fox and Woldorff, 1994).

---

[2] Although there is general agreement that the fMRI signal derives from the excessive inflow of oxygenated blood (referred to as "Watering the whole garden for the sake of one flower" by Malonek and Grinvald, 1996), the precise mechanism by which neural activity and oxygen consumption trigger increased flow is poorly understood. However, two recent studies describe novel mechanisms in the pathway linking neuronal activation to blood flow.

Stamler et al. (1997) has shown that the binding of O_2 to Hbr leads to an allosteric change that promotes the binding of nitric oxide (NO) to HbO_2. When HbO_2 is converted to Hbr by active neurons, the NO group is released, promoting the local inflow of blood from arterioles. This study predicts that the BOLD signal is actually well localized (i.e., within 200mm) to the region of activation. Work by Shulman (Cognitive Neuroscience Institute, 1997) has recently shown BOLD signal localized to a single cortical barrel, supporting this view of localized BOLD signal (in disagreement with Malonek and Grinvald, 1996, who argue for a much broader dispersal of signal following a discrete triggering neural event).

Shulman and colleagues (Sibson et al., 1997) have recently demonstrated a nearly one to one stochiometry (.90) between glutamate neurotransmitter synthesis and glucose consumption: Given the consistent relation between glucose consumption and blood flow (see Jeuptner and Weiler, 1995, for a review), Shulman's argument suggests that increases in the BOLD signal are the result of increases in glutamate synthesis, and that decreases in BOLD signal (e.g., Gehi, Moore et al., 1996; see below) are decreases in glutamate synthesis (i.e., neuronal inhibition of excitatory neurons). Because Shulman and colleagues' measurements have been conducted under hyperammonemic states, however, their conclusions should be regarded as preliminary (M. Raichle, conversation, 7/11/97).

Mapping the Cortical Organization of the PoCG in Humans using fMRI

I mapped the extent and mediolateral location of palm activation in the human PoCG, and the anterior-posterior segregation of multiple areas around the central sulcus using fMRI. The goal of these studies is manifold. The first goal of these studies was to assess quantitatively the organization of somatosensory function in normal subjects using fMRI, and to compare the pattern of these results to the "gold standard" of cortical mapping, in vivo electrical stimulation studies. Consistent with the classic literature, studies using PET and fMRI have detected activation within the PoCG during tactile sensory stimulation (Boecker et al., 1996; Burton et al., 1997; Coghill et al., 1994; Disbrow et al., in press; Hammeke et al., 1994; Pardo et al., 1997). Studies using PET have also recapitulated the overall pattern of somatotopy described in the Penfield homunculus (Drevets et al., 1995). To date, however, studies of tactile stimulation using fMRI have not provided a quantitative localization of activation within the PoCG. A second goal of this work was to extend beyond the Penfield's findings. Despite the tremendous contribution of Penfield and colleagues to our understanding of human cortical organization, they nonetheless employed a relatively low resolution method with a non-natural stimulus. It is unclear whether differences reported between Penfield's homunculus and the organization of the monkey PoCG (e.g., differences in the mediolateral representation of the somatotopic map and the presence of multiple areas in the monkey) are differences that arise in human cortical organization or in the techniques employed.

To examine the relation between the organization and reorganization, I have also investigated the capacity for plasticity in the human cortex following complete spinal cord injury (SCI). To assess the possible link between cortical map reorganization and perception, I have recorded the pattern of referred sensations in these patients. To investigate the physiological consequences of deafferentation, I have scanned 2 subjects with spinal-cord injury, including a subject with phantom pain.

Some of the results presented here have been included in previous reports (Gehi, 1996; Gehi et al., 1996; Moore et al., 1996; Moore et al., 1997; Moore et al., 1998; Moore et al., submitted).

Experiment 1: Characterization of Somatosensory Activation within the Mediolateral Extent of the Human PoCG with fMRI at 1.5 T

To define the position and extent of somatosensory activation within the human PoCG, we scanned subjects in a 1.5 T magnet during tactile stimulation of the palm, forearm, finger and thumb.

Methods

Functional Imaging Techniques

Subjects (N = 5 right-handed subjects, age 19-26, 4 women) were scanned with a head coil in a 1.5 T General Electric (GE) scanner modified for echo-planar imaging (EPI) by ANMR systems. An asymmetric spin-echo pulse sequence was employed to minimize the contribution of large vessels to the functional signal (Baker et al., 1993). Prior to functional scanning, a T1-weighted high-resolution (10 slices, 1.56 mm x 1.56 mm x 7 mm resolution; TE = 40 msec) scan was taken in the same slice plane as the functional images. These images were later used to localize functional activation anatomically. Functional scans (T2* weighted, asymmetric spin-echo sequence; TR = 2500 msec; TE = 70 msec) consisted of 10 slices oriented in the coronal oblique plane approximately parallel to the course of the PoCG (3.125 mm x 3.125 mm x 7 mm resolution: Figure 1A). A total of 96 images was taken per slice during each 4:00 min functional scan. Subjects received 8-10 scans per session.

Stimulation Parameters

Subjects received punctate tactile input with a $5.88_{log10.mg}$ von Frey hair at a rate of ~3 Hz. During stimulation, the subject's hand was supported with firm deformable foam cushioning. Stimulation was presented during 20 sec epochs alternated with 20 sec epochs of rest. Two types of tactile scans were conducted: Palm and forearm stimulation, and forefinger and thumb stimulation. During the palm and forearm scans, stimuli were presented in the following order; palm - off - forearm - off - palm+forearm - off - palm+forearm - off - forearm - off - palm - off. During thumb and forefinger scans, stimuli were presented in the following order; thumb - off - forefinger - off - thumb+forefinger - off - thumb+forefinger - off - forefinger - off - thumb - off. Stimuli were presented across the palm with the exception of the thenar eminence, the glabrous surface of the thumb and forefinger, and a ~3 in square region on the volar surface of the forearm. In one subject, stimuli were presented in alternating 30 sec epochs (palm - off - arm - off - palm - off - arm - off, similar pattern for thumb and finger beginning with the thumb). Stimuli were presented to the left or right side of the body on different functional scans.

Statistical Analyses

Individual scans were analyzed using the Kolmogorov-Smirnov (KS) nonparametric statistic (Xiong et al., 1996). Stimulation epochs were compared with neighboring epochs of no stimulation, and balanced for the order of the control epochs (i.e., control data were taken from epochs preceding and following stimulation). A statistical threshold of $p < .05$ was employed.

Anatomical Analyses

To have a consistent space for the comparison of activation position and extent within the PoCG, we developed the following approach to linearizing and

normalizing its anatomy. The basic transformation was to measure PoCG length as a single line from the medial to the lateral edge of the PoCG, and then to localize activation as a percentage of the total length of this linearized gyrus (Figure 1A). The central sulcus was identified by two anatomical landmarks: (a) The intersection of the superior frontal sulcus with the precentral sulcus; and, (b) the ascension of the cingulate sulcus in its marginal sulcus branch to the dorsal surface of the hemisphere (the central sulcus is the first sulcus anterior to the marginal sulcus in a sagittal view within ~6-10 mm lateral to the midline). The most posterior and medial section that included the PoCG in coronal view was then defined as Slice 1, and the length of the PoCG from the cingulate sulcus to the point where the PoCG left the slice plane within that section was recorded. This process was repeated for the more anterior slices until the point 1 cm above the lateral sulcus was reached. This point was defined as the end of the PoCG to avoid contamination of our measurements by activation in somatosensory representations within the Sylvian fissure (e.g., area SII). Functional activation was then assessed in each slice, and the position and size of each region of activation was measured. The length of the gyrus, which ranged from 90 to 120 mm in our sample, was then measured, and the position of activation regions along this length were translated into the percentage of the total length of the PoCG in that hemisphere (Figure 1A).

The benefits of this approach are threefold. First, straightening and normalizing the PoCG allows the quantitative comparison of the position of individual activations and the extent of activation along the PoCG across subjects. Second, it helps to align activation that originates in a single cortical representation but that is sectioned by the plane of the slice. Third, it allows the simultaneous visualization of activation in multiple slices along the PoCG, a kind of graphic display that is impossible in coronal oblique sections.

Data were quantified in three ways using this technique (Figures 1-4). A *region of activation* corresponded to a contiguous cluster of pixels that showed significant activation during the task, within one slice. The position of each region of activation was measured as a distance along the PoCG. An *overlapping region of activation* was defined as a location where several regions of activation, taken from different slices, overlapped in extent when the data were projected onto the normalized PoCG length. A *center of activation* was defined as the mean of the centers of each region of activation in a given hemisphere, and the *mean center of activation* is the mean position of each center of activation across hemispheres. These terms are graphically illustrated in Figures 1 through 4.

Figure 1 Anatomical reconstruction techniques for the localization of functional data A. In all experiments, coronal oblique sections were taken approximately parallel to the course of the PoCG (angled black lines over the brain). The red arrows mark the central sulcus. Stacks of vertical boxes represent the area of the PoCG in successive coronal oblique sections. In Experiment 1 and Experiment 4, the length of the PoCG from medial to lateral (lines within PoCG sections) was measured, and the distance of each activation (colored boxes) along this length was measured. Each one of these boxes corresponds to a *region of activation*. This measurement permitted the reconstruction of activation along a single length, which could then be normalized to permit comparisons across different brain sizes (bottom horizontal box). This also aided in the reduction of multiple activation sites across slices to a single *overlapping region of activation* (e.g., the red and yellow boxes overlapping in the bottom reconstruction). B. Data from Experiments 2 and 3 were displayed on reconstructed 3D brains. Using this approach, functional data were displayed on models derived from white matter/grey matter borders. Three models that were used for visualization analysis, from left to right, were the expanded white/gray matter model, the white matter model, and the inflated white matter brain (dark gray are sulci, light gray gyri). Red arrows indicate the central sulcus.

Figure 1

A.

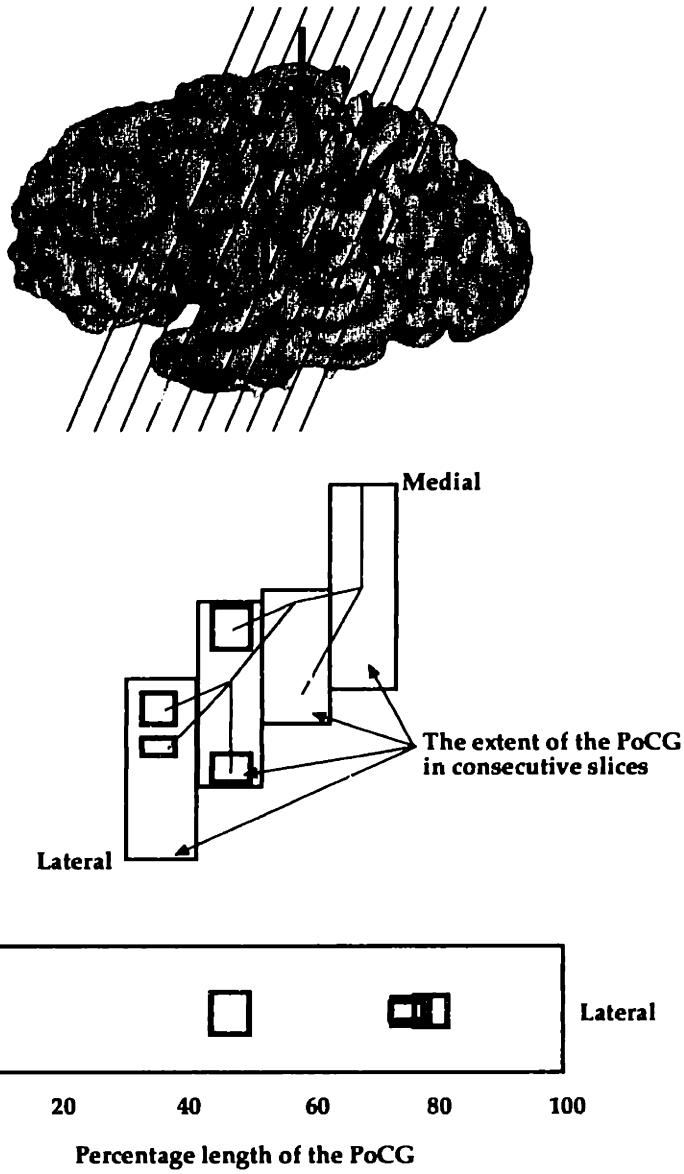
Medial
The extent of the PoCG
in consecutive slices
Lateral
Medial
Lateral
0
20
40
60
80
100
Percentage length of the PoCG

B.

Results

During tactile stimulation of the palm, the number of distinct regions of activation within the PoCG in a given hemisphere ranged from 1 to 14 (4.9 +/- 3.8 SD, N = 10 hemispheres), and the number of overlapping regions of activation ranged from 1 to 6 (3.0 +/- 2.0; Figure 2). All regions of activation were located within the lateral 80% of the PoCG or, approximately, lateral to the crest of the PoCG at the midline, and a majority (34/49, 69.4%) of the regions of activation were located within the lateral 50% of the linearized PoCG (Figure 3). The center of activations in each hemisphere was localized to a region between the 40% to 80% distance within the PoCG (mean center of activation 63.0% +/- 8.9 SD; Figures 2 and 4).

Forearm, thumb and finger stimulation demonstrated fewer total regions of activation than the palm (forearm 1.5 +/- 1.8 SD: finger 2.5 +/- 1.3: thumb 2.0 +/- 1.2), and fewer activated hemispheres (forearm 7/10: finger 9/10: thumb 9/10). The distribution of activation regions for these three representations was bimodal in shape, with a peak at 50% to 60%, and a second peak at 90% to 100% of the PoCG length (Figure 3). Within individual subjects, somatotopy (as predicted by the Penfield homunculus) was assessed by comparison of the centers of activation within a hemisphere. Using this method, somatotopy was maintained in 48% of comparisons. The average location of mean centers of activation for forearm, finger, and thumb stimulation (Figure 4) were localized to the region activated by the palm (see table in Figure 4).

Figure 2 Reconstructed activation for the left hemisphere following right palm stimulation in 5 subjects for 1.5 T scans The position of each *region of activation* is displayed as a percentage of the total length of the PoCG, stretching from medial (0) to lateral (100). Red boxes indicate each *region of activation*: Gold bars indicate the position of the *center of activation* for that hemisphere.

Figure 2

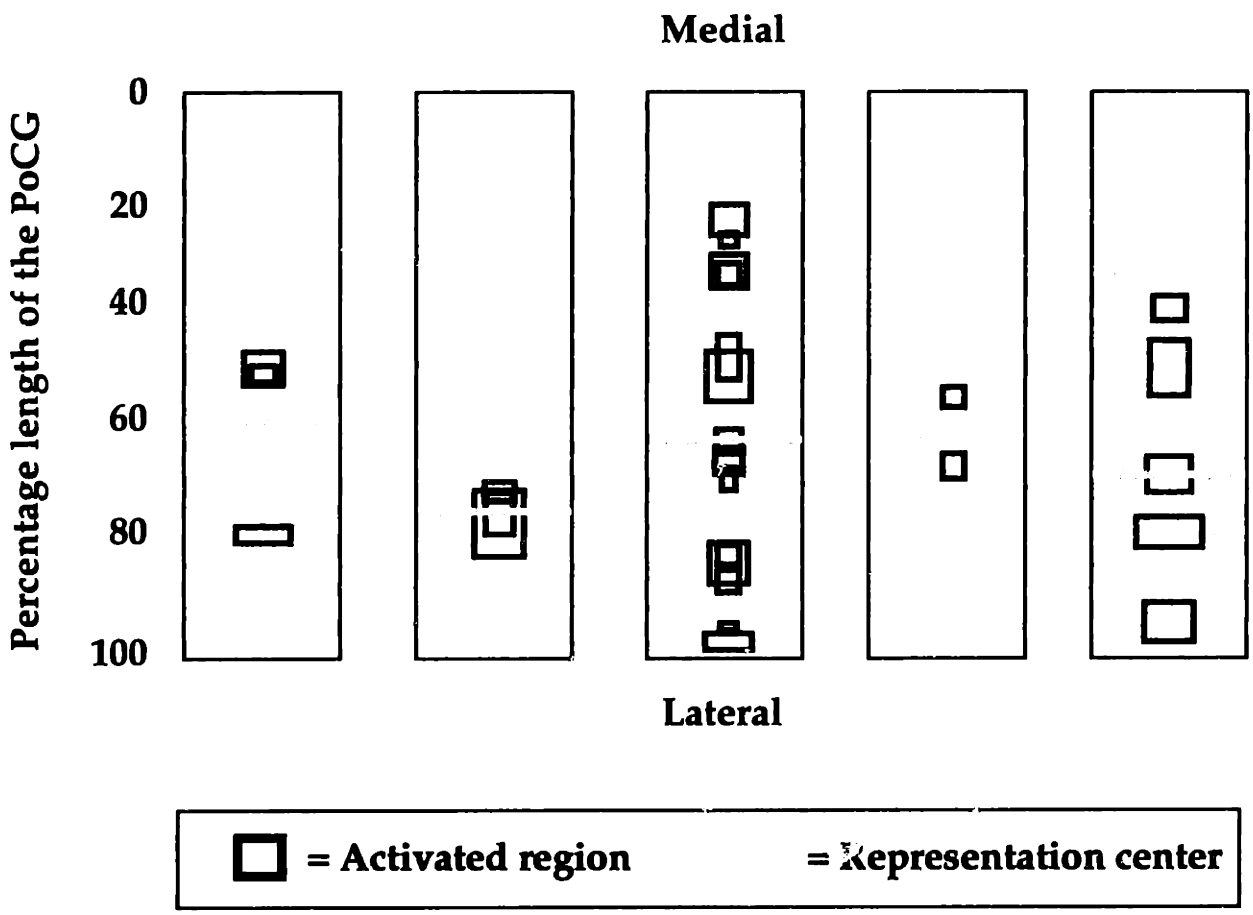
Medial
Percentage length of the PoCG
0
20
40
60
80
100
Lateral
= Activated region
= Representation center

Figure 3 Histograms of the position of activation across subjects *Top histogram* The position of region of activations evoked by palm stimulation is plotted for all subjects (N = 10 hemispheres). Note that all activations are localized to the lateral 80% of the gyrus, and the majority of activations are localized to the lateral 50% of the gyrus. *Bottom histogram* The normalized position of forearm (red), finger (green) and thumb (blue) regions of activation (N = 10 hemispheres). Note the bimodal distribution of the histogram, with a peak at 50-60% of the total PoCG length and a second peak 90-100% of the PoCG length.

Figure 3

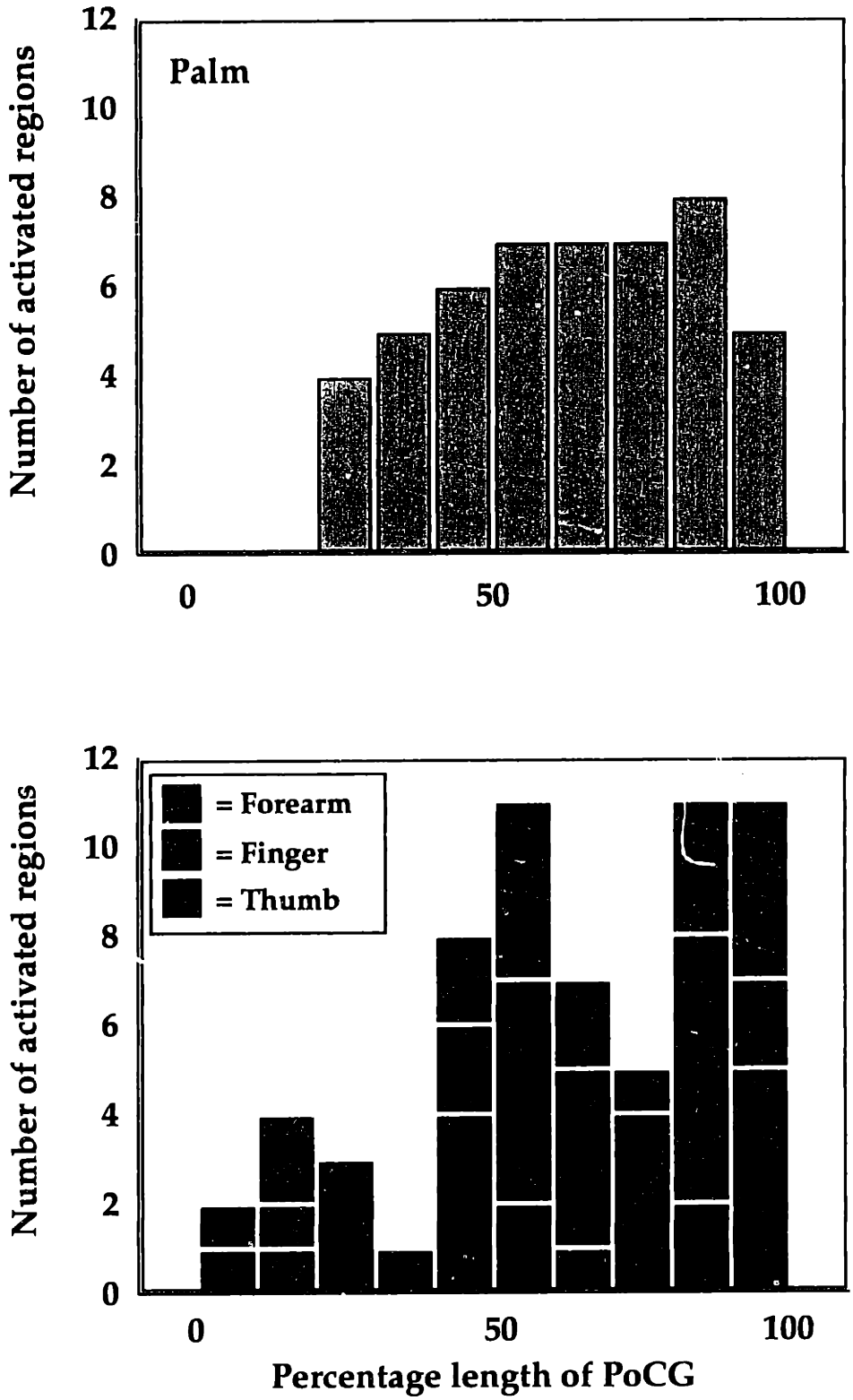
Palm
Number of activated regions
12
10
8
6
4
2
0
0
50
100
= Forearm
= Finger
= Thumb
Number of activated regions
Percentage length of PoCG

Figure 4 Position of mean activation centers The center of activation for each hemisphere was averaged to form a composite somatotopic map of the *mean center of activation* (A = forearm; F = finger; P = palm; T = thumb). Data are shown in relation to the Penfield homunculus (from Penfield and Rasmussen, 1950). The table displays the mean +/- SD for the centers of activation for each representation.

Figure 4

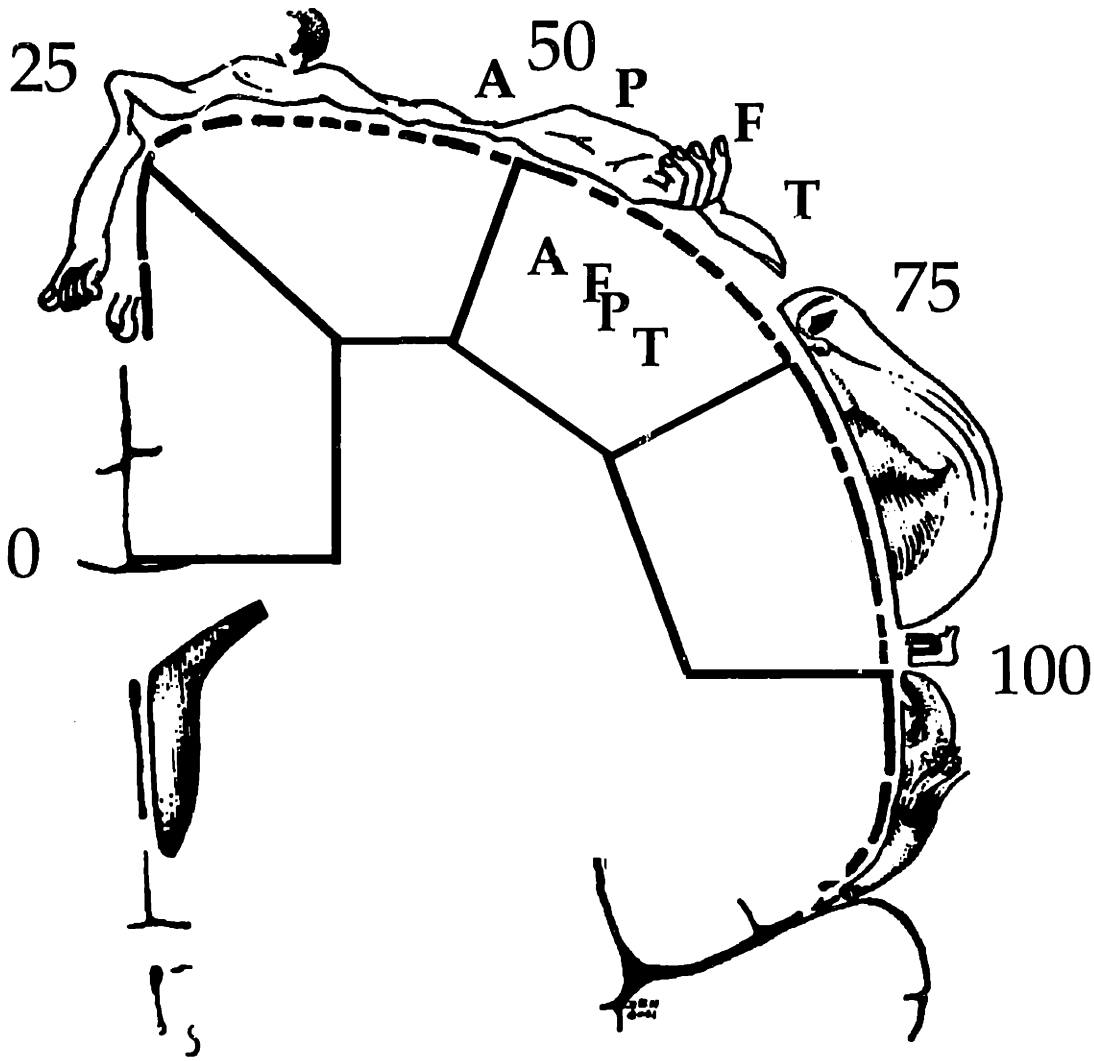

Area Stimulated	Forearm (A)	Palm (P)	Forefinger (F)	Thumb (T)
Average Position (N = 10 hem.)	56.9 +/- SD 22	63.0 +/- SD 8.9	60.0 +/- SD 15.7	68.8 +/- SD 13.7

Discussion

In Experiment 1, tactile stimulation of the palm evoked regions of activation in the contralateral PoCG in all subjects. Evoked activity was located in the lateral two-thirds of the gyrus across subjects, and in up to 6 overlapping regions of activation throughout the lateral extent of the PoCG in a single subject. Fitted to the Penfield homunculus, the spread of signal we observed suggests overlap between the hand and putative face representation. Although Penfield and Rasmussen (1950) reported that ~30% of the stimulation sites within the hand representation evoked overlapping sensations in the hand and in at least one other peripheral region (e.g., hand and forearm), these coincident perceptions originated from areas that were more local within the map. The spread of this activation was greater than that predicted by Penfield and colleagues.

In agreement with the Penfield homunculus, the center of activation in Experiment 1 during stimulation of the forearm, finger and thumb was localized to the same region of the PoCG as the palm. However, the precise somatotopic ordering of the center of activation of these areas in individual subjects occurred at chance levels (48%). Further, unlike palm activation, arm stimulation activated the PoCG in only 7 of 10 contralateral hemispheres, and finger and thumb stimulation each demonstrated a single example of non-activation (9 of 10 hemispheres).

There are several potential methodological causes for the extensive spread of activation observed in Experiment 1. First, because of the exploratory nature of the Experiment, we employed a permissive statistical threshold ($p < 0.05$), that inflated the probability of type 1 error (Locasio et al., 1997). Second, the reconstruction technique we used traced a single length of the PoCG. This simplification has several advantages, including facilitating the quantitative comparison of activation patterns between subjects, control for variance in the size of the PoCG, and the alignment of activations that were located in different functional slices that are actually part of a single contiguous activation (Figure 1). Nevertheless, this technique may have failed to identify overlap in activated regions within the gyrus. Finally, despite our attempts to truncate the measured length of the PoCG to avoid contamination with activation in area SII, the activation we observed may have constituted spread of signal from SII upwards into the measured region of the PoCG. This overlap is suggested by the most lateral peak (90%-100%) within the distribution of activations for the forearm, finger and thumb.

Experiment 2: Characterization of Somatosensory Activation within the Mediolateral Extent of the Human PoCG with fMRI at 3 T

To address the questions posed by Experiment 1, we replicated the tactile stimulation paradigm with improved scanning techniques. These included scanning with a 3 T magnet, increased number of functional scans and stimulus epochs per subjects, and 3D whole brain visualization techniques (Sereno et al., 1995).

Methods

Imaging Techniques

Right-handed subjects (N = 5, age 20-31 yr, 2 female) were scanned in a 3 T General Electric scanner with a GE birdcage head coil. Two subjects (not included in the total N) were eliminated from analysis post hoc; the first subject because she was lefthanded, and the second subject because he suffered from chronic repetitive strain injury syndrome. Both subjects nonetheless activated the predicted regions of the PoCG. Before and after functional scanning, a high resolution T1-weighted anatomical scan was taken (TE = 57 msec). Functional scans consisted of 16 slices oriented in a coronal oblique plane approximately parallel to the course of the central sulcus (voxel size = 3.125 mm x 3.125 mm x 4 mm: TR = 2000 msec TE = 50 msec; Figure 1). A total of 128 images per slice were taken for each 4:16 minute functional scan. Each subject received a minimum of 2 functional scans that were averaged prior to data analysis.

Stimulation Parameters

A functional scan consisted of periods of stimulation (16 sec) alternated with periods of no stimulation (16 sec), for a total of 8 cycles of on/off stimulation. Tactile stimulation of the palm was administered as in Experiment 1. In addition, two subjects received stimulation of the glabrous surface of the middle finger at a rate of 3 Hz (2 functional scans per subject). Subjects were instructed to keep their eyes closed during functional imaging and open between scans.

Statistical Analyses

Frequency-based and t-test statistical analyses were performed on a voxel by voxel basis in all subjects. In the first approach, a Fourier analysis was performed on the activation in each voxel over the full functional scan period. An F-test was then conducted, comparing the ratio of the signal at the stimulus frequency with all other frequencies. The second method pooled activation across stimulation epochs and compared it with the signal during non-stimulation epochs, with a 2 sec hemodynamic delay (Chapter 2, Figure 1) factored into the rise and fall time of the BOLD signal. Almost identical activation maps were generated by these two analyses. Analysis of the volume of the cortical area in the PreCG and PoCG region in 3 subjects (Cardviews), recommended a Bonferroni correction for the analysis of 2000 pixels ($p < 0.01$, corrected p value).

Anatomical Analyses

Inflated brain analysis techniques were conducted as described in Sereno et al., 1995 and Tootell et al., 1997 (Figure 1B). An initial SPGR high-resolution anatomical scan was taken for each subject (128 slice, 1.0 cubic mm; head coil, 1.5 T

GE or Siemens scanner). From this scan, the grey-white matter border was defined using a region-growing approach, and this border was tesselated to form a surface. The surface was fitted against MRI data, and clear surface defects were corrected, if needed, by manual inspection. Following each functional scanning session, the surface was aligned with the high-resolution T1 scan (1.5 mm x 1.5 mm x 4 mm), to correct for differences in the orientation and position of the brain in individual experiments. Functional data were then interpolated onto the surface and the brain was inflated by an algorithm that employed curvature reduction and local area-preserving terms (Dale and Sereno, 1993).

Results

In Experiment 2, we employed a 3 T magnet, which has higher signal and signal-to-noise ratio than the 1.5 T magnet (Thulborn et al., 1998), and used the reconstruction techniques of Dale and Sereno (1993). In this study, we found that all subjects (N = 5) demonstrated a region of activation in the PoCG at the level of the first posterior bend of the central sulcus (Figure 5). This finding is in agreement with fMRI activation of the motor hand representation, which has been localized to the corresponding region of the precentral gyrus (Fink et al., 1997; Grafton et al., 1996; Porro et al., 1996; Rao et al., 1995; Sanes et al, 1995; Yousry et al., 1997). This area, the extent of the PoCG within the first posterior curve of the central sulcus, will be referred to as the *hand area*. In addition to activation in the hand area, and in agreement with Experiment 1, all subjects also demonstrated activation lateral to the hand area within the PoCG. Although the pattern of lateral activation was more variable than that seen within the hand area, activation was present in 3 of 5 subjects in a region ~1 cm lateral to the hand area activation, and in 4 of 5 subjects as a dorsal extension of activation in the Sylvian fissure (putative area SII; Figure 5).

Finger (N = 2) and forearm (N = 4) were also stimulated in a subset of subjects. During finger stimulation, both subjects demonstrated activation within the anatomically defined hand area that was lateral to and overlapping with activation of the palm (Figure 6). Arm stimulation failed to activate the PoCG in Experiment 2 in individual subjects (N = 0/4)[3].

Figure 5 Palm activation at 3 T displayed on the inflated brain *Top boxes* Activation from 3 subjects is displayed on inflated (top row) and white/gray matter models (bottom row) of the brain. As demonstrated in white/gray matter models of these three hemispheres, activation was observed in three locations along the PoCG during palm stimulation: The hand area, a region lateral and proximal to the hand area, and in the invasion of activation by area SII into the PoCG. These two areas correspond with the two peaks in the distribution of finger, thumb and forearm activation locations in Figure 4. *Bottom inflated brain* The location of these three activations is shown on an inflated brain, enclosed in each ROI is the number of subjects that demonstrated activation in this region.

---

[3] We have recently used a new averaging technique to combine funcitonal signal across subjects (Moore, Dale and Fischl, unpublished observations). Using this technique, palm activation demonstrated a segregation of activation within the PoCG analogous to that predicted by the position of the palm at the border of areas 3b and 1 and within area 2 in the macaque monkey (Nelson et al., 1980). Further, averaging across subjects brought out a significant ($p < .01^{40}$) signal following arm stimulation. However, because the precision of this averaging technique is being assessed (e.g., SII activation was significantly shifted away from the position observed in individual subjects), the data were too preliminary to report at the time of submission.

Figure 5

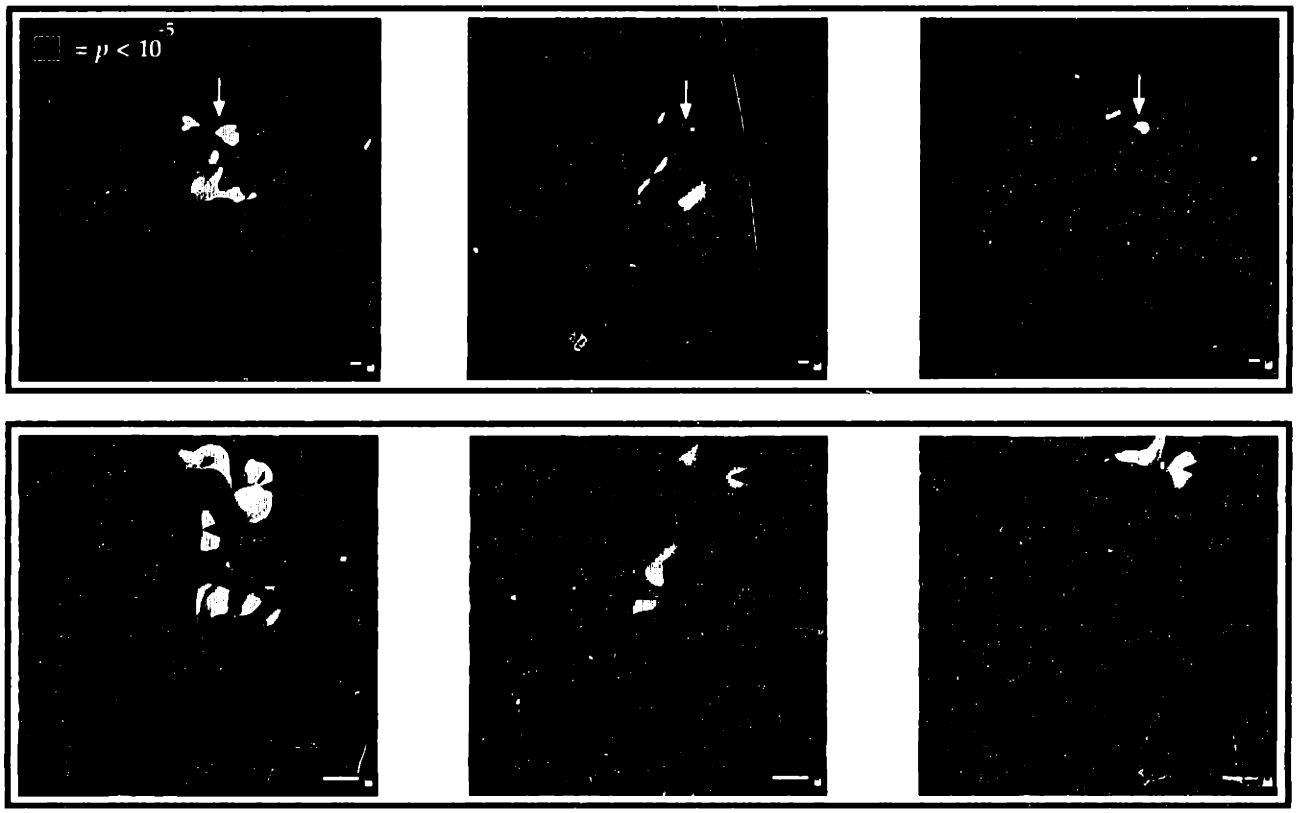

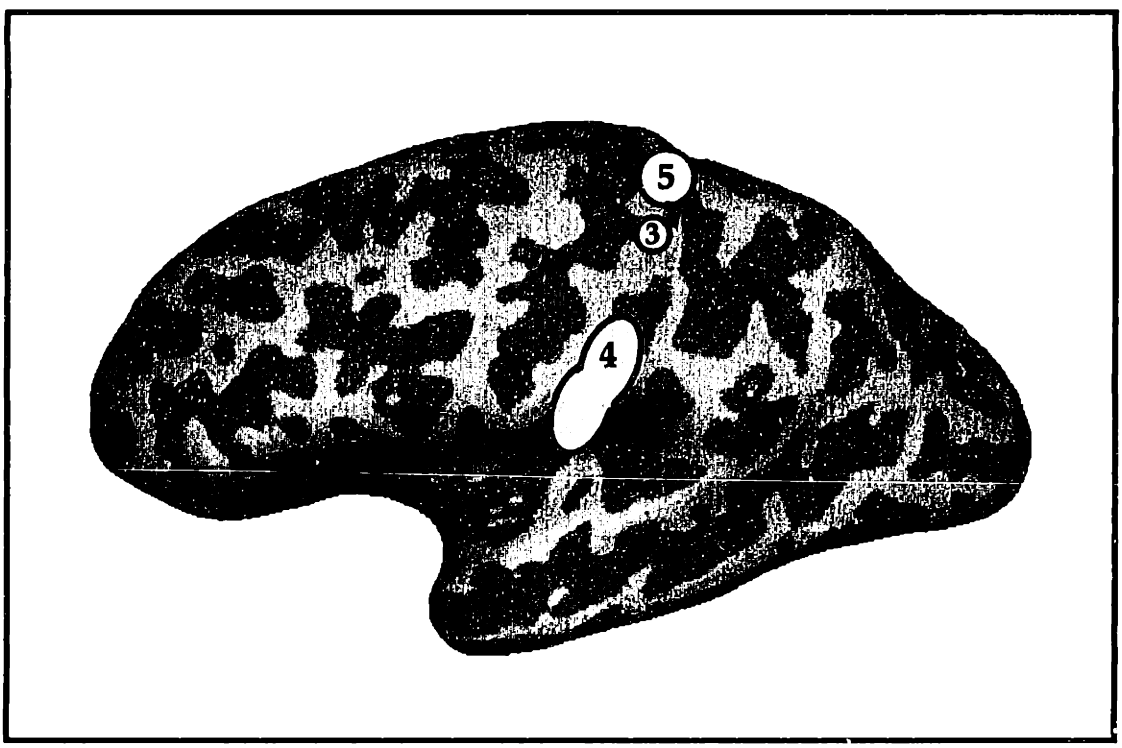

Discussion

Activation in the Hand Area

Experiment 2 confirmed and refined the observations made in Experiment 1. As in the first study, stimulation of the palm activated the contralateral PoCG in all subjects, and this activation was limited to the lateral two-thirds of the gyrus. The most medial activation was observed in the hand area of the PoCG, identified as the first posterior bend of the central sulcus. This region is located at approximately the mediolateral position of the PoCG suggested by Penfield and colleagues as the position of the hand representation and, the position of the hand representation in the first posterior bend of the central sulcus can be seen in their reconstruction of individual stimulation-defined homunculi (e.g., Figures 13 and 16 of Penfield and Rasmussen, 1950). More complete analysis of activation within the hand area is presented in Experiment 3.

Activation Lateral to the Hand Area

In agreement with the first study, activation was also observed more laterally within the PoCG during palm stimulation: In Experiment 2, we observed activation in three PoCG zones during tactile stimulation of the palm. The consistency of multiple activation sites across our two studies suggests that it is not the product of the permissive statistical threshold we employed (Experiment 2 was conducted with a rigorous Bonferroni correction for multiple tests). Further, the mean number of overlapping regions of activation in Experiment 1 (3.0 +/- 2.0 SD) is in good general agreement with the 3 regions of activation we observed in Experiment 2 (Figure 5).

The lateral palm activation we observed proximal to the hand area may be the representation of input from the medial nerve of the palm, as suggested by detailed electrophysiogical mapping studies in the monkey. Nelson et al. (1980, Figure 10; see also Kaas et al., 1979, Figure 2) reported a segregation of the palm representation in the macaque monkey in areas 3b and 1 into two distinct representations of the ulnar and medial nerves, separated by the representation of the digits, and Merzenich et al. (1978; Kaas et al., 1979) reported a continuous, somatotopically organized representation of the palm stretching from medial to lateral. Because we did not stimulate the thenar eminence of the palm, we would predict more robust activation in the ulnar representation of the glabrous surface of the palm, and weaker activation, driven only by contact on the pads adjacent to the fingers, in the radial palm representation. This expected pattern is consistent with our data: In all subjects, the hand area representation was activated, while in 3 of 5 subjects, a more lateral area was activated. In two subjects, this activation extended from the hand area, suggesting a continuous representation, and in 1 subject the more lateral activation area was distinct, suggesting a fractured palm representation.

The second, more lateral region of activation observed in 4 subjects corresponds to a dorsal spread of signal into the PoCG from activation in the Sylvian fissure. Penfield and Rasmussen (1950) observed area SII as posterior to the intersection of the PoCG and Sylvian fissure, and in individual cases (e.g., Figures 60 and 71 of Penfield and Rasmussen, 1950), this representation was located in the postcentral sulcus. Our data are in agreement with this localization, as we observed activation extending from the edge of the Sylvian fissure dorsally through the postcentral sulcus, overlapping with the edge of the PoCG (Figure 5). This observation is also in agreement with several PET studies (Seitz and Roland, 1992; Burton et al., 1997; Coghill et al., 1994; Prado et al., 1997) that have more recently

localized SII to the parietal operculum. The extent of activation in area SII into the PoCG in Experiment 2 suggests that the more lateral activation peak observed in Experiment 1, that appeared to overlap with the face representation, was probably the result of activation in parietal operculum that is continuous with SII.

Somatotopy at 3 T

With the 3 T magnet, our limited sample of finger stimulation scans (N = 2) in Experiment 2 suggest that the failure to recover fine somatotopy is an artifact of the reconstruction and/or the 1.5 T imaging techniques we employed in Experiment 1. Using the 3 T scanner, an increased number of stimulus cycles, and Dale and Sereno reconstruction techniques, we observed that the center of finger activation in the anatomical hand area is lateral to the center of palm activation, and the extent of activation of these two representations is overlapping. This finding is in agreement with Penfield and Rasmussen (1950), who reported that finger representations are lateral and adjacent to (and often overlapping with) the palm representation. This finding is also in agreement with fMRI studies of somatotopic ordering in motor cortex, where neighboring representations have shifted centers of mass but overlapping extent (Kleinschmidt et al., 1997; Rao et al., 1995; Sanes et al., 1995).

The inability to resolve fine somatotopy in Experiment 1 is probably the result of several factors, including the lower signal-to-noise ratio of the 1.5 T scanner and of our stimulation paradigm, and variability introduced by our straightening and normalizing techniques. The method we used for identifying the "center" of the representation may also have contributed to this error, as we defined the center as the mean of the position of regions of activation along the gyrus. The overlap of the most lateral extent of the gyrus by activation in the Sylvian sulcus was included in our PoCG sample, and may have shifted the representation laterally within the gyrus (e.g., Figure 4). The divided/extended palm representation we observe at 3 T may also have contributed, as palm activation extended through the finger representation (N = 2) or was rerepresented on the lateral edge of the finger representation (N = 1) in three subjects, predicting the overlap in the average center of activations we observed at 1.5 T in these two representations.

Stimulation of the forearm in Experiment 2 failed to activate the PoCG in any subject. This finding is in general agreement with the results of Experiment 1, where 3 of 10 cases failed to activate the PoCG despite the use of a permissive statistical threshold. In contrast, we observed activation in the parietal operculum at the position of SII during arm stimulation (Coghill et al., 1994; Penfield and Rasmussen, 1950) in 3 of 4 number of subjects (data not shown). Failure to activate the forearm representation within the PoCG may be the result of the relatively smaller and more variable representation of the forearm within the primate PoCG (Merzenich et al., 1978).

Comparison of Experiments 1 and 2

Experiment 2 provided several methodological improvements over Experiment 1. We employed increased frequency of stimulus epochs, an improvement that reduced noise in the signal (McCarthy et al., 1996), and increased the statistical power. Further, (a) we sampled data at approximately double the spatial in-plane resolution (3 T magnet, 4 mm vs. 1.5 T magnet, 7 mm), (b) the 3 T added approximately twice the signal-to-noise ratio achieved in the 1.5 T (Thulborn et al., 1998), and (c) the signal amplitude we observed was increased by use of a non-

asymmetric spin-echo sequence (Baker et al., 1993). These improvements taken into account, the reconstruction techniques employed at 1.5 T nevertheless captured many key aspects of map organization within the PoCG: (a) Activation at 1.5 T with the linearized gyrus was localized to the lateral two-thirds of the PoCG; (b) it demonstrated the same mean number (3) of overlapping regions as the 3 T; (c) the center of the palm activations was localized to approximately the same region of the PoCG predicted by the Penfield homunculus; and, (d) the activation of the lateral extent of the PoCG by activity spreading from SII was observed. We conclude that the reconstruction techniques employed at 1.5 T, if combined with more robust imaging measures, provide a useful quantitative approach to the estimation of activation and spread within the PoCG. This approach has utility because it controls for the size of the PoCG in individual subjects, and because more elaborate reconstruction techniques require additional scanning and computational manipulations, limiting the population of subjects that can be analyzed.

Experiment 3: Segregation of Multiple Somatosensory Areas within the Human Central Sulcus Region

To this point, the analysis presented has focused on the mediolateral organization of function within the human PoCG. As discussed in the introduction to this Chapter, there is also an anterior-posterior segregation of function within the central sulcus region of the monkey: Several distinct areas in this region code for separate submodalities of somatosensory input (Kaas et al., 1979; Jones and Porter, 1980). To investigate the presence of these areas in the human, we have scanned subjects at 3 T during tactile and proprioceptive/motor stimulation of the hand.

Methods

Scanning methods were identical to those in Experiment 2 with the following exceptions.

Stimulation Parameters

Proprioceptive/motor scans were presented with the same alternating stimulation cycle as the tactile scans. During the proprioceptive/motor task, subjects held their arm bent at the elbow with their hand above their chest and flexed and extended the metacarpal and interphalangeal joints of the fingers and thumb of the right hand at a rate of 3 Hz (Rao et al., 1996; Schlaug et al., 1996), without touching the fingers to either neighboring digits or to the palm surface (as if squeezing an imaginary tennis ball). The 3 Hz rate of motor output was maintained through training prior to scanning and through an auditory metronome input played to the subject. Due to the noise generated by the scanner, one subject was unable to discriminate consistently the metronome, and squeezed at a self-paced rate of 2-5 Hz (this subject was able to detect the "go" and "stop" commands at the beginning and end of each activation epoch). All subjects were visually monitored for compliance with squeezing rate during the scanning session. Functional scans were counter-balanced for scan order within subjects, with the caveat that a tactile scan was always first. Subjects were instructed to keep their eyes closed during functional imaging and open between scans.

Anatomical Analyses

As a companion analysis to the functional segregation of somatosensory representations, we used the sulcal and gyral pattern in individual subjects to demarcate anatomical borders in the human subject that corresponded to areal borders within the primate. We defined seven anatomical regions of interest centered over the hand representation in each subject (Figure 8, top diagram), that correlated with the cytoarchitectonic areas surrounding the central sulcus: Brodmann areas 6, 4, 3a, 3b, 1 and 2 (Brodmann, 1909; Geyer et al., 1997; White et al., 1997). In addition, a seventh area was defined in the depth of the postcentral sulcus. Although there is between subject variability in the correspondence between cytoarchitecture and gross human neuroanatomy (see Geyer et al., 1997 for a detailed assessment of radioligand binding in the PoCG; White et al., 1997, for a detailed assessment of the extent of 4, 3a and 3b in humans; and, Jones and Porter, 1980, for a review of the variability in the localization of area 3a in humans and primates), separate examinations of the pattern of cytoarchitecture within the human PreCG and PoCG agree on the following associations across subjects at the level of

the hand area: Area 6 can be localized to the crest of the PreCG, area 4 to the anterior wall of the central sulcus, area 3a to the depth of the central sulcus, area 3b to the posterior bank of the central sulcus, area 1 to the crest of the central sulcus, and area 2 to the posterior bank of the PoCG. Because the extent of these areas in the transition points between horizontal wall and crest of gyri is probabilistic within the human population, activation that was ambiguous in location (e.g., on the edge of a gyral crown) was marked as activation in a border region (thin wedges of the Figure 8 color-coded maps), to help reduce the probability of misattribution. The segregation of activation into these areas was completed by two independent observers (C. M. and A. Gray), with agreement on all assignments to the areas listed except 1 (34/35, 97%).

Results

In all subjects, tactile stimulation of the hand activated two distinct foci, a PreCG region and a PoCG region, segregated by a "gap" region of non-activation. This pattern can be seen in the palm and finger activation maps in Figure 6 (left and center columns of brain maps). In contrast, proprioceptive/motor stimulation activated the PreCG, the gap region, and the PoCG in all subjects (Figure 6, righthand column of activation maps). Using the borders functionally defined by the palm tactile activation task, time series were generated in each subject for the PreCG and PoCG regions, and for the gap. As predicted by the statistical maps, the PreCG and the PoCG tactile regions showed increased percentage signal change during the tactile task, while no change was observed in the gap region (Figure 7, first set of time series). During proprioceptive/motor activation, all three regions defined in the tactile task demonstrated increased percentage signal change (Figure 7, second set of time series). Signal increase in the gap region was significantly greater during the proprioceptive/motor task than during the tactile task, but there was no significant difference in the amplitude of signal increase in the PoCG and PreCG regions for the two stimulation paradigms (*PreCG*: tactile, .97% +/- .30 SD vs. proprioceptive/motor, 1.13 +/- .53: *PoCG*: .93 +/- .17 vs. 1.44 +/1 .58: $p > .05$: *Gap*: tactile .17 +/- .29 vs. proprioceptive/motor 1.7 +/- .71: $p < .01$; Figure 7, bar graphs).

As a companion analysis to the functional segregation of somatosensory representations, we used the sulcal and gyral pattern in individual subjects to demarcate anatomical borders in the human subject that correspond to Brodmann area borders. We found that the depth of the central sulcus, corresponding to Brodmann area 3a, was active in only 1 of 5 subjects during tactile stimulation, while the same region was activated in all subjects during proprioceptive/motor stimulation (Figure 8; Table 1).

Table 1: Localization of Activation During Tactile and Proprioceptive/Motor Tasks

Stimuli\Areas	6	4	3a	3b	1	2	dPoCS
Tactile	5	2	1	5	5	4	1
Proprioceptive/Motor	5	5	5	5	5	3	1

Numbers in each cell = subjects activating this portion of the PoCG. See Figure 8 and text for details.

*Figure 6 **Activation within the hand area during proprioceptive/motor and tactile tasks is segregated to distinct cortical areas** Top* On the filled white/gray matter model, the position of the hand area in the first posterior genu of the PoCG is marked by the black box. The black arrow shows the position of the central sulcus. A cartoon of the hand area on the right shows the position of the PreCG, central sulcus and PoCG for the white matter models displayed below. *Bottom* Activation is shown for 2 subjects during palm tactile, finger tactile and proprioceptive/motor tasks. During the tactile tasks, activation was observed in a PreCG and a PoCG region but not in a gap region spanning the central sulcus. During the proprioceptive/motor task, all three regions defined by the tactile task were activated. Note also that the mediolateral extent of tactile activation for the finger and palm stimulation is coextensive with the activation during proprioceptive/motor activation, which recruits muscles from both the fingers and the palm.

Figure 6

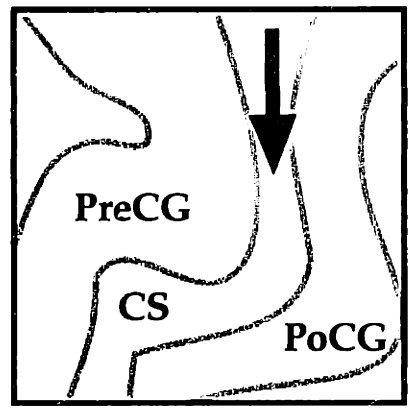

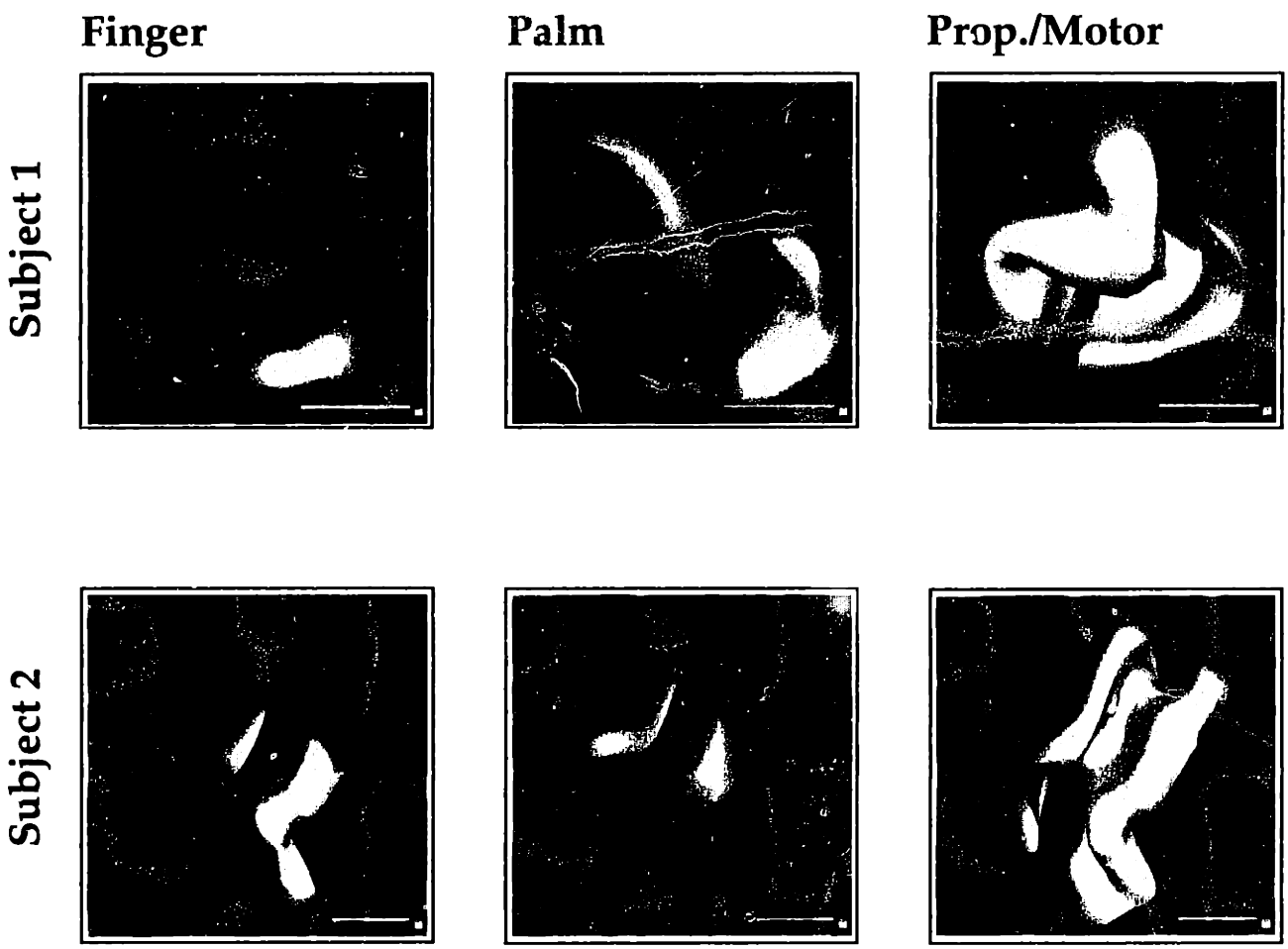

Figure 7 Timecourse of activation in the PreCG, gap and PoCG regions for tactile and proprioceptive/motor tasks *Top graphs* As predicted by the statistical maps, increased percentage signal change during tactile stimulation is observed in the PreCG (purple) and PoCG (yellow) regions but not in the gap region (red). During proprioceptive/motor task, activation is observed in all three regions. Grey background indicates the duration of the task (16 sec). Each trace represents the average of 6 stimulation epochs within a given subject, in turn averaged across 5 subjects. *Bottom bar charts* The mean percentage signal change for the period 4 sec to 20 sec following the onset of the task. Striped bars indicate signal change during the proprioceptive/motor task, solid bars signal change during the tactile task. Asterisk indicates significantly greater signal increase in the gap region during proprioceptive/motor than tactile stimulation ($p < .01$). Each bar is the mean +/- SD for activation averaged across 5 subjects.

Figure 7

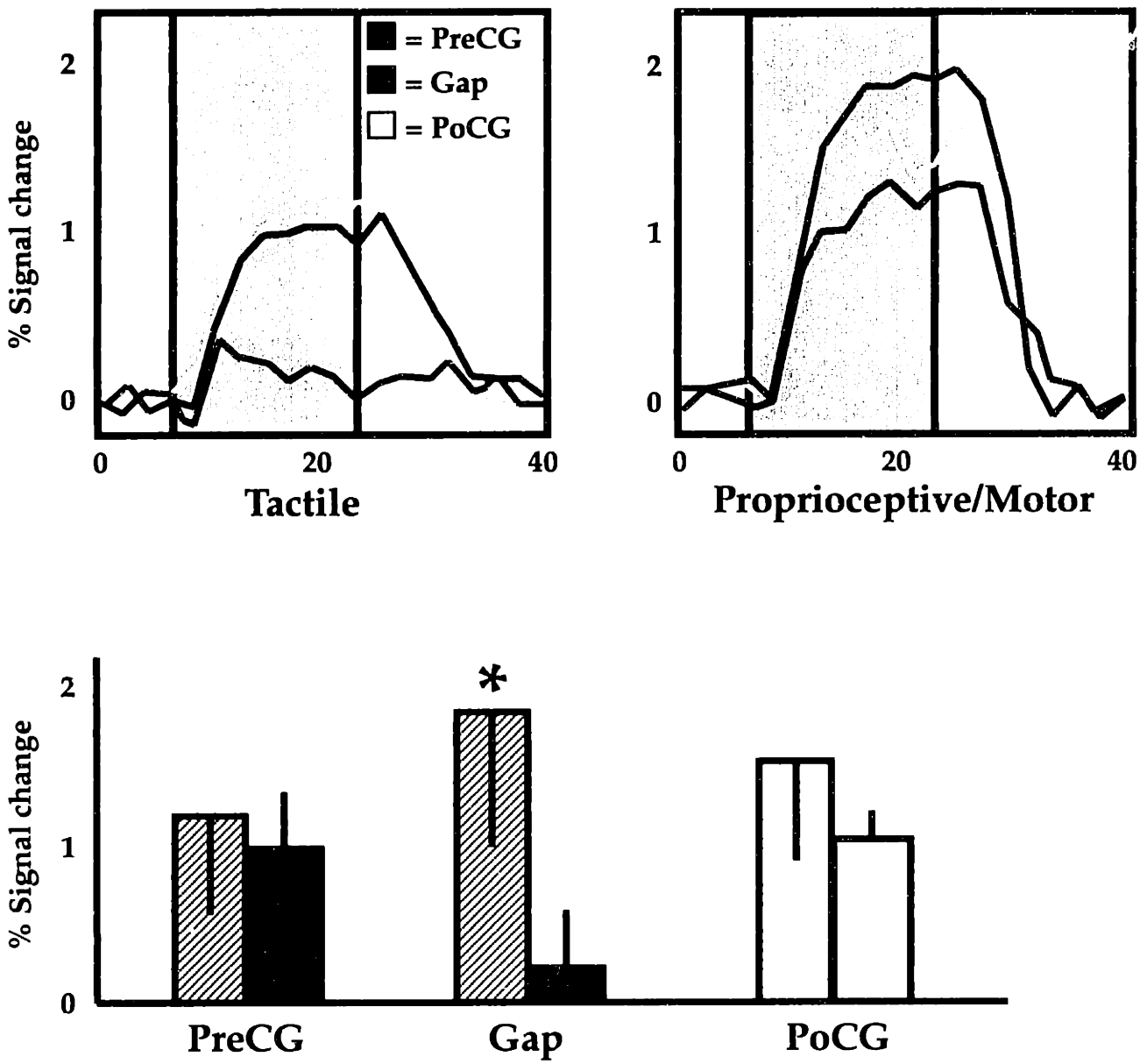
= PreCG
= Gap
= PoCG
% Signal change
2
1
0
0
20
40
Tactile
Proprioceptive/Motor
*
PreCG
Gap
PoCG

Figure 8 Activation in discrete gross anatomical foci during tactile and proprioceptive/motor stimulation *Top box* The presence of activation was quantified in 7 distinct regions within the central sulcus hand area. The corresponding Brodmann areas are displayed within each anatomically defined region on a sagittal cross-section (PoCS marks the depth of the postcentral sulcus). Between regions, borders (non-numbered wedges) were defined to reduce the probability of misattribution of activation. The position of the PoCG, PreCG and precentral sulcus (PreCS), and central sulcus (CS) is marked to orient the reader. *Bottom color-coded plots* Color-coding corresponds to the number of subjects demonstrating activation in each region. Activation during tactile stimulation was localized to the PoCG (areas 3b, 1 and 2) and the PreCG (area 6), but was present in only one subject in the depth of the central sulcus (area 3a). Activation during proprioceptive/motor stimulation was present in the PreCG, PoCG and central sulcus regions, but did not extend beyond area 2 into the depth of the postcentral sulcus.

Figure 8

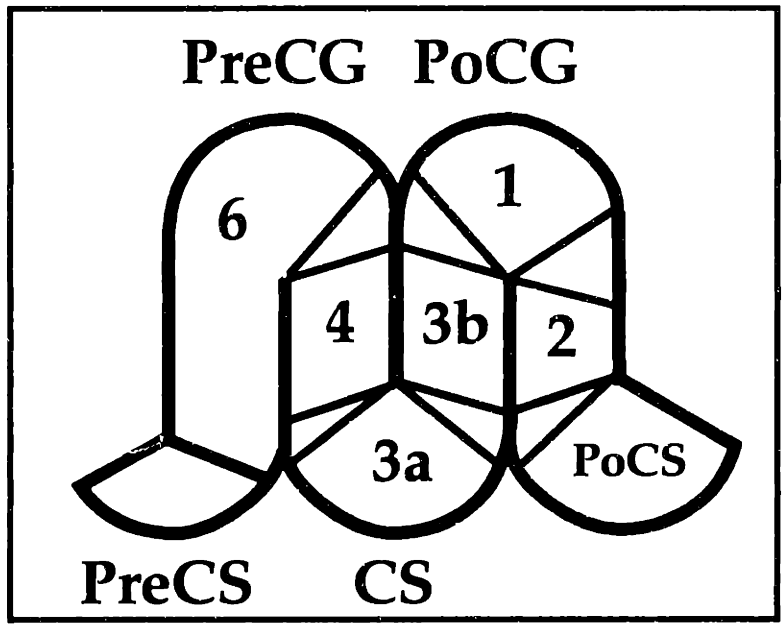

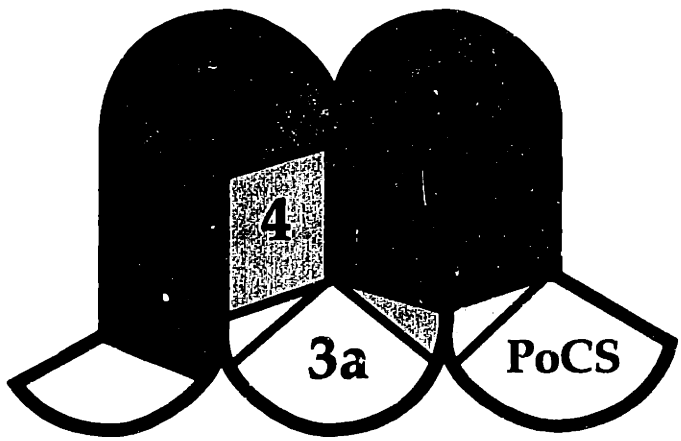

Tactile

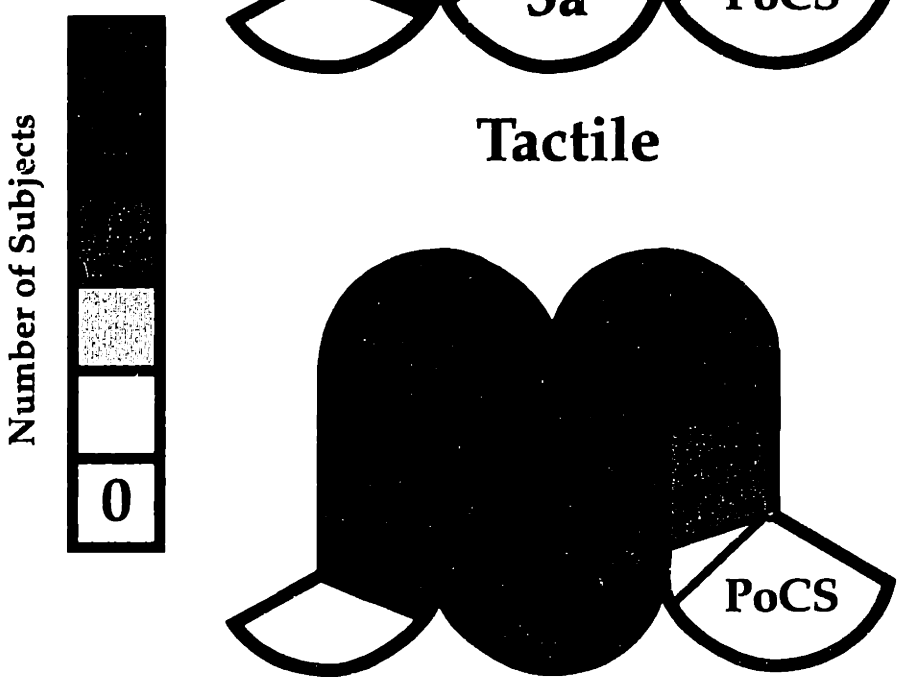

Proprioceptive/Motor

Discussion

These results provide the first conclusive evidence for the segregation in the human of multiple somatosensory areas in the region surrounding the central sulcus. Using fMRI, we resolved activation in three distinct, functionally defined representations within the hand area during tactile and proprioceptive/motor stimulation: A PoCG region, a gap region and a PreCG region. During tactile stimulation, the PoCG and PreCG region were activated, defining an unresponsive gap region between them. The position of these activations correspond to areas 3b, 1 and 2 for the PoCG activation, area 3a for the gap region, and area 6 for the PreCG region. These areas have been shown to possess similar response properties in the monkey, suggesting that organization in the human cortex is analogous to that seen in the monkey.

The assignment of activation to Brodmann areas defined by sulcal/gyral landmarks within the central sulcus region is probabilistic within the human population (Brodmann, 1909; Jones and Porter, 1980; White et al., 1997). However, we believe these assumptions are reasonable, given the conservative estimation of areal attribution (use of border regions) and the consistent localization of these regions in the hand representation across recent studies of receptor binding and cytoarchitecture in human cortex (Geyer et al., 1997; White et al., 1997). Further, the goal of areal attribution in this study is to examine the distribution of activations across subjects relative to the anatomy surrounding the PoCG. If areal attribution based on anatomical landmarks is incorrect in a minority of subjects[4], the activation pattern is nonetheless ubiquitous in our sample, and conclusions drawn from stimulation are reasonable to apply to the population (i.e., the position of the Gap region correlates with the probable position of area 3a within our sample).

Correspondence with the Monkey Literature

Definition of Putative Human Area 3a

The selective activation of putative area 3a during proprioceptive/motor but not tactile stimulation is predicted by recordings in the monkey (Jones and Porter, 1980; Iwamura et al., 1993; Kaas et al., 1979; Rencanzone et al., 1992a). Area 3a in the monkey receives input from the ventral posterior superior nucleus of the thalamus (Cusick et al., 1985), which encodes exclusively deep and proprioceptive inputs. Neurons in area 3a are effectively driven by proprioceptive and deep receptor inputs, but only a minority (~10% to ~25%; Iwamura et al., 1993; Rencanzone et al., 1992a) of neurons in this area, localized to the border of area 3b, respond to superficial contact of the skin surface. The definition of area 3a in the human and monkey has been the subject of some debate, as this region shows greater anatomical variability between subjects and has less rigid anatomical borders than other regions within the central sulcus region (Jones and Porter, 1980; White et al., 1997; but see Geyer et al., 1997). Our functional mapping suggests that area 3a has predictable and relatively well-defined physiological borders in the human.

Activation in the PoCG and PreCG During Tactile Input

---

[4] In one subject, activation was observed within the central sulcus, and the gap occured in the border region between the depth of the central sulcus and the anterior wall of the central sulcus (areas 3a and 4 in Figure 8). Given the unanimity of the gap pattern of activation, it is reasonable to suggest that in fact physiological mapping in this subject *predicts anatomical variability* in the position of area 3a.

In agreement with investigations of the non-human primate using extracellular recording electrodes, we observed tactile activation in the PoCG in the location of areas 3b, 1 and 2 (Chapman and Ageranioti-Belanger, 1991; Johnson and Hsiao, 1992; Iwamura et al., 1993; Kaas et al., 1979; Manger et al., 1997; Merzenich et al., 1978; Nelson et al., 1980; Paul et al., 1972; Sur et al., 1980, 1984). In the monkey, areas 3b and 1 possess discrete tactile receptive fields (Johnson and Hsiao, 1992; Merzenich et al., 1978; Nelson et al., 1980), with rapidly and slowly adapting response properties (Paul et al., 1972; Sur et al., 1980, 1984). As one would predict, the punctate von Frey stimulus employed in our study also effectively drives suprathreshold activity in area 3b neurons in macaque cortex (Jain et al., 1997).

The description of tactile representations within areas 3b, 1 and 2 (e.g., separate palm representations) may be beyond the functional resolution of the current study. However, it is interesting to note that two subjects (subject CM and the lefthanded subject who was excluded from the study) showed discrete activation during palm stimulation on the anterior crest of the PoCG and in a discrete foci within putative area 2, the pattern predicted by suprathreshold mapping studies in macaque and owl monkey cortex (Kaas et al., 1979). Further, recent analysis of these data using a newly developed averaging technique defines two separate representations within the PoCG corresponding to the predicted positions of the palm in areas 3b/1 and 2 (C. Moore, A. Dale and B. Fischl, unpublished observations).

Activation during tactile stimulation in the PreCG area, corresponding to area 6, is predicted by the presence of tactile receptive fields in the macaque monkey (Gentilucci et al., 1988; Rizzolatti et al., 1981) and by the effect of lesions to this area, which induce somatosensory neglect for the contralateral side (Rizzolatti et al., 1983). Surprisingly, we did not observe consistent activation (N = 2 of 5 subjects) in the posterior bank of the PreCG during tactile input, a region that corresponds to area 4. Area 4 has been shown to have distinct tactile and deep/proprioceptive maps in the primate (Strick and Preston, 1982), a dissociation that is supported by receptor binding and PET studies in the human (Geyer et al., 1995). While it is possible that the correspondence between the gross anatomy and distinct Brodmann areas is not maintained for this region of the PreCG, this possibility is unlikely given the reliable localization of area 4 to the posterior bank of the PreCG in humans (Brodmann, 1909; White et al., 1997; Geyer et al., 1995).

Activation in the PreCG and PoCG During Proprioceptive/Motor Input

Activation in the PreCG during the proprioceptive/motor task is predicted by surgical stimulation (e.g., Penfield and Rasmussen, 1950) and functional imaging studies (e.g., Kim et al., 1993; Rao et al., 1993). The PoCG activation zone was also activated in the proprioceptive/motor task. This activation is consistent with several functional imaging studies that have reported activation that spans the PreCG, central sulcus and PoCG during tasks that combine proprioceptive/motor grasping type-movements with tactile stimulation (Boecker et al., 1996; Grafton et al., 1996; O'Sullivan et al., 1994; Rizzolatti et al., 1996) and without tactile stimulation (Fink et al., 1997). Our findings are also in agreement with several studies reporting modulation of firing in neurons in areas 3b and 1 during and prior to movement of the hand (Jiang et al., 1990a, 1990b; Lebedev et al., 1994; Prud'homme et al., 1994; see Nelson, 1996 for a review), and with the reciprocal connection of area 1 with primary motor cortex (Cusick et al., 1985; Jones and Porter, 1980; Stepniewska et al., 1993). Activation in areas 3b and 1 is also consistent with recordings from unanesthetized

monkey preparations (Iwamura et al., 1993), which show that approximately 40% of all neurons on the anterior border of area 3b are deep or proprioceptive in character, and that approximately 20% of neurons in area 1 are deep or proprioceptive in character.

The activation of areas 3b and 1 in the human is, however, in disagreement with recordings from anesthetized Owl monkey (Merzenich et al., 1978), where *none* of the receptive fields in areas 3b and 1 were found to be deep or proprioceptive. This disagreement may be explained by the premovement activity described above, or by the filtering effects of anesthesia on less robust inputs. Recordings in monkey somatosensory cortex (Arezzo et al., 1981; see also Armstrong-James and George, 1988 and Chapin and Lin, 1984 for similar findings in the rat) have shown that weaker inputs within the central sulcus region are suppressed under barbiturate anesthetic, creating a sharper segregation of submodalities than exists in the awake behaving state (see also Conclusion).

Putative Human Area 2

In the human, area 2 is located in the posterior bank of the PoCG (Geyer et al., 1997; Brodmann, 1909[5]). In owl (Merzenich et al., 1978) and macaque monkeys (Iwamura et al., 1985, 1993; Nelson et al., 1980), area 2 contains both tactile and proprioceptive receptive fields, with a greater concentration of tactile receptive fields located at the anterior border of area 2 (Merzenich et al., 1978; Iwamura et al., 1993). The posterior bank of the PoCG was activated in our study in 4 of 5 subjects during tactile stimulation of the palm, and 3 of 5 subjects during proprioceptive/motor activation. Our findings are in agreement with a recent PET study that reported activation spanning the anterior and posterior banks of the PoCG following contact on the fingertips with moving gratings, and the activation of the posterior bank of the PoCG during passive movement of the fingers (Burton et al., 1997), and with activation in the postcentral sulcus during a variety of haptic manipulation tasks (Grafton et al., 1996; O'Sullivan et al., 1994).

The failure to activate area 2 in individual subjects in our study during proprioceptive/motor or tactile activity may reflect the integrative function of area 2: In the primate, neurons in this area are often driven exclusively by the combination of tactile and proprioceptive/motor input (Iwamura et al., 1985). In support of this view, we have recently observed consistent activation in area 2 in individual subjects (N = 3/3 and 5/5) during two tasks that require integration of tactile and proprioceptive input (C. Moore, S. Corkin, C. Stern, A. Gray and A. Dale, unpublished observations). Activation in the depth of the postcentral sulcus was observed in only one subject for both tasks. This region is difficult to drive in monkeys with either proprioceptive or tactile input, with less than 40% of neurons with detectable receptive fields (Iwamura et al., 1993).

---

[5] Recent studies (J. Kaas, unpublished observations) in the human suggest that the position of area 2 is further up the posterior bank of the PoCG than previously reported. Using this position to correlate with our phsyiological data, we observe activation in putative area 2 in all subjects during contralateral stimulation of the palm.

Experiment 4: Cortical Reorganization in SCI Subjects: Perceptual Report and fMRI

To assess the capacity for reorganization in the human cortex, we have examined subjects with spinal-cord injury (SCI). This population of human subjects provides an extreme challenge to the reorganizational capacity of the cortex, because several centimeters of the cortical map are deafferented. To assess this reorganization, we have used two methods, perceptual reports and fMRI. The first gives insight into the possible connection between reorganization and perceptual changes (Ramachandran, 1993), and the second a means for observing corresponding physiological change.

Methods

Subjects

Subjects were male SCI patients (N = 8) with complete traumatic lesions at the thoracic level (between T3 and T10, Table 2). Subjects were referred to us for study at the MIT Clinical Research Center and the Massachusetts General Hospital Nuclear Magnetic Resonance Center by Dr. Sandra Kostyk of the West Roxbury VA Hospital Spinal Cord Unit and Dr. Alyssa LeBel of the Massachusetts General Hospital Pain unit. All subjects experienced their injury > 1 yr prior to participation in this study.

Table 2: SCI Subjects

Age	*Level*	*Reported phantom sensations*
41 (DP)	T5	None
38 (CC)	T7(R)/T9 (L)	Constant, painful
37 (RH)	T6*	Evoked (reference zone), non-painful
32 (DH)	T7	Evoked (reference zone), painful and non-painful
48	T8	Evoked and spontaneous, painful
47	T3	Spontaneous (rare), non-painful
58	T10	None
76	T4	None

* Subject was later reported to have limited sacral sparing (see text for details).

Clinical Report

Subjects (N = 8) received a questionnaire asking them to detail the sensory effects of their injury. This questionnaire was accompanied by an oral interview.

Imaging Techniques, Anatomical Analyses and Data Analyses

Subjects (N = 3: first 3 subjects in Table 2) were scanned in a 1.5 T magnet as described in Experiment 1. Stimulation epochs were of the same length as Experiment 1, but were presented without the hand+arm condition (hand - off - arm - off - hand - off - arm - off - hand - off - arm - off). Data analysis was performed as described in Experiment 1.

Results

Perceptual Reports

In addition to the loss of somatosensory perception beneath the level of injury, subjects reported the following sensory phenomena.

Increased Sensitivity Proximal to the Lesion

In all SCI subjects (N = 8), increased sensitivity in the band of skin above the level of injury was reported for the time period immediately following the injury. The duration of this sensitivity and its intensity varied among subjects. Two subjects reported sustained allodynia.

Phantom Sensations

Five subjects reported phantom sensations. In three of them, these sensations could be evoked by sensory stimulation. The range of phenomena that evoked phantom sensations included two broad categories: Somatosensory and non-specific stimulation. Non-specific stimulation was observed in all three subject with evoked phantoms. This category included stimuli as diverse as lying down at night to relax (this phenomenon was also reported in a single amputee subject with phantom pain, C. Moore and S. Corkin, unpublished observations), and sudden loud noises. In one subject, phantom sensations occurred spontaneously without a clear connection to a prior sensory stimulus, and in another (CC) phantom pain was constant beneath his level of injury.

In two subjects, phantom sensations were evoked from discrete reference zones. In subject DH, contact on the right forearm evoked sensations in the ribs at the level of injury. Subject RH reported three discrete reference zones (Figure 9). On the chest above the level of injury, light tactile touch was referred to the genital region. This reference zone had a precise organization, in which the direction of tactile movement (green arrow) was recapitulated in this phantom sensation. Two sites on the head also evoked referred sensations in RH: Tapping on the top of the head was referred to the sacral region and contact on the back of the head to a region on the back below the level of injury. At 6 months following our examination, this subject recovered a small region of non-specific sacral sparing, overlapping or near to the referred sensations in region A and the green box of Figure 9. This recovery is interesting to note, as it is in agreement with the pattern of referred sensations in subject DH, who also referred sensations to a region of mixed deafferenation at his level of his injury on the trunk.

Figure 9 Reference zones in a T6 lesion SCI subject (RH) *Upper Figures* Boxes above the line of injury mark dermal areas that evoked referred sensations to below the line of injury (corresponding boxes). The green arrow represents a maintained sense of directional contact in the phantom sensation evoked at this reference zone. *Lower homunculus* The proximity of reference zones and their projected phantom perceptions is shown on the Penfield homunculus. Note that while these areas are in the same overall region of the map, they are not necessarily adjacent.

Figure 9

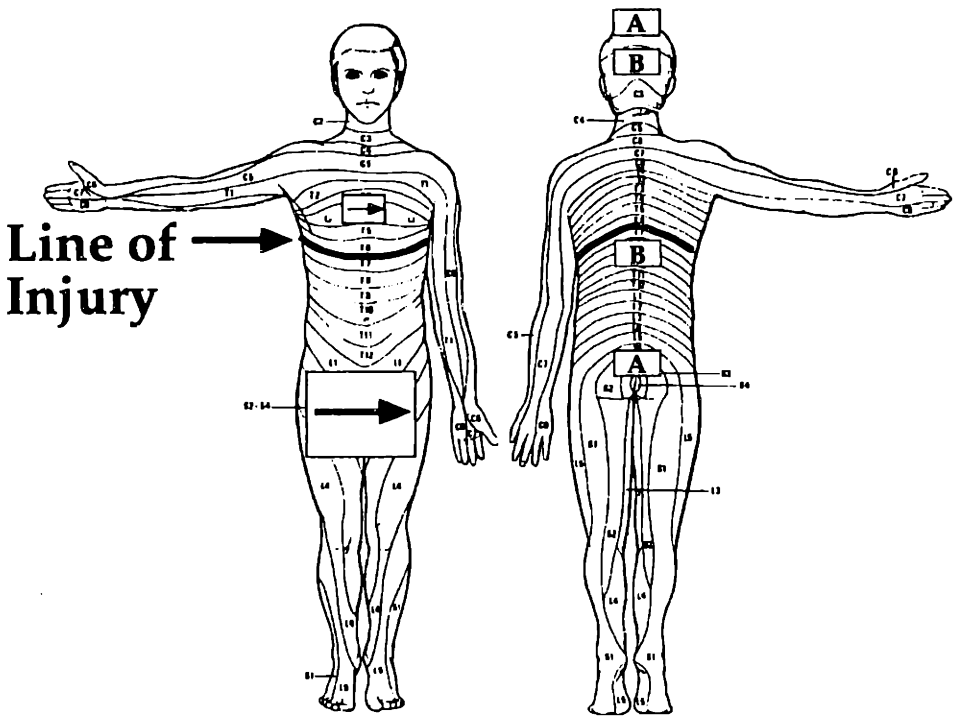

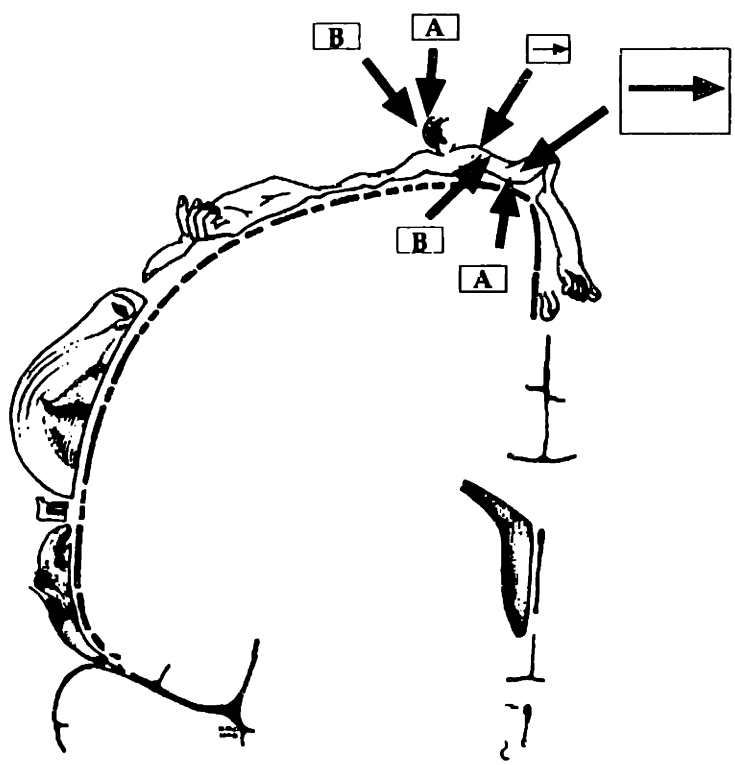

FMRI

Three SCI subjects were scanned in the 1.5 T magnet with a head coil. In one subject (RH), head motion during the scan precluded detailed analysis of the fMRI data, although a clear pattern of sensory evoked fMRI signal in a region corresponding to the palm representation could be observed in the raw data. Of the two remaining subjects, one subject had constant phantom sensations beneath the level of injury (T7, right side, T9, left side), and one subject did not possess phantom sensations. In both subjects, we observed a normal extent and number of overlapping activations (z-score > .05) following stimulation of the right palm (*Number of overlapping regions of activation* Phantom subject: 1 overlapping region of activation; Non-phantom subject, 3 regions: *Extent of regions of activation* Phantom subject, 42.1% to 72.8% of the length of normalized PoCG; Non-phantom subject, 68.1% to 79%) and arm (*Number of regions of activation* Phantom subject, 2. Non-phantom subject, 4; *Extent of regions of activation* Phantom subject, 53.2% to 68.0%: non-phantom subject, 39.3% to 79.0%). In these two subjects, the percentage increase in fMRI signal during palm stimulation was greater (phantom subject) or equal to (SCI Non-phantom subject) the amplitude of signal in the NCS with the highest observed percentage signal change during palm stimulation (Figure 10; compare also the average signal change in the NCS population scanned at 3 T during tactile stimulation in Figure 7).

Figure 10 Activation in the palm representation of an SCI with phantom perceptions and an SCI without phantom perceptions A. Color-coded activation maps are displayed for coronal oblique slices through the PoCG region. Color indicates significant activation during palm stimulation. Yellow boxes outline the area from which the timecourses on the right were generated. Within the timeplots, circles indicate raw data, black lines indicate data convolved with a [1 1 1] filter, and red lines indicate activation levels summed over 10 time-point (20 sec) epochs. B. The amplitude of palm activation signal in the hand area is greater for the SCI with phantom sensations then for the SCI without phantom sensations or the highest signal observed in an NCS (Experiment 1).

Figure 10

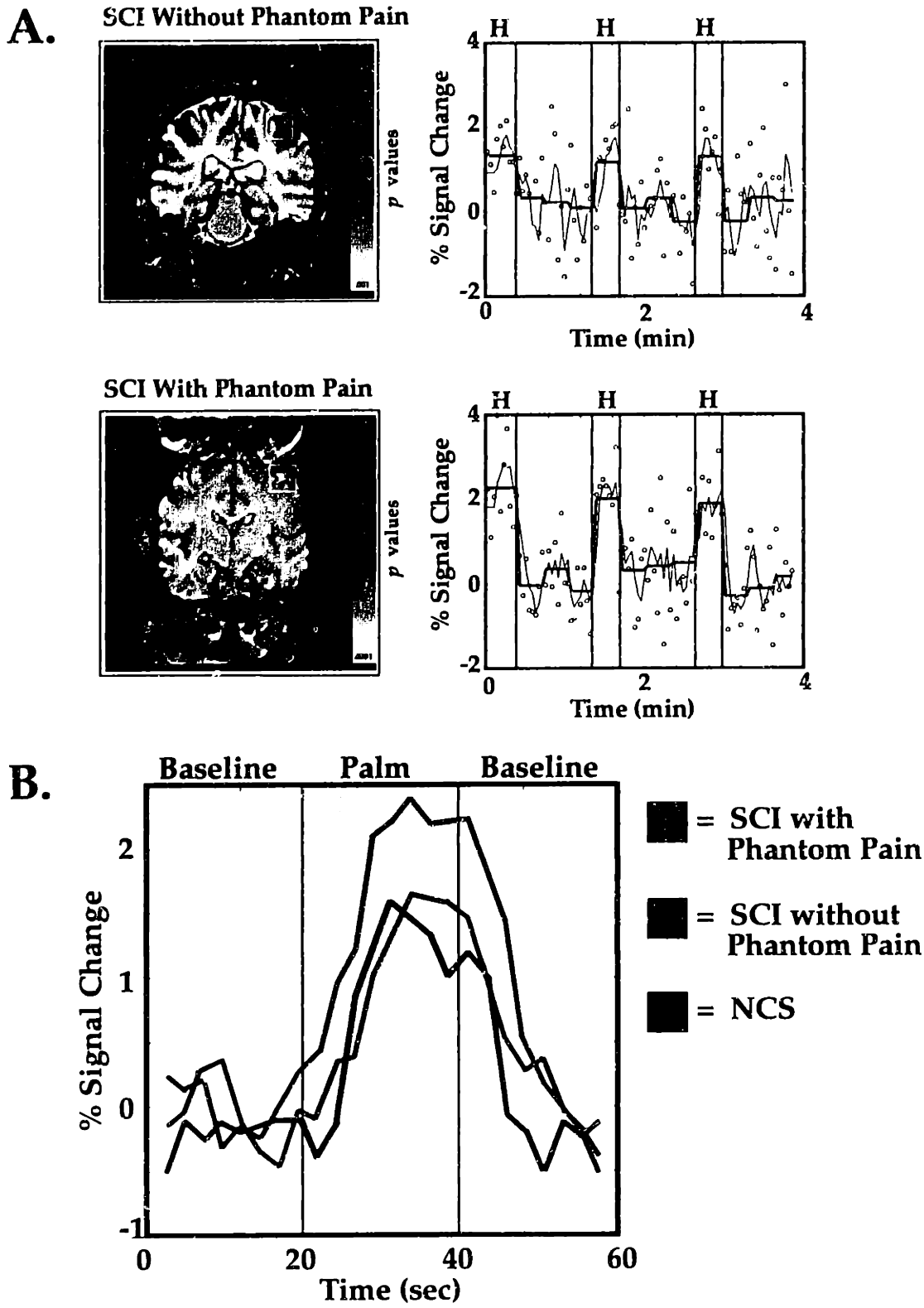
A.
SCI Without Phantom Pain
p values
H
H
H
% Signal Change
4
2
0
-2
0
2
4
Time (min)
SCI With Phantom Pain
p values
H
H
H
% Signal Change
4
2
0
-2
0
2
4
Time (min)
B.
Baseline
Palm
Baseline
% Signal Change
2
1
0
-1
0
20
40
60
Time (sec)
= SCI with Phantom Pain
= SCI without Phantom Pain
= NCS

Discussion

In SCI subjects, I observed increased sensitivity at the level of injury, somatotopic organization of reference zones and increased fMRI signal in extant representations in SCI subjects. Each of these findings support the suggestion that cortical remapping occurs in humans following SCI.

Sensory Changes Following SCI

Increased Sensitivity at the Level of Injury

Several authors have reported increased sensitivity immediately above the level of injury in SCI subjects (e.g., Tasker, 1990). As described in the Introduction, increased tactile acuity should be a consequence of the decrease in receptive field size that accompanies cortical reorganization. The precise mechanism by which cortical expansion would induce increased sensitivity (as opposed to increased acuity) is unclear, but increased cortical area subserving the band above the level of injury would suggest increased psychophysical capability, potentially including sensitivity. This finding is in agreement with Haber (1958), who reported increased pressure sensitivity on the upper arm ipsilateral to lower arm amputation.

Evoked Phantom Sensations Following SCI

In two subjects, discrete reference zones were observed in regions that are within the same section of the cortical map as the deafferented region: Contact on the forearm (subject DH) and contact on the chest or head (subject RH) evoked phantom sensations to the deafferented region. This finding supports the hypothesis presented by Ramachandran (1993) that cortical reorganization may underlie phantom sensations. In both cases, the reference zone was within the same cortical area on the map as the evoked phantom, but was not proximal on the body surface, suggesting that peripheral mechanisms for the generation of phantom sensations did not support this phenomenon.

In both subjects, sensations were referred to regions that overlapped poorly afferented regions: The sacral region in subject RH and the line of injury in the thoracic region in subjects RH and DH. This finding, while preliminary, suggests that diminished but maintained sensory input may contribute to the perception of phantom limbs. A simple linear model suggests that the combintation of input from the reference zone with degraded input from the border region crosses threshold of activation that is a prerequisite for conscious perception, evoking the conscious percept of the phantom limb.

In both cases, the reference zones were near to, but not directly adjacent to, the deafferented zone according to the Penfield homunculus. There are at least three potential explanations for this finding. First, this finding suggests that reorganization driving the phantom percept may occur at a different level of processing (e.g., subcortical structures) where there is a different progression of representations[6]. Second, it may reflect variability in the cortical map. Consistent with this proposal, Merzenich et al. (1987) have observed considerable intersubject variability in the organization of the hand representation of areas 3b and 1 in owl

---

[6] Following the completion and approval of this thesis, the author scanned patient DH and observed activation in the putative chest and forearm region in the PoCG during stimulation of his forearm reference zone. In contrast, stimulation in an adjacent site on the forearm that did not evoke referred sensations activated only the putative forearm region. A gap in the activatio n pattern in this region between the arm and chest suggests that the second hypothesis, of subcortical reorganization, is the most plausible one, and that in agreement with the work of Florence and Kaas (1996), cortical reorganization in the primate is driven by subcortical change.

and macaque monkeys. Third, it could provide evidence against the correlation between remapping and phantom sensations, although the localization of reference zone and phantom sensation to the same somatotopic region of the PoCG is remarkable if it is not the result of central reorganization.

Greater fMRI Signal During Palm Stimulation in an SCI Subject with Phantom Pain

In the subject with phantom pain, we observed a greater percentage signal change during palm stimulation than was observed in NCS. While the interpretation of this finding is limited by its singularity, this result is nonetheless in agreement with our findings in Chapter 2, where we observed not only an expansion of neighboring representations into a sensory deafferented region (the cut vibrissa representation), but also an increased signal change in the center of the uncut vibrissa representation. Further, this finding is in agreement with Flor et al. (1995), who reported a shift in organization correlated with the percept of phantom pain, and it is in agreement with Kew et al. (1994), who observed an increased signal in representations proximal to the deafferented zone.

A potential confound in relating the amplitude of the BOLD signal change to neural activity is the metric we have employed, increased inflow of HbO_2 measured in an fMRI scanner. Several lines of reasoning suggest, however, that our result may actually reflect an increase in neural activation in the center of the representation. First, a similar increase was observed during action potential receptive field mapping of the uncut vibrissa representation (Armstrong-James et al., 1994). Second, increased signal within the extant representation has been observed using a variety of techniques (suprathreshold electrical recordings, intrinsic signal imaging, fMRI and PET). Third, similar results have now been demonstrated following a CNS lesion (Chapter 3), a PNS lesion (Kew et al., 1994) and a non-invasive reorganization of the pattern of peripheral input (Chapter 2; Armstrong-James et al., 1994).

Our findings, when taken with these previous studies, suggest that cortical reorganization may result not only in expansion of representations into cortex receiving less perceptually relevant information, but also in a change in the organization within the extant representation. As discussed in Chapter 2, one mechanism for amplitude increase within the extant representation would be an activity dependent down regulation of disinhibition: As described in Chapter 1, inhibition is centered on the center of excitation, suggesting that a release from inhibition would increase the amplitude of activity within a representation. In support of this suggestion, Garraghty et al. (1994) have reported decreased cortical GAD staining in the monkey following PNS lesions (see also Welker et al., 1989), although these studies report changes selective to the deafferented cortex that may not be able to explain increases in the extant representation. Further, in potential contrast with a disinhibition hypothesis, Merzenich et al. (1983) have observed a decrease in receptive field size in the extant representation following transection of the median nerve, whereas one would predict increased receptive field size following decreased inhibition (Chapter 1; Dykes et al., 1984; Larmour and Dykes, 1988; Kyrazi et al., 1996).

General Discussion

Correspondence of fMRI Findings with the Monkey Literature

A consistent theme of these findings is a closer agreement with the monkey literature than with prior mapping studies of human cortex. For example, recent human studies using subdural electrode grids (Nii et al., 1996) have suggested that the position of motor and tactile representations is variable across subjects, and can be located on either side of the central sulcus. In contrast, our findings suggest that distinct maps encoding tactile and proprioceptive/motor activity are present in both the PreCG and the PoCG, and that the borders of these maps define an area that is specifically responsive to proprioceptive/motor activity. The correlation between our findings and those in the monkey is enhanced by the observation that our findings in the unanesthetized human are in best agreement with unanesthetized monkey mapping studies (e.g., Iwamura et al., 1993). The agreement of our data with monkey studies may arise from several factors: (a) The greater spatial resolution of fMRI; (b) the ability to scan a number of normal subjects; (c) controlled experimental conditions; and, (d) the ability to analyze data from individual subjects, thereby avoiding decreased resolution through averaging.

This correspondence gives support to the assumption that monkey cortex is a viable model for understanding human cortical organization and reorganization in the PoCG (Florence et al., 1996; Johnson and Hsiao, 1992). It also provides evidence from another species that the segregation of somatosensory cortical areas is preserved in evolution (Kaas, 1983; Krubitzer, 1995).

Can fMRI go Beyond the Monkey Literature?

The emphasis I have placed on the analogy between the human and monkey begs the question of whether fMRI is capable of generating novel findings in the human without the predictive and interpretive insight provided by monkey mapping studies. In one sense, the converse is true: Because of the agreement between the human and monkey literature, there is greater confidence in more subtle (e.g., non-activation of putative area 4 in our study) and novel findings with fMRI. This confidence is particularly relevant in studies of cortical reorganization and in the study of regions where organization may more substantially differ across species (e.g., posterior parietal lobe).

CONCLUSION

This thesis has examined the organization and reorganization of somatosensory cortex at a number of levels and over a number of timescales. In conclusion, I offer commentary on some prevalent themes throughout the work.

Common Themes in Cortical Processing in Rat and the Human

As demonstrated in Chapters 1 and 2, adult rat SI is less dissimilar from other somatosensory cortices than previously believed. Like sensory cortex in other systems and other species, rat SI demonstrates context-dependent reorganization and longer-term plasticity. Nevertheless, the analogy between rat and primate somatosensory cortex is clearly not a precise one, nor is it the goal of this thesis to suggest they operate by identical mechanisms. That said, it is still constructive to consider findings from each together.

Prevalence of Cortical Plasticity

Evidence from all three Chapters support the suggestion that cortical reorganization is part of the normal function of perceptual processing. Subthreshold cortical receptive fields provide an extensive substrate for rapid interactions and a potential field over which longer-term reorganization can occur. Reorganization at short (frequency-dependent sharpening of the vibrissa representation) and longer-time scales (vibrissa trimming/pairing) was characterized in the rat SI cortex, demonstrating that cortical change can readily take place following relatively subtle and non-invasive changes in the pattern of sensory input. Similar changes were suggested by the somatotopic organization of reference zones and by fMRI images from a spinal-cord injured subject with phantom sensations. The similar pattern of change in the center of an extant representation following vibrissa trimming/pairing and spinal-cord injury suggest that plasticity over longer time scales may operate by similar mechanisms in the rat and primate (but see Jain et al., 1995). Further, the faciliity with which cortical reorganization occured in rat SI cortex suggests that the plasticity induced by more invasive manipulations (e. g., spinal cord injury) may reflect the mechanisms engaged in the processing of sensory input and/or in short- and longer-term learning.

Segregation of Areas in Human and Rat SI

A second prevalent theme of this work is the segregation of functional "areas" in the context of different patterns of sensory stimulation. In the human, putative area 3a was activated by proprioceptive/motor but not tactile input. In rat SI, the putative septa was activated during low frequency (1 Hz) but less so by high frequency stimulation. Krubitzer (1995) has proposed the evolution of discrete cortical processing modules such as barrels as the evolutionary forerunner of segregation of a new cortical area. The frequency dependent suppression of responses in the septa and beyond suggest that this uncoupling may be a physiological harbinger of future evolutionary areal segregation. In this context it is interesting to note the spatial segregation of adaptation properties within primate SI, the RA and SA columns (Sur et al., 1981, 1984).

Dynamic Regulation of the Action Potential Threshold in Human and Rat SI

Rat and human cortex demonstrated a broader overlap in cortical input than might have been anticipated from previous studies. In the rat, subthreshold receptive fields within a given column extended over a field of 25 vibrissa. In the

human, the PoCG tactile activation region received not only tactile but also proprioceptive/motor input. As described in Chapter 3, several lines of evidence, particularly recording in the unanesthetized primate, predict this overlap. The divergence of our findings with those of Merzenich et al. (1978) suggest a sharpening of the cortical representation during anesthesia (Arezzo et al., 1981). This finding is predictable in the context of previous studies of the effects of anesthesia on suprathreshold receptive fields, and it suggests that primate somatosensory cortex, like adult rat SI, has an adjustable threshold for action potential activity in a given area. Further, this dynamic thresholding may play a role in human perception, as it appears to in the rat (Chapter 2).

Context-dependent Inhibitory Sharpening of Representations in Human and Rat SI

An implication of our findings in Chapters 1 and 2, and of pervious work in the visual and somatosensory cortex, is that a key function of subthreshold receptive field input is the amplification of a feature or spatial location (Zipser et al., 1996). We have observed in rat SI (Chapter 1) that smaller surround inputs are differentially suppressed by inhibition, suggesting that these inputs should be further suppressed during multi-vibrissa interactions (Brumberg et al., 1996). We have recently observed (Gehi, 1996; Gehi et al., 1996) that the human cortex also demonstrates consistent lateral inhibition during tactile stimulation. In contrast to the weak or nonexistent activation in the human PoCG during arm stimulation (Chapter 3, Experiments 1 and 2), we consistently observed *decreased* fMRI signal in the PoCG lateral to the arm representation during tactile stimulation. While the origins of "inhibition" of an fMRI signal are unresolved, this finding suggests that within the human cortex, perception of contact is amplified by inhibition of neighboring representations. In a similar finding, Drevets et al., (1995) have reported that the anticipation of contact in a specific peripheral location leads to decreased PET signal in surrounding representations (e.g., in the foot representation during anticipation of hand contact). In this regard, it is also interesting to note that we have recently observed ipsilateral inhibition within the hand area during tactile stimulation (Moore et al., submitted).

Cortical Plasticity versus Subcortical Plasticity: Emergent Plasticity

The processing level at which somatotopic plasticity occurs is a subject of some debate. Several studies have presented evidence for purely cortical reorganization (Diamond et al., 1994; Wang et al., 1995): Our findings (Chapter 1) of large subthreshold receptive fields in rat SI also provide a substrate (if not evidence) that the cortex may be the locus of longer-term cortical reorganization. A wealth of studies also have demonstrated reorganization in subcortical structures. Even prior to the influential reports of cortical reorganization in the primate cortex following nerve transection, Wall (1977) demonstrated the unmasking of latent inputs in the spinal cord following nerve cut. Similarly, following amputation there are expanded termination zones from extant, neighboring inputs to the dorsal horn and cuneate nucleus (Florence and Kaas, 1996).

Given the emerging view that plasticity is an integral component of perceptual processing, and given the evidence that subcortical reorganization is possible, it would be surprising to have to wait to observe changes in this basic feature of sensory organization until a processing stage as progressed as the cortex. Conversely, the prevalence of dynamic organization at many stages of processing

suggests that *levels of sensory processing should be uniquely plastic for what they uniquely encode*: The level at which a feature emerges should be the first level at which plasticity for that feature occurs. In this context, it is interesting to note that Simons and Carvell (1989; Simons, 1995) have argued that the primary thalamocortical response transformation in rat SI is the constraint of the suprathreshold receptive field during whisking, and that we observe dynamic modulation of this transformation at frequencies relevant to whisking behavior.

Future Directions

This thesis presents several possible lines of research. In conclusion, I briefly suggest a few future directions for this work.

Correlation Between Organization within Specific Human Cortical Areas and Sensory Processes

As reviewed above, lesion studies have suggested that specific cortical areas subserve distinct submodalities of somatosensory perception (Semmes et al., 1974). Reorganization within these areas, on short and long timescales should, therefore, also be related to changes in perceptual set or acuity.

Long-term, Area-specific Cortical Reorganization Amputees will often report phantom sensations that are restricted to a specific submodality of perception, e.g., either only a cramping feeling in the palm (proprioceptive), or only a pins and needles sensation (tactile). These specific perceptual phenomena suggest that reorganization may exclusively occur in a subset of cortical areas. Correlation of reorganization in a specific area with phantom perceptions would help to relate specific human cortical areas with the processes of perception they support.

Dynamic Area-specific Cortical Reorganization A variety of phenomena, including the effects of increasing frequency, can also be examined within specific cortical areas. Area-specific changes in organization can then be directly related to changes in perception under the same stimulation conditions (e.g., tests of increased tactile acuity with increased frequency of stimulation).

Effects of Multimodal Input on the Organization of Distinct Cortical Areas The changes in cortical organization seen with different levels of anesthesia, i.e., between a multi-modal cortex and a strictly segregated cortex, suggest that one important mechanism for sensory processing in the human may be the selective coupling and uncoupling of cortical areas during different perceptual tasks or motor sets. This suggestion presents several lines of experimentation, including the integration of submodalities of somatosensory input and the integration of visual and somatosensory input. Examination of cortical mapping within specific areas in the context of conflicting input from other sources (e.g., seeing contact on one finger while the neighboring finger is being stimulated) would provide insight into how these cortical areas operate in concert to integrate multimodal information (e.g., shifts in the finger activation with biasing visual input). Given the relatively large surface area over which signal can be sampled in an fMRI experiment, multiple visual and somatosensory cortical areas could be evaluated under these stimulus conditions.

Integration of Cortical Map with Primate Data An important component of this research plan is to actively integrate the examination of human cortex with fMRI with concurrent work in the monkey. Specifically, detailed electrophysiological mapping studies in the primate can be used to investigate the receptive field

changes that underlie larger scale reorganization that are elucidated with fMRI in the human subject.

Interactions examined with whole-cell recording during different contexts of vibrissa stimulation

One implication of this thesis is that increasing frequency of stimulation transforms the organization of the vibrissa representation: Further, pervious work has emphasized the importance of multiple vibrissa interactions (e.g., Brumberg et al., 1996). Given the importance of these factors to sensory processing, whole cell recording during varying patterns of sensory stimulation (e.g., deflection of a series of vibrissa emulating directional movement along the vibrissa) would provide detailed insight into the roles of excitation and inhibition in the more complex and realistic inputs to these receptive fields. Further, the activation of several vibrissae in concert (emulating whisking) would give insight into the role of global context on the processing of single vibrissa deflections (e.g., Brumberg et al., 1996), and the role of ongoing patterns of input to the characteristics of the sensory response (Abbott et al., 1997).

APPENDIX

Comparison of Subthreshold and Intrinsic Optical Signal Spread in Rat SI Cortex

Despite the success of intrinsic-signal optical imaging and other techniques in replicating the localization of electrophysiological function in animals and in man, the relation between neuronal activity and hemodynamic change is still only poorly understood. Studies using antidromic stimulation and nerve section (reviewed in Jeuptner and Weiler, 1995) have demonstrated that 2-deoxyglucose changes are driven by presynaptic input. In agreement with these studies, optical imaging and extracellular suprathreshold recording in the cat visual cortex (Das and Gilbert, 1995; Toth et al., 1996) suggest that the divergence of the optical signal is significantly greater than the divergence of suprathreshold activity. In contrast with these studies, Frostig and colleagues (Frostig et al., 1994; S. Masino, personal communication; R. Frostig, Barrels Symposium, 10/25/97) have reported a 1 to 1 correspondence between the spread of optical signal and the spread of suprathreshold receptive fields in the rat SI vibrissa representation.

To provide a connection between the subthreshold receptive fields recorded in Chapter 1 and the mapping metric I used to assess the organization and reorganization of rat SI in Chapter 2, I have compared the spread of subthreshold activity recorded in the rat barrel cortex with the spread of intrinsic optical signal.

Methods

In this experiment, the first frame of the data collection epoch was divided into the mean of frames 2, 3 and 4, i.e., dividing the signal 0-500 msec after the onset of sensory stimulation into data acquired 500-2000 msec after the onset of stimulation. This approach takes advantage of the delay in onset of the optical signal to allow for the most temporally proximal baseline acquisition (Figure 1A of Chapter 2). In Experiments 1 and 2 of Chapter 2, the data were susceptible to amplitude shifts in the underlying baseline (Arieli et al., 1996): While these shifts were less frequently observed in Experiment 2, they were prevalent in Experiment 1. The use of a more temporally local baseline alleviates some of the effect of these shifts.

Results

As demonstrated in Figure 3 of Chapter 2, the optical signal generated by stimulation of a single vibrissa diverges over a significant portion of the 4.25 mm x 3.5 mm region of cortical area imaged. Vibrissa 1- and 2-away from the primary vibrissa evoked consistent signal in the center of the primary vibrissa representation (N = 6 rats: primary vibrissa, .24% +/- .03 SEM, N = 18 vibrissae; 1-away, .14 +/- .03, N = 22; 2-away, .08 +/- .03, N = 8: $p < .05$: Signal averaged under a 100 μm radius disk). The relative amplitude of this signal, taken as a percentage of the amplitude of the signal evoked in the center of the primary vibrissa representation, is shown in Appendix Figure 1 (1-away, 58% +/- 4 SEM; 2-away, 33 +/- 14). For comparison, the relative amplitude of subthreshold input to supragranular neurons (N = 5), recorded at approximately the depth at which we imaged (325 μm to 475 μm), was quantified (Figure 1). As described in Chapter 1 (see Figure 4 of Chapter 1), the fall off in supragranular signal decreased in amplitude as a function of distance from the primary vibrissa (primary vibrissa, 9.6 mV +/- 1.2 SEM, N = 5 vibrissae; 1-away, 6.5 +/- 1.0, N = 6; 2-away, 4.9 +/- 1.1, N = 8). Extracellular recordings made using identical anesthetic and similar stimulation regimens are also shown in Figure 1 (Diamond et al., 1994, by permission of the author). The fall-off in suprathreshold signal spread is considerably steeper than that observed in optical signal or

suprathreshold signal spread (see also the focal nature of suprathreshold receptive fields in Chapter 1).

Discussion

We found that the fall off in optical signal spread fell between the rate of fall off in subthreshold and suprathreshold signal spread for neurons recorded at the same cortical depth. This finding suggests that optical signal shows greater divergence than suprathreshold signal spread. This finding is in agreement with studies in cat visual cortex that have demonstrated extension of the optical signal beyond the edge of the suprathreshold receptive field (Das and Gilbert, 1995; Toth et al., 1996; Toth et al., 1997) and, more generally, with findings demonstrating that presynaptic activity can drive metabolic cortical signals (see Jeuptner and Weiller, 1995, for a review). Das and Gilbert (1995) observed that the suprathreshold activation zone in visual cortex occupied only 5% of the total cortex demonstrating optical signal spread. We have measured a different metric, the rate of fall off in the relative strength of the signal, but our data also suggest that the spread of the optical signal is significantly greater than the spread of suprathreshold signal.

We have compared the fall-off in signal of a single vibrissa deflection in the subthreshold and suprathreshold receptive field mapping studies with the signal generated by 5 Hz stimulation in the optical mapping study. As described in the Chapter 2, 5 Hz stimulation evokes a more discrete divergence of optical signal than 1 Hz stimulation, suggesting that this comparison may have underestimated the spread of optical signal. If we have, in fact, underestimated the fall-off in optical signal, this brings our findings into better agreement with previous studies that have suggested a subthreshold correlate of optical signal, and into sharper contrast with studies that report the correlation of suprathreshold and optical signals (Frostig et al., 1994; R Frostig, Barrels Symposium, 10/25/98; S. Masino, personal communication).

The differences between our findings and those of Frostig and colleagues may be the result of methodological differences in imaging and analysis techniques. Frostig and colleagues (Chen-Bee and Frostig, 1996; Chen-Bee et al., 1996; Frostig, 1994; Masino et al., 1993; Masino and Frostig, 1996; Prakash et al., 1996) quantify spread of optical signal as the full width at half maximal of the peak signal generated, whereas we analyzed fall-off in signal over a constant distance from the center of the representation. Their method of defining the border of the representation artificially reduces the spread of the signal within the cortex, and may explain the different results achieved by the two groups. Other methodological differences include the following: Depth of focus (300 μm vs. 450 μm) in the cortex; subtraction of an analogue reference image from the data image prior to digitization; and, they employ a 5x5 gaussian smoothing filter prior to analysis. However, these differences do not immediately suggest a reason for differences in our findings.

Figure 1 Rate of fall-off in optical, suprathreshold and subthreshold signal spread
The slope of the decrease in optical signal strength (blue line) falls between that observed for subthreshold (red line) and suprathreshold (black line) signal spread. Suprathreshold data are reproduced with permission from Diamond et al. (1994).

REFERENCES

Abbott, L. F., Varela, J. A., Sen, K., Nelson, S. B. (1997) Synaptic depression and cortical gain control. Science 275:220-224.

Ageranioti-Belanger, S. A., Chapman, C. E. (1992) Discharge properties of neurons in the hand area of primary somatosensory cortex in monkeys in relation to the performance of an active tactile discrimination task. Exp Brain Res 91:207-228.

Agmon, A., Connors, B. W. (1991) Thalamocortical responses of mouse somatosensory (barrel) cortex in vitro. Neuroscience 41:365-380.

Agmon, A., Connors, B. W. (1992) Correlation between intrinsic firing patterns and thalamocortical synaptic responses of neurons in mouse barrel cortex. J Neurosci 12:319-329.

Allard, T., Clark, S. A., Jenkins, W. M., Merzenich, M. M. (1991) Reorganization of somatosensory area 3b representations in adult owl monkeys after digit syndactyly. J Neurophysiol 66:1048-1058.

Amitai, Y., Connors, B. W. (1995) Intrinsic physiology and morphology of single neurons in neocortex. In: Cerebral Cortex (E. G. Jones and I. T. Diamond, eds.), pp. 299-331. New York, NY, Plenum Press.

Arezzo, J. C., Vaughan, H. G. Jr, Legatt, A. D. (1981) Topography and intracranial sources of somatosensory evoked potential in the monkey. II. Cortical components. Electroencephalogr Clin Neurophysiol 51:1-18.

Arieli, A., Sterkin, A., Grinvald, A., Aertsen, A. (1996) Dynamics of ongoing activity: explanation of the large variability in evoked cortical responses. Science 273:1868-1871.

Armstrong-James, M., Callahan, C. A., Friedman, M. A. (1991) Thalamo-cortical processing of vibrissal information in the rat. I. Intracortical origins of surround but not centre-receptive fields of layer IV neurones in the rat S1 barrel field cortex. J Comp Neurol 303:193-210.

Armstrong-James, M., Callahan, C. A. (1991) Thalamo-cortical processing of vibrissal information in the rat. II. Spatio-temporal convergence in the thalamic ventral posterior medial nucleus (VPm) and its relevance to generation of receptive fields of S1 cortical "barrel" neurones. J Comp Neurol 303:211-224.

Armstrong-James, M., Diamond, M. E., Ebner, F. F. (1994) An innocuous bias in whisker use in adult rats modifies receptive fields of barrel cortex neurons. J Neurosci 6978-6991.

Armstrong-James, M., Fox, K. (1987) Spatio-temporal convergence and divergence in the rat S1 "barrel" cortex. J Comp Neurol 263:265-281.

Armstrong-James, M., Fox, K., Das-Gupta, A. (1992) Flow of excitation within rat barrel cortex on striking a single vibrissa. J Neurophysiol 68:1345-1358.

Armstrong-James, M., George, M. J. (1988) Influence of anesthesia on spontaneous activity and receptive field size of single units in rat Sm1 neocortex. Exp Neurol 99:369-387.

Armstrong-James, M., Welker, E., Callahan, C. A. (1993) The contribution of NMDA and non-NMDA receptors to fast and slow transmission of sensory information in the rat SI barrel cortex. J Neurosci 13:2149-2160.

Baker, J. R., Hoppel, B. E., Stern, C. E., Kwong, K. K., Weisskoff, R. M., Rosen, B. R. (1995) Dynamic functional imaging of the complete human cortex using gradient-echo and asymmetric spin echo echo-planar magnetic resonance imaging. *Soc. Mag. Res. Med. Abs. 12.*

Bear. M. F., Cooper, L. N., Ebner, F. F. (1987) A physiological basis for a theory of synapse modification. Science 237:42-48.

Bindmann, L. J., Murphy, K. P. S. J., Pockett, S. (1988) Postsynaptic control of the induction of long-term changes in efficacy of transmission at neocortical synapses in slices of rat brain. J Neurophysiol 60:1053-1065.

Boecker, H., Khorram-Sefat, D., Kleinschmidt, A., Merboldt, K.-D., Hanicke, W., Requardt, M., Frah, J. (1996) High-resolution functional magnetic resonance imaging of cortical activation during tactile exploration. Human Brain Mapping 3:236-244.

Bonhoeffer, T., Grinvald, A. (1996) Optical imaging based on intrinsic signals: The methodology, in: Brain Mapping: The Methods (A. W. Toga and J. C. Mazziotti, eds.), pp. 55-97. San Diego, CA, Academic Press.

Bors, E. (1951) Phantom limbs of patients with spinal cord injury. AMA Arch Neurol Psych 66:610-631.

Brodmann, K. (1994) Localisation in the cerebral cortex (L. J. Garey, Trans.). London: Smith-Gordon. (Original work published 1909).

Brumberg, J. C., Pinto, D. J., Simons, D. J. (1996) Spatial gradients and inhibitory summation in the rat whisker barrel system. J Neurophysiol 76:130-140.

Burton, H., MacLeod, A. M., Videen, T. O., Raichle, M. E. (1997) Multiple foci in parietal and frontal cortex activated by rubbing embossed grating patterns across fingerpads: A positron emission tomography study in humans. Cereb Cortex 7:3-17.

Cahusac, P. M. B. (1995) Synaptic plasticity induced in single neurones of the primary somatosensory cortex in vivo. Exp Brain Res 107:241-253.

Carlson, M. (1980) Characteristics of sensory deficits following lesions of Brodmann's areas 1 and 2 in the postcentral gyrus of Macaca mulatta. Brain Res 204:424-430.

Carvell, G. E., Simons, D. J. (1988) Membrane potential changes in rat SmI cortical neurons evoked by controlled stimulation of mystacial vibrissae. Brain Res 448:186-191.

Carvell, G. E., Simons, D. J. (1990) Biometric analyses of vibrissal tactile discrimination in the rat. J Neurosci 10:2638-2648.

Castro-Alamancos, M. A., Connors, B. W. (1996) Short-term synaptic enhancement and long-term potentiation in neocortex. Proc Natl Acad Sci USA 93:1335-1339.

Castro-Alamancos, M. A., Connors, B. W. (1996) Short-term plasticity of a thalamocortical pathway dynamically modulated by behavioral state. Science 272:274-277.

Castro-Alamancos, M. A., Connors, B. W. (1995) Different forms of synaptic plasticity in somatosensory and motor areas of the neocortex. J Neurosci 15:5324-5333.

Chapin, J. K. (1986) Laminar differences in sizes, shapes, and response profiles of cutaneous receptive fields in the rat SI cortex. Exp Brain Res 62: 549-559.

Chapin, J. K., Lin. C.-S. (1984) Mapping the body representation in the SI cortex of anesthetized and awake rats. J Comp Neurol 229:199-213.

Chapman, C. E., Ageranioti-Belanger, S. A. (1991) Discharge properties of neurones in the hand area of primary somatosensory cortex in monkeys in relation to the performance of an active tactile discrimination task. I. Areas 3b and 1. Exp Brain Res 87:319-339.

Chen-Bee, C. H., Kwon, M. C., Masino, S. A., Frostig, R. D. (1996) Areal extent quantification of functional representations using intrinsic signal optical imaging. J. Neurosci Methods 68:27-37.

Chen-Bee, C. H., Frostig, R. D. (1996) Variability and interhemispheric asymmetry of single-whisker functional representations in rat barrel cortex. J Neurophysiol 76:884-893.

Chmielowska, J., Carvell, G.E., Simons, D.J. (1989) Spatial organization of thalamocortical and corticothalamic projection systems in the rat Sm1 barrel cortex. J Comp Neurol 285:325-338.

Chubbyk, J. G. (1966) Small-motion biological stimulator. APL Tech Dig May-June:18-23.

Clark, S. A., Allard, T., Jenkins, W. M., Merzenich, M. M. (1988) Receptive fields in the body-surface map in adult cortex defined by temporally correlated inputs. Nature 332:444-445.

Coghill, R. C., Talbot, J. D., Evans, A. C., Meyer, E., Gjedde, A., Bushnell, M. C., Duncan, G. H. (1994) Distributed processing of pain and vibration by the human brain. J Neurosci 14:4095-4108.

Cohen, M. S., Bookheimer, S. Y. (1994) Localization of brain function using magnetic resonance imaging. Trends Neurosci 17:268-277.

Cohen, D. A. D., Prud'homme, M. J. L., Kalaska, J. F. (1994) Tactile activity in primate primary somatosensory cortex during active arm movements: Correlation with receptive field properties. J Neurophysiol 71:161-172..

Constanzo, R. M., and Gardener, E. P. (1980) A quantitative analysis of responses of direction-sensitive neurons in somatosensory cortex of awake monkeys. J Neurophysiol 43: 1319-1341.

Corkin, S. (1964) Somesthetic function after focal cerebral damage in man. Doctoral dissertation, McGill University, Montreal.

Corkin, S., Milner, B., Rasmussen, T. (1970) Somatosensory thresholds: Contrasting effects of postcentral-gyrus and posterior parietal-lobe excisions. Arch Neurol 23:41-58.

Cusick, C. G., Steindler, D. A., Kaas, J. H. (1985) Corticocortical and collateral thalamocortical connections of postcentral somatosensory cortical areas in squirrel monkeys: A double-labeling study with radiolabeled wheatgerm agglutinin conjugated to horseradish peroxidase. Somatosensory Research 3:1-31.

Dale, A., Sereno, M. I. (1993) Improved localization of cortical activity by combining EEG and MEG with MRI cortical surface reconstruction: A linear approach. J Cog Neuro 5:162-176.

Dale, A. M., Buckner, R. L. (1997) Selective averaging of rapidly presented individual trials using fMRI. Human Brain Mapping 5:329-340.

Das, A. Gilbert, C. G. (1995) Long-range horizontal connections and their role in cortical reorganization revealed by optical recording of cat primary visual cortex. Nature 375:780-784.

Deisz R. A., Prince, D. A. (1989) Frequency-dependent depression of inhibition in guinea-pig neocortex in vitro by GABA-B receptor feedback on GABA release. J. Physiol. London 412: 513-554.

Delacour, J., Houcine, O., Talbi, B. (1987) "Learned" changes in the responses of the rat barrel field neurons. Neuroscience 23:63-71.

Dettmers, C., Connelly, A., Stephan, K. M., Turner, R., Friston, K. J., Frackowiak, R. S. J., Gadian, D. G. (1996) Quantitative comparison of functional magnetic resonance imaging with positron emission tomography using a force-related paradigm. Neuroimage 4:201-209.

Devor, M., Wall, P. D. (1981) Plasticity in the spinal cord sensory map following peripheral nerve injury in rats. J Neurosci 1:679-684.

DeYoe, E. A., Carman, G. J., Bandettini, P., Glickman, S., Wieser, J., Cox, R., Miller, D., Neitz, J. (1996) Mapping striate and extrastriate visual areas in human cerebral cortex. Proc Natl Acad Sci USA 93:2382-2386.

Diamond, M. E., Armstrong-James, M., Ebner, F. F. (1992a) Experience-dependent plasticity in adult rat barrel cortex. Proc Natl Acad Sci USA 90:2082-2085.

Diamond, M. E., Armstrong-James, M., Ebner, F. F. (1992b) Somatic sensory responses in the rostral sector of the posterior group (POm) and in the ventral posterior medial nucleus (VPm) of the rat thalamus. J Comp Neurol 318:462-476.

Diamond, M. E., Huang, W., Ebner, F. F. (1994) Laminar comparison of somatosensory cortical plasticity. Science 265:1885-1888.

Dinse, H. R., Rencanzone, G. H., Merzenich, M. M. (1993) Alterations in correlated activity parallel ICMS-induced representational plasticity. Neuroreport 5:173-176.

Disbrow, E., Buoncore, M., Anotgnini, J., Carstens, E., Rowley, H. A. (in press) The somatosensory cortex: A comparison of the response to noxious, thermal. mechanical and electrical stimuli using functional magnetic resonance imaging. Human Brain Mapping.

Drevets, W. C., Burton, H., Videen, T. O., Snyder, A. Z., Simpson, J. R. Jr, Raichle, M. E. (1995) Blood flow changes in human somatosensory cortex during anticipated stimulation. Nature 373:249-252.

Dykes, R. W., Landry, P., Metherate, R., Hicks, T. P. (1984) Functional role of GABA in cat primary somatosensory cortex: Shaping receptive fields of cortical neurons. J Neurophysiol 6:1066-1093

Dykes, R. W., Larmour, Y. (1988) Neurons without demonstrable receptive fields outnumber neurons having receptive fields in samples from the somatosensory cortex of anesthetized or paralyzed cats and rats. Brain Res 440:133-143.

Dykes, R. W., Ruest, A. (1985) What makes a map in somatosensory cortex? In: Cerebral Cortex (A. Peters and E. G. Jones, eds.), pp. 1-29. New York, NY, Plenum Press.

Elbert, T., Flor, H., Birbaumer, N., Knecht, S., Hampson, S., Larbig, W., Taub, E. (1994) Extensive reorganization of the somatosensory cortex in adult humans after nervous system injury. Neuroreport 5:2593-2597.

Engel, S. E. (1996) Looking into the black box: New directions in neuroimaging. Neuron 17:375-378.

Faggin, B. M., Nguyen, K. T., Nicolelis, M. A. L. (1997) Immediate and simultaneous sensory reorganization at cortical and subcortical levels of the somatosensory system. Proc Natl Acad Sci 94:9428-9433.

Ferster, D., Jagadeesh, B. (1992) EPSP-IPSP interactions in cat visual cortex studied with in vivo whole-cell patch recording. J Neurosci 12:1262-1274.

Fink, G. R., Frackowiak, R. S. J., Pietrzyk, U., Passingham, R. E. (1997) Multiple nonprimary motor areas in human cortex. J Neurophysiol 77:2164-2174.

Flor, H., Elbert, T., Knecht, S., Weinbruch, C., Pantev, C., Birbaumer, N., Larbig, W., Taub, E. (1995) Phantom-limb pain as a perceptual correlate of cortical reorganization following arm amputation. Nature 375:482-484.

Florence, S. L., Jain, N., Pospichal, M. W., Beck, P. D., Sly, D. L., Kaas, J. H. (1996) Central reorganization of sensory pathways following peripheral nerve regeneration in fetal monkeys. Nature 381:69-71.

Florence, S. L., Kaas, J. H. (1996) Large-scale reorganization at multiple levels of the somatosensory pathway follows therapeutic amputation of the hand in monkeys. J Neurosci 15:8083-8095.

Fogassi, L., Gallese, V., Fadiga, L., Luppino, G., Matelli, M., Rizzolatti, G. (1996) Coding of peripersonal space in inferior premotor cortex (area F4). J Neurophysiol 76:141-156.

Fox, P. T., Raichle, M. E. (1986) Focal physiological uncoupling of cerebral blood flow and oxidative metabolism during somatosensory stimulation in human subjects. Proc Natl Acad Sci USA 83:1140-1144.

Fox, P. T, Woldorff, M. G. (1994) Integrating human brain maps. Curr Opin Neurobiol 4:151-156.

Fregnac, Y., Shulz, D., Thorpe, S., Bienenstock, E. (1988) A cellular analogue of visual cortical plasticity. Nature 333:367-370.

Friedman, A., Gutnick, M. J. (1987) Low-threshold calcium electrogenesis in neocortical neurons. Neurosci Letters 81:117-122.

Frostig, R. D. (1994) What does in vivo optical imaging tell us about the primary visual cortex in primates? In: Cerebral Cortex (A. Peters and K. S. Rockland, eds.), pp. 331-358. New York, NY, Plenum Press.

Garraghty, P. E., Florence, S. L., Kaas, J. H. (1990) Ablations of areas 3a and 3b of monkey somatosensory cortex abolish cutaneous responsivity in area 1. Brain Res 528:165-169.

Garraghty, P. E., Hanes, D. P., Florence, S. L., Kaas, J. H. (1994) Pattern of peripheral deafferentation predicts reorganizational limits in adult primate somatosensory cortex. Somatosensory Motor Res 11:109-117.

Garraghty, P. E., Kaas, J. H. (1991) Large-scale functional reorganization in adult monkey cortex after peripheral nerve injury. Proc Natl Acad Sci USA 88:6976-6980.

Garraghty, P. E., LaChica, E. A., Kaas, J. H. (1991) Injury-induced reorganization of somatosensory cortex is accompanied by reductions in GABA staining. Somatosensory Motor Res 8:347-354.

Anil Gehi, (1996) Somatotopic mapping of the human somatosensory cortex using functional magnetic resonance imaging (fMRI). Masters thesis, Massachusetts Institute of Technology, Cambridge.

Gehi, A., Moore, C. I., Corkin, S., Rosen, B. R. & Stern, C. E. (1996) FMRI of Somatosensory Cortex: Somatotopy and Lateral Inhibition Within the Postcentral Gyrus. *Soc. Neurosci. Abs., 22.*

Gentilucci, M., Fogassi, L., Luppino, G., Matelli, M., Cabarda, R., Rizzolati, G. (1988) Functional organization of inferior area 6 in the macaque monkey. I. Somatotopy and the control of proximal movements. Exp Brain Res 71:475-490.

Geyer, S., Ledberg, A., Schleicher, A., Kinomura, S., Schorman, T., Burgel, U., Klinberg, T., Larsson, J., Zilles, K., Roland, P. E. (1995) Two different areas within the primary motor cortex of man. Nature 382:805-807.

Geyer, S., Schleicher, A., Zilles, K. (1997) The somatosensory cortex of human: Cytoarchitecture and regional distribution of receptor-binding sites. Neuroimage 6:27-45.

Gil, Z., Amitai, Y., Castro-Alamancos, M. A., Connors, B. W. (1996) Different frequency modulation and GABAb involvement at thalamocortical and intracortical synapses. *Soc. Neuro. Abs.* 22.

Glazewski, S., Fox, K. (1996) Time course of experience-dependent synaptic potentiation and depression in barrel cortex of adolescent rats. J Neurophysiol 75:1714-1729.

Grafton, S. T., Fagg, A. H., Woods, R. P., Arbib, M. A. (1996) Functional anatomy of pointing and grasping in humans. Cerebral Cortex 6:226-237.

Haber, W. B. (1958) Reactions to loss of limb: Physiological and psychological aspects. Annals NY Acad Sci 74:14-24.

Halligan, P. W., Marshall, J. C., Wade, D. T., Davey, J., Morrison, D. (1993) Thumb in cheek? Sensory reorganization and perceptual plasticity after limb amputation. Neuroreport 4:233-236.

Hammeke, T. A., Yetkin, F. Z., Mueller, W. M., Morris, G. L., Haughton, V. M., Rao, S. M., Binder, J. R. (1994) Functional magnetic resonance imaging of somatosensory stimulation. Neurosurgery 35:677-681.

Head, H. (1920) Studies in neurology. Vol. II. London: Henry Frowde and Hodder and Stoughton, Ltd.

Hellweg, F. C., Schultz, W., Creutzfeldt, O. D. (1977) Extracellular and intracellular recordings from cat's cortical whisker projection areas: Thalamocortical response transformation. J Neurophysiol 40:463-479.

Hyvarinen, J., Poranen, A. (1978) Movement-sensitive and direction and orientation-selective cutaneous receptive fields in the hand area of the post-central gyrus in monkeys. J Physiol 283:523-527.

Innocenti, G. M., Manzoni, T. (1972) Response patterns of somatosensory cortical neurones to peripheral stimuli. An intracellular study. Arch Ital Biol 110:322-347.

Istvan, P. J., Zarzecki, P. (1994) Intrinsic discharge patterns and somatosensory inputs for neurons in raccoon primary somatosensory cortex. J Neurophysiol 72:2827-2839.

Iwamura, Y., Tanaka, M., Sakamoto, M., Hikosaka, O. (1985) Vertical neuronal arrays in the postcentral gyrus signaling active touch: A receptive field study in the conscious monkey. Exp Brain Res 58:412-420.

Iwamura, Y., Tanaka, M., Sakamoto, M., Hikosaka, O. (1993) Rostrocaudal gradients in the neuronal receptive field complexity in the finger region of the alert monkey's postcentral gyrus. Exp Brain Res 92:360-368.

Iwamura, Y., Iriki, A., Tanaka, M. (1994) Bilateral hand representation in the postcentral somatosensory cortex. Nature 369:554-556.

Iwamura, Y., Tanaka, M. (1996) Representation of reaching and grasping in the monkey postcentral gyrus. Neuroscience Letters 214:147-150.

Jack, C. R., Jr, Thompson, R. M., Butts, R. K., Sharbrough, F. W., Kelly, P. J., Hanson, D. P., Riederer, S. J., Ehman, R. L., Hangiandreou, N. J., Cascino, G. D. (1994) Sensory motor cortex: Correlation of presurgical mapping with functional MR imaging and invasive cortical. Radiology 190:85-92.

Jagadeesh, B., Wheat, H. S., Ferster, D. (1993) Linearity of summation of synaptic potentials underlying direction selectivity in simple cells of the cat visual cortex. Science 262:1901.

Jain, N., Catania, K. C., Kaas, J. H. (1997) Deactivation and reactivation of somatosensory cortex after dorsal spinal cord injury. Nature 386:495-498.

Jain, N., Florence, S. L., Kaas, J. H. (1995) Limits on plasticity in somatosensory cortex of adult rats: Hindlimb cortex is not reactivated after dorsal column section. J Neurophysiol 73:1537-1546.

Jenkins, W. M., Merzenich, M. M., Ochs, M. T., Allard, T., Guic-Robles, E. (1990) Functional reorganization of primary somatosensory cortex in adult owl moneys after behaviorally controlled tactile stimulation. J Neurophysiol 63:82-104.

Jensen, K.F. and Killackey, H.P. (1987) Terminal arbors of axons projecting to the somatosensory cortex of the adult rat I. The normal morphology of specific thalamocortical afferents. J Neurosci 7:3529-3543.

Jeuptner, M., Weiler, C. (1995) Review: Does measurement of regional cerebral blood flow reflect synaptic activity?--Implications for PET and fMRI. Neuroimage 2:148-156.

Jiang, W., Chapman, C. E., Lamarre, Y. (1990) Modulation of somatosensory evoked responses in the primary somatosensory cortex produced by intracortical microstimulation of the motor cortex in the monkey. Exp Brain Res 80:333-344.

Johnson, K. O., Hsiao, S. S. (1992) Neural mechanisms of tactual form and texture perception. In: Annual Review of Neuroscience (W. M. Cowan, E. M. Shooter, C. F. Stevens, R. F. Thompson, eds.), pp. 227-250. Palo Alto, CA, Annual Reviews.

Jones, E. G. (1985) Connectivity of the primate sensory-motor cortex. In: Cerebral Cortex (A. Peters, and E. G. Jones, eds.), pp. 113-184. New York, NY, Plenum Press.

Jones, E. G., Porter, R. (1980) What is area 3a? Brain Res Rev 2:1-43.

Kaas, J. H. (1983) What, if anything, is SI? Organization of first somatosensory area of cortex. Physiology Reviews 63:206-231.

Kaas, J. H. (1989) Why does the brain have so many visual areas? J Cog Neuro 1:121-135.

Kaas, J. H., Nelson, R. J., Sur, M., Dykes, R. W., Merzenich, M. M. (1984) J Comp Neurol 226:111-140.

Kaas, J. H., Garraghty, P. E. (1991) Hierarchical, parallel, and serial arrangements of sensory cortical areas: Connection patterns and functional aspects. Curr Opin Neurobiol 1:248-251.

Kaas, J. H., Nelson, R. J., Sur, M., Lin, C.-S., Merzenich, M. M. (1979) Multiple representations of the body within the primary somatosensory cortex of primates. Science 204:521-523.

Kawakami, Y., Ashida, H. (1993) Long-lasting potentiation of field potentials in primary and secondary somatosensory cortex. Brain Res 605:147-154.

Margaret Keane (1991) Dissociations among priming effects after cerebral lesions: Evidence for neurally distinct memory systems. Doctoral dissertation, Massachusetts Institute of Technology, Cambridge.

Keller, A. (1995) Synaptic organization of the barrel cortex. In: Cerebral Cortex (E. G. Jones and I. T. Diamond, eds.), pp. 221-262. New York, NY, Plenum Press.

Kety, S. S. (1996) In: History of Neuroscience in Autobiography (L. Squire, ed.), pp. 382-413. Washington, D. C., Society for Neuroscience.

Kew, J. J. M., Ridding, M. C., Rothwell, J. C., Passingham, R. E., Leigh, P. N., Sooriakumaran, S., Frackowiack, R. S. J., Brooks, D. J. (1994) Reorganization of cortical blood flow and transcranial magnetic stimulation maps in human subjects after upper limb amputation. J Neurophysiol 72:2517-2524.

Killackey, H. P., and Leshin, S. (1975) The organization of specific thalamocortical projections to the posteromedial barrel subfield of the rat somatosensory cortex. Brain Res 86:469-472.

Kim, S.-G., Ashe, J., Georgopolous, A. P., Merkle, H., Ellerman, J. M., Menon, R. S., Ogawa, S., Ugurbil, K. (1993) Functional imaging of human motor cortex at high magnetic field. J Neurophysiol 69:297-301.

Kim, H. G., Beierlein, M., Connors, B. W. (1995) Inhibitory control of excitable dendrites in neocortex. J Neurophysiol 4:1810-1814.

Kleinschmidt, A., Nitschke, M. F., Frahm., J. (1997) Somatotopy in the human motor cortex hand area. A high resolution functional MRI study. European J Neurosci 9:2178-2186.

Knecht, S., Henningsen, H., Elbert, T., Flor, H., Hohling, C., Pantev, C., Taub, E. (1996) Reorganizational and perceptual changes after amputation. Brain 119:1213-1219.

Koralek, K. A., Jensen, K. F., Killackey, H. P. (1988) Evidence for two supplementary patterns of thalamic input to the rat somatosensory cortex. Brain Res 463:346-351.

Krubitzer, L. (1995) The organization of neocortex in mammals: are species differences really so different? Trends Neurosci 18:408-417.

Kryazi, H. T., Carvell, G. E., Brumberg, J. C., Simons, D. J. (1996) Quantitative effects of GABA and bicuculline methiodide on receptive field properties of neurons in real and simulated whisker barrels. J Neurophys 75:547-560.

Kyrazi, H. T., Simons, D. J. (1993) Thalamocortical response transformations in simulated whisker barrels. J Neurosci 13:1601-1615.

Kwong, K., Belliveau, J. W., Chesler, D. A., Goldberg, I. E., Weisskoff, R. M., Poncelet, B. P. et al., (1992) Dynamic magnetic resonance imaging of human brain activity during primary sensory stimulation. Proc Natl Acad Sci USA 89:5675-5679.

Lebedev, M. A., Denton, J. M., Nelson, R. J. (1994) Vibration-entrained and premovement activity in monkey primary somatosensory cortex. J Neurophysiol 72:1654-1673.

Lebedev, M. A., Nelson, R. J, (1996) High-frequency vibratory sensitive neurons in monkey primary somatosensory cortex: Entrained and nonentrained responses to vibration during the performance of vibratory-cued hand movements. Exp Brain Res 111:313-325.

Lee, S. M., Ebner, F. F. (1992) Induction of high-frequency activity in the somatosensory thalamus of rats in vivo results in long-term potentiation of responses in SI cortex. Exp Brain Res 90:253-261.

Lee, S. L., Friedberg, M. H., Ebner, F. F. (1994a) The role of GABA-mediated inhibition in the rat ventral posterior medial thalamus. I. Assessment of receptive field changes following thalamic reticular nucleus lesions. J Neurophys 71:1702-1715.

Lee, S. L., Friedberg, M. H., Ebner, F. F. (1994b) The role of GABA-mediated inhibition in the rat ventral posterior medial thalamus. II. Differential effects of GABAa and GABAb receptor antagonists on responses of VPm neurons. J Neurophys 71:1716-1726.

Lee, S. M., Weisskopf, M. G., Ebner, F. F. (1991) Horizontal long-term potentiation of responses in rat somatosensory cortex. Brain Res 544:303-310.

Li, C. X., Waters, R. S. (1996) In vivo intracellular recording and labeling of neurons in the forepaw barrel subfield (FBS) of rat somatosensory cortex: Possible physiological and morphological substrates for reorganization. Neuroreport 7:2261-2272.

Lin, W., Kuppusarmy, K., Haacke, E. M., Burton, H. (1995) Functional MRI in human somatosensory cortex activated by touching textured surfaces. J Mag Res Imaging 565-572.

Locasio, J. J., Jennings, P. J., Moore, C. I., Corkin, S. (1997) Time series analysis in the time domain and resampling methods for studies of functional magnetic resonance brain imaging. Human Brain Mapping 5:168-193.

Lu, S-M., Lin, R.C.-S. (1993) Thalamic afferents of the rat barrel cortex: A light- and electron-microscopic study using phaseolus vulgaris leucoagglutinin as an anterograde tracer. Somatosens Mot Res 10:1-16.

Lund, J. P., Sun, G.-D., Lammare, Y. (1994) Cortical reorganization and deafferentation in adult macaques. Science 265:546-548.

Malonek, D., Dirnagl, U., Lindauer, U., Yamada, K., Kanno, I., Grinvald, A. (1997) Vascular imprints of neuronal activity: relations between the dynamics of cortical blood flow, oxygenation, and volume changes following sensory stimulation. Proc Natl Acad Sci USA 94:14826-14831.

Malonek, D., Grinvald, A. (1996) Interactions between electrical activity and cortical microcirculation revealed by imaging spectroscopy: Implications for functional brain mapping. Science 272:551-554.

Manger, P. R., Woods, T. M., Jones, E. G. (1996) Representation of face and intra-oral structures in area 3b of macaque monkey somatosensory cortex. J Comp Neurol 371:513-521.

Markram, H., Tsodyks, M. (1996) Redistribution of synaptic efficacy between neocortical pyramidal neurons. Nature 382:807-810.

Masino, S. A., Kwon, M. C., Dory, Y., Frostig, R. D. (1993) Characterization of functional organization within rat barrel cortex using intrinsic signal optical imaging through a thinned skull. Proc Natl Acad Sci USA 90:9998-10002.

Masino, S. A., Frostig, R. D. (1996) Quantitative long-term imaging of the functional representation of a whisker in rat barrel cortex. Proc Natl Acad Sci USA 93:5022-5027.

McCarthy, G., Puce, A., Luby, M., Belger, A., Allison, T. (1996) Magnetic resonance imaging studies of functional brain activation: Analysis and interpretation. Electroencephalogr Clin Neurophysiol Suppl 47:15-31.

McCasland, J. S., Woolsey, T. A. (1988) High-resolution 2-deoxyglucose mapping of functional cortical columns in mouse barrel cortex. J Comp Neurol 278:555-569.

McCormick, D. A., Connors, B. W., Lightaall, J. W., Prince, D. A. (1985) Comparative electrophysiology of pyramidal and sparsely stellate neurons of the neocortex. J Neurophys 54:782-806.

Merzenich, M. M., Jenkins, W. M., Johnston, P., Schreiner, C., Miller, S. L., Tallal, P. (1996) Temporal processing deficits of language -learning impaired children ameliorated by training. Science 271:77-81.

Merzenich, M. M., Kaas, J. H. (1980) Principles of organization of sensory-perceptual systems in mammals, in: Progress in Psychobiology and Physiological Psychology (9), pp. 1-42. San Diego, CA, Academic Press.

Merzenich, M. M., Kaas, J. H., Sur, M., Lin, C.-S. (1978) Double representation of the body surface within cytoarchitectonic, areas 3b and 1 in "SI" in the owl monkey (*Aotus trivirgatus*). J Comp Neurol 181:41-74.

Merzenich, M. M., Kaas, J. H., Wall, J., Nelson, R. J., Sur, M., Felleman, D. (1983) Topographic reorganization of somatosensory cortical areas 3b and 1 in adult monkeys following restricted deafferentation. Neuroscience 8:33-55.

Merzenich, M. M., Nelson, R. J., Kaas, J. H. ,Stryker, M. P., Jenkins, W. M., Zook, J. M., Cyander, M. S., Schoppmann, A. (1987) Variability in hand surface representations in areas 3b and 1 in adult owl and squirrel monkeys. J Comp Neurol 258:281-296.

Merzenich, M. M., Nelson, R. J., Stryker, M. P., Cyander, M. S., Schoppman, A., Zook, J. M. (1984) Somatosensory cortical map changes following digit amputation in adult monkeys. J. Comp. Neurol. 224:591-605.

Keller, A. (1995) Synaptic organization of the barrel cortex. In: Cerebral Cortex (E. G. Jones and I. T. Diamond, eds.), pp. 221-262. New York, NY, Plenum Press.

Merzenich, M. M., Rencanzone, G. H., Jenkins, W. M., Allard, T. T., Nudo, R. J. (1988) Cortical representational plasticity. In: Neurobiology of Neocortex (P. Rakic and W. Singer, eds.). pp. 41-67. John Wiley and Sons, Limited.

Merzenich, M. M., Sameshima, K. (1993) Cortical plasticity and memory. Curr Opin Neurobiology 3:187-196.

Montoro, R. J., Lopez-Barneo, J., Jassik-Gershenfield, D. (1988) Differential burst firing modes of neurons of the mammalian visual cortex in vitro. Brain Res, 460:168-172.

Moore, C. I. (1998) Intracellular in vivo recording and intrinsic-signal optical imaging in rat somatoesnsory cortex: Barrels X proceedings. Somatosensory and Motor Res, 15:54.

Moore, C. I., Gehi, A., Corkin, S., Rosen, B. R., Stern, C. & Dale, A. (1997) Basic and Fine Somatotopy in Human SI. *The Cognitive Neuroscience Conference abstracts, 4.*

Moore, C. I., Gehi, A., Guimereas, A. R., Corkin, S., Rosen, B. R. & Stern, C. E. (1996) Somatotopic Mapping of Cortical Areas SI and SII Using FMRI. *2nd International Conference on Functional Mapping of the Human Brain abstracts.*

Moore, C. I., Nelson, S. B. (1994) In Vivo Whole Cell Recording of Vibrissa-Evoked Synaptic Responses in Rat Somatosensory Cortex. *Soc. Neurosci. Abs., 20.*

Moore, C. I., Sheth, B., Basu, A., Nelson, S. & Sur, M. (1996) What is the Neural Correlate of The Optical Imaging Signal? Intracellular Receptive Field Maps and Optical Imaging in Rat Barrel Cortex. *Soc. Neurosci. Abs., 22.*

Moore, C. I., Sheth, B. R., Sur, M. (1995) Intrinsic-signal optical imaging of somatosensory cortex before and after patterned stimulation of rat vibrissae. *Soc. Neurosci. Abs. 21.*

Moore, C. I., Sur, M. (1997) Cortical plasticity and LTP. Behav and Brain Sciences, 20:623-624.

Mountcastle, V. B., Powell, T. P. S., (1959) Neural mechanisms subserving cutaneous sensibility, with special reference to the role of afference inhibition in sensory perception and discrimination. Bull Johns Hopkins Hosp 105: 173-200.

Nelson, R. J. (1996) Interactions between motor commands and somatic perception in sensorimotor cortex. Curr Opin Neurobiol 6:801-810.

Nelson, R. J., Sur, M., Felleman, D. J., Kaas, J. H. (1980) Representation of the body surface in postcentral parietal cortex of *Macaca fascicularis*. J Comp Neurol 192:611-643.

Nelson, S., Toth, L., Sheth, B., Sur, M. (1994) Orientation selectivity of cortical neurons during intracellular blockade of inhibition. Science 265:774-777.

Nicolelis, M. A., Lin, R.-C., Woodward, D. J., Chapin, J. K. (1993) Induction of immediate spatio-temporal changes in thalamic networks by peripheral block of ascending cutaneous information. Nature 361:533-536.

Nicolelis, M. A., Baccala, L. A., Lin, R. C., Chapin, J. K. (1995) Sensorimotor encoding by synchronous neural ensemble activity at multiple levels of the somatosensory system. Science 268:1353-1358.

Nii, Y., Uematsu, S., Lesser, R. P., Gordon, B. (1996) Does the central sulcus divide motor and sensory functions? Cortical mapping of human hand areas as revealed by electrical stimulation through subdural grid electrodes. Neurology 46:360-367.

Ogawa, S., Tank, D. W., Menon, R., Ellerman, J. M., Kim, S. G., Merkle, H., et al. (1992) Intrinsic signal changes accompanying sensory stimulation: Functional brain mapping with magnetic resonance imaging. Proc Natl Acad Sci USA 89:5951-5955.

O'Sullivan, B. T., Roland, P. E., Kawashima, R. (1994) A PET study of somatosensory discrimination in man. Microgeometry versus macrogeometry. Eur J Neurosci 6:137-148.

Pardo, J. V., Wood, T. D., Costello, P. A., Pardo, P. J., Lee, J. T. (1997) PET study of the localization and laterality of lingual somatosensory processing in humans. Neurosci Lett 234:23-26.

Parker, J. L., Wood, M. L., Dostrovsky, J. O. (1998) A focal zone of thalamic plasticity. J Neurosci 18:548-558.

Paul, R. L., Merzenich, M., Goodman, H. (1972) Representation of slowly adapting and rapidly adapting cutaneous mechanoreceptors of the hand in Brodmann's areas 3 and 1 of *Macaca mulatta*. Brain Res 36:229-249.

Parker, J. L., Wood, M. L., Dostrovsky, J. O. (1998) A focal zone of thalamic plasticity. J Neurosci 18:548-558.

Paxinos, G., Watson, C. (1986) The rat brain in stereotaxic coordinates (2nd ed.). Sydney: Academic Press.

Penfield, W., Rasmusson, T. (1950) *The Cerebral Cortex of Man: A Clinical Study of Localization of Function.* New York, NY: Hafner.

Pettit, M. J., Schwark, H. D. (1993) Receptive field organization in dorsal column nuclei during temporary denervation. Science 262:2054-2056.

Pinto, D. J., Brumber, J. C., Simons, D. J., Ermentrout, G. B. (1996) A quantitative population model of whisker barrels: Re-examining the Wilson-Cowan equations. J Comp Neuro 3:247-264.

Pons, T. P., Kaas, J. H. (1985) Connections of area 2 of somatosensory cortex with the anterior pulvinar and subdivisions of the ventroposterior complex in macaque monkeys. J Comp Neurol 240:16-36.

Pons, T. P., Garraghty, P. E., Friedman, D. P., Mishkin, M. (1987) Physiological evidence for serial processing in somatosensory cortex. Science 237:417-420.

Pons, T. P., Garraghty, P. E., Ommaya, A. K., Kaas, J. H., Taub, E., Mishkin, M. (1991) Massive cortical reorganization after sensory deafferentation in adult macaques. Science 252:1857-1860.

Porro, C. A., Francescato, M. P., Cettolo, V., Diamond, M. E., Baraldi, P., Zuiani, C., Bazzocchi, M., di Prampero, P. E. (1996) J Neurosci 16:7688-7698.

Bradley Postle (1997) The cognitive mechanisms and neural substrates underlying repetition priming. Doctoral dissertation, Massachusetts Institute of Technology, Cambridge.

Prakash, N., Cohen-Cory, S., Frostig, R. D. (1996) Rapid and opposite effects of BDNF and NGF on the functional organization of the adult cortex in vivo. Nature 381:702-706.

Prud'homme, M. J. L., Cohen, D. A. D., Kalaska, J. F. (1994) Tactile activity in primate primary somatosensory cortex during active arm movements: Cytoarchitectonic distribution. J Neurophysiol 71:173-181.

Ramachandran, V. S. (1993) Behavioral and magnetoencephalographic correlates of plasticity in the adult human brain. Proc Natl Acad Sci USA 90:10413-10420.

Rao, S. M., Binder, J. R., Bandettini, P. A., Hammeke, T. A., Yetkin, F. Z., Jesmanowicz, A., Lisk, L. M., Morris, G. L., Mueller, W. M., Estkowski, L. D., Wong, E. C., Haughton, V. M., Hyde, J. S. (1993) Functional magnetic resonance imaging of complex human movements. Neurology 43:2311-2318.

Rao, S. M., Binder, J. R., Hammeke, T. A., Bandettini, P. A.,, Bobholz, J. A., Frost, J. A., Myklebust, B. M., Jacobson, R. D., Hyde, J. S. (1995) Somatotopic mapping of the human primary motor cortex with functional magnetic resonance imaging. Neurology 45:919-924.

Rao, S. M., Bandettini, P. A., Binder, J. R., Bobholz, J. A., Hammeke, T. A., Stein, E. A., Hyde, J. S. (1996) Relationship between finger movement rate and functional magnetic resonance signal change in human primary motor cortex. J Cereb Blood Flow Metab 16:1250-1254.

Reid, R. C., Soodak, R. E., Shapley, R. M. (1991) Direction selectivity and spatio-temporal structure of receptive fields of simple cells in cat striate cortex. J Neurophysiol 66:505-529.

Rencanzone, G. H., Merzenich, M. M., Jenkins, W. M. (1992a) Frequency discrimination training engaging a restricted skin surface results in an emergence of a cutaneous response zone in cortical area 3a. J Neurophysiol 67:1057-1070.

Rencanzone, G. H., Merzenich, M. M., Jenkins, W. M., Grajski, K. A., Dinse, H. R. (1992b) Topographic reorganization of the hand representation in cortical area 3b of owl monkeys trained in a frequency-discrimination task. J Neurophysiol 67:1031-1056.

Riddoch, G. (1941) Phantom limbs and body shape. Brain 64:197-222.

Rizzolatti, G., Scandolara, C., Matelli, M, Gentilucci, M. (1981) Afferent properties of periarcuate neurons in macaque monkeys. I. Somatosensory responses. Behav Brain Res 2:125-146.

Rizzolatti, G., Camarda, L., Fogassi, M., Gentilucci, M., Luppino, G., Matelli, M. (1988) Functional organization of inferior area 6 in the macaque monkey. II. Area F5 and the control of distal movements. Exp Brain Res 71:491-507.

Rizzolatti, G., Fadiga, L., Matelli, M., Bettinardi, V., Paulesu, E., Perani, D., Fazio, F. (1996) Exp Brain Res 111:246-252.

Rizzolatti, G., Matelli, M., Pavesi, G. (1983) Deficits in attention and movement following the removal of postarcuate (area 6) and prearcuate (area 8) cortex in macaque monkeys. Brain 106:655-673.

Sanes, J. N., Donaghue, J. P., Thangaraj, V., Edelman, R. R., Warach, S. (1995) Shared neural substrates controlling hand movements in human motor cortex. Science 268:1775-1777.

Schlaug, G., Sanes, J. N., Thangaraj, V., Darby, D. G., Jancke, L., Edelman, R. R., Warach, S. (1996) Neuroreport 7:879-883.

Schroeder, C. E., Seto, S., Arezo, J. C., Garraghty, P. E. (1995) Electrophysiological evidence for overlapping dominant and latent inputs to somatosensory cortex in squirrel monkeys. J Neurophysiol 74:722-732.

Seitz, R. J., Roland, P. E. (1992) Vibratory stimulation increases and decreases the regional cerebral blood flow and oxidative metabolism: a positron emission tomography (PET) study. Acta Neurol Scand 86:60-67.

Semmes, J., Porter, L. (1972) A comparison of precentral and postcentral cortical lesion on somatosensory discrimination in the monkey. Cortex 8:249-264.

Semmes, J., Porter, L., Randolph, M. C. (1973) Further studies of anterior postcentral lesions in monkeys. Cortex 10:55-68.

Sereno, M. I., Dale, A. M., Reppas, J. B., Kwong, K. K, Belliveau, J. W., Brady, T. J, Rosen, B. R., Tootell, R. B. H. (1993) Borders of multiple visual areas in humans revealed by functional magnetic resonance imaging. Science 268:889-893.

Sheth, B. R., Moore, C. I., Sur, M. (1998) Temporal modulation of spatial borders in rat barrel cortex. J Neurophysiol 79:464-470.

Shulman, R. G. (1997, July) Seminar presented at the McDonnell-Pew cognitive neuroscience retreat, Hanover, NH.

Sibson, N. R., Dhankhar, A., Mason, G. F., Behar, K. L., Rothman, D. L., Shulman, R. G. (1997) In vivo 13C NMR measurements of cerebral glutamine synthesis as evidence for glutamate-glutamine cycling. Proc Natl Acad Sci USA 94:2699-2704.

Silva, A., Rasey, S. K., Wall, J. T. (1994) Rapid changes in the size of nerve dominance aggregates in primate somatosensory cortex after nerve injury. *Soc. Neurosci. Abs., 20.*

Simons, D. J. (1978) Response properties of vibrissa units in the rat SI somatosensory neocortex. J Neurophysiol 41:798-820.

Simons, D. J. (1983) Multi-whisker stimulation and its effects on vibrissa units in rat SmI barrel cortex. Brain Res 276:178-182.

Simons, D. J. (1985) Temporal and spatial integration in the rat SI vibrissa cortex. J Neurophysiol 54:615-635.

Simons, D. J., Carvell, G. E. (1989) Thalamocortical response transformation in the rat vibrissa/barrel system. J Neurophysiol 61:311-330.

Simons, D. J., Carvell, G. E., Hershey, A. E., Bryant, D. P. (1992) Responses of barrel cortex neurons in awake rats and effects of urethane anesthesia. Exp Brain Res 91:259-272.

Simons, D. J. (1995) Neuronal integration in the somatosensory whisker/barrel cortex. In: Cerebral Cortex (E. G. Jones and I. T. Diamond, eds.), pp. 263-297. New York, NY, Plenum Press.

Simpson, W. A. (1989) The step method: A new adaptive psychophysical procedure. Perception and Psychophysics 45:572-576.

Stamler, J. S., Jia, L., Eu, J. P., McMahon, T. J., Demchenko, I. T., Bonaventura, J., Gernert, K., Piantadosi, C. A. (1997) Blood flow regulation by S-nitrosohemoglobin in the physiological oxygen gradient. Science 276: 2034-2037.

Stepniewska, I, Preuss, T. M., Kaas, J. H. (1993) Architectonics, somatotopic organization and ipsilateral cortical connections of the primary motor area (M1) of owl monkeys. J Comp Neurol 330:238-271.

Stevens, J. C., Patterson, M. Q. (1995) Dimensions of spatial acuity in the touch sense: Changes over the life span. Somatosensory and Motor Res 12:29-47.

Strick, P. L., Prestion, J. B. (1982) Two representations of the hand in area 4 of a primate. II. Somatosensory input organization. J Neurophysiol 48:150-159.

Mriganka Sur (1980) Some principles of organization of somatosensory cortex Doctoral dissertation, Vanderbilt University, Nashville.

Sur, M., Merzenich, M. M., Kaas, J. H. (1980) Magnification, receptive field area, and "hypercolumn" size in areas 3b and 1 of adult somatosensory cortex in owl monkeys. J Neurophysiol 44:25-311.

Sur, M., Wall, J. T., Kaas, J. H. (1981) Modular segregation of functional cell classes within the post-central somato-sensory cortex of monkeys. Science 212:1059-1061.

Sur, M., Wall, J. T., Kaas, J. H. (1984) Modular distribution of neurons with slowly adapting and rapidly adapting responses in area 3b of somatosensory cortex in monkeys. J Neurophysiol 4:724-744.

Swadlow, H. A., (1992) Monitoring the excitability of neocortical efferent neurons to direct activation by extracellular current pulses. J Neurophysiol 68:605-619.

Tasker, R. R. (1990) Pain resulting from central nervous system pathology (central pain). In: The Management of Pain (J. J. Bonica, ed.). Philadelphia, PA, Lea and Febiger.

Taylor, L., Jones, L. (1997) Effects of lesion invading the postcentral gyrus on somatosensory threshold on the face. Neuropsychologia 35:953-961.

Teuber, H.-L., Krieger, H. P., Bender, M. B. (1949) Reorganization of sensory function in amputation stumps: Two-point discrimination. Federal Proceedings 8:156.

Thulborn, K. R., Talagala, S. L., Chang, T., Tasciyan, B., McCurtain, B., Sweeney, J. A. (1998, March). Sensitivity advantage for fMRI at 3.0 Tesla over 1.5 Tesla [6 paragraphs]. Available WEB site, Univ. Wisconsin Medical College.

Tommerdahl, M., Delemos, K. A., Vierck, C. J. Jr, Favorov, O. V., Whitsel, B. L. (1996) Anterior parietal cortical response to tactile and skin-heating stimuli applied to the same skin site. J Neurophysiol 75:2662-2670.

Tootell, R. B., Reppas, J. B., Kwong, K. K., Malach, R., Born, R. T., Brady, T. J., Rosen, B. R., Belliveau, J. W. (1995) Functional analysis of human MT and related visual cortical areas using magnetic resonance imaging. J Neurosci 15:3215-3230.

Toth, L. J., Rao, S. C., Kim, D.-S., Somers, D., Sur, M. (1996) Subthreshold facilitation and suppression in primary visual cortex revealed by intrinsic signal imaging. Proc Natl Acad Sci USA 93:9869-9874.

Toth, L. J., Kim, D.-S., Rao, S. C., Sur, M. (1997) Integration of local inputs in visual cortex. Cerebral Cortex 7:703-710.

Turrigiano, G. G., Leslie, K. R., Desai, N. S., Rutherford, L. C., Nelson, S. B. (1998) Activity-dependent scaling of quantal amplitude in neocortical neurons. Nature 391:892-896.

Tootell, R. B. H., Mendola, J. D., Hadjikhani, N. K., Ledden, P. J., Liu, A. K., Reppas, J. B., Sereno, M. I., Dale, A. M. (1997) Functional analysis of V3A and related areas in human visual cortex. J Neurosci 17:7060-7078.

Valbo, A. B., Hagbarth, K.-E., Torebjork, H. E., Wallin, B. G. (1979) Somatosensory, proprioceptive and sympathetic activity in human peripheral nerves. Physiol Rev 59:919-957.

Van Essen, D. C., Anderson, C. H., Felleman, D. J. (1992) Information processing in the primate visual system: an integrated systems perspective. Science 255:419-423.

Wall, P. D. (1977) The presence of ineffective synapses and the circumstances which unmask them. Phil Trans R Soc Lond B 278:361-372.

Wang, X., Merzenich, M. M., Sameshima, K., Jenkins, W. M. (1995) Remodeling of adult hand representation in adult cortex determined by timing of tactile stimulation. Nature 378:71-75.

Weinstein, S. (1968) Intensive and extensive aspects of tactile sensitivity as a function of body part, sex, and laterality. In: The Skin Senses (D. R. Kenshalo, ed.). pp. 195-222. Springfield, Ill, Thomas.

Welker, C. (1971) Microelectrode delineation of fine grain somatotopic organization of SmI cerebral neocortex in albino rat. Brain Res 26:259-275.

Welker, C. (1976) Receptive fields of barrels in the somatosensory neocortex of the rat. J Comp Neurol 166:173-190.

Welker, E., Soriano, E., Van der Loos (1989) Plasticity in the barrel cortex of the adult mouse: Effects of peripheral deprivation on GAD-immunoreactivity. Exp Brain Res 74:441-452.

Welker, E., Rao, R. B., Dorfi, J., Melzer, P., Van der Loos, H. (1992) Plasticity in the barrel cortex of the adult mouse: Effects of chronic stimulation upon deoxyglucose uptake in the behaving animal. J. Neurosci. 12:153-170.

White, L. E., Andrews, T. J., Hulette, C., Richards, A., Groelle, M., Paydarfar, J., Purves, D. (1997) Structure of the human sensorimotor system. I: Morphology and cytoarchitecture of the central sulcus. Cereb Cortex 7:18-30.

Wilson, C. J. (1993) The generation of natural firing patterns in neostriatal neurons. Prog Brain Res, 99:277-297.

Wilson, M. A., McNaughton, B. L. (1993) Dynamics of the hippocampal ensemble code for space. 261:1055-1058.

Wong-Riley, M. T., Welt, C. (1980) Histochemical changes in cytochrome oxidase of cortical barrels after vibrissal removal in neonatal and adult mice. Proc Natl Acad Sci USA, 77:2333-2337.

Woods, R. P. (1996) Correlation of brain structure and function, in: Brain Mapping: The Methods (A. Toga and J. C. Mazziotti, eds.), pp., New York, NY, Plenum Press.

Woolsey, C. N., Marshall, W. H., Bard, P. (1942) Representation of cutaneous tactile sensibility in cerebral cortex of monkey as indicated by evoked potentials. Bull Johns Hopkins Hosp, 70:399-441.

Woolsey, T. A., Van der Loos, H. (1970) The structural organization of layer IV in the somatosensory region (SI) of mouse cerebral cortex. The description of a cortical field composed of discrete cytoarchitectonic units. Brain Res 17:205-242.

Xiong, J, Gao, J.-H., Lancaster, J. L., Fox, P. (1996) Assessment and optimization of functional MRI analyses. Human Brain Mapping 4:153-167.

Yousry, T. A., Schmid, U. D., Alkadhi, H., Schmidt, D., Peraud, A., Beuttner, A., Winkler, P. (1997) Localization of the motor hand area to a knob on the precentral gyrus: A new landmark. Brain, 120:141-157.

Zador, A. M., Dobrunz, L. E. (1997) Dynamic synapses in the cortex. Neuron 19:1-4.

Zarzecki, P., Witte, S., Gordon, D. C., Kirchberger, P., Rasmusson, D. D. (1993) Synaptic mechanisms of cortical representational plasticity: Somatosensory and corticocortical EPSPs in reorganized raccoon SI cortex. J Neurophysiol 5:1422-1432.

Zhu, J., Connors, B. W.)1994) Intrinsic firing patterns and whisker-evoked synaptic responses of neurons in rat SmI cortex. *Soc Neurosci Abs, 20.*

Zipser, K., Lamme, V. A., Schiller, P. H. (1996) Contextual modulation in primary visual cortex. J Neurosci 16:7376-7389.